ALMA MATER STUDIORUM · UNIVERSITÀ DI BOLOGNA

Dipartimento di Fisica e Astronomia

Dottorato di Ricerca in Fisica
CICLO XXXV

Finite Group Lattice Gauge Theories for Quantum Simulation

Presentata da
Sunny Pradhan

Coordinatore Dottorato
Prof. Michele Cicoli

Supervisore
Prof. Elisa Ercolessi

Esame Finale Anno 2023

"*More is different*"

– P. W. Anderson

Abstract

The present manuscript focuses on Lattice Gauge Theories based on finite groups. For the purpose of Quantum Simulation, the Hamiltonian approach is considered, while the finite group serves as a discretization scheme for the degrees of freedom of the gauge fields. Several aspects of these models are studied. First, we investigate dualities in Abelian models with a restricted geometry, using a systematic approach. This leads to a rich phase diagram dependent on the super-selection sectors. Second, we construct a family of lattice Hamiltonians for gauge theories with a finite group, either Abelian or non-Abelian. We show that is possible to express the electric term as a natural graph Laplacian, and that the physical Hilbert space can be explicitly built using spin network states. In both cases we perform numerical simulations in order to establish the correctness of the theoretical results and further investigate the models.

Declaration

This manuscript is based on the results presented in the following works:

- <u>SP</u>, A. Maroncelli, E. Ercolessi
  Discrete Abelian lattice gauge theories on a ladder and their dualities with quantum clock models
  `arXiv:2208.04182` (submitted)

- A. Mariani, <u>SP</u>, E. Ercolessi
  Hamiltonians and gauge-invariant Hilbert space for Yang-Mills theories with finite gauge group
  `arXiv:2301.12224` (submitted)

The following works are not discussed in this thesis:

- <u>SP</u>, E. Ercolessi
  Long-range Kitaev chains and Toeplitz matrices
  (in preparation)

- F. Dell'Anna, <u>SP</u>, E. Ercolessi, C. Degli Esposti Boschi
  Quantum Fisher Information and multipartite entanglement in spin-1 chains
  (in preparation)

Contents

Introduction

Gauge theories are an essential ingredients in our microscopical description of fundamental laws and are a cornerstone of contemporary physics. In high-energy physics, they underlie the Standard Model that describe the elementary particles and their interaction. While in Condensed Matter (CM), gauge theories emerge as effective descriptions of strongly correlated phenomena, such as superconductivity or the fractional Hall effect.

Lattice Gauge Theories (LGTs) are one of the most promising methods for non-perturbative studies of gauge theories [1]. First developed by Wilson in 1974 for investigating quark confinement [2], it is now going through a renaissance period due to the growing field of *Quantum Simulation* (QS) [3]. The work by Wilson opened up the possibility of simulating Quantum Field Theories, in particular QCD, in regimes that are not accessible through perturbative methods. Unfortunately, the numerical simulations can also be limited, due to some intrinsic issues of the methodologies used. One infamous example is the sign problem in the presence of a finite chemical potential.

Regardless of numerical techniques, the simulation on classical devices of quantum systems is inherently limited, due to the exponential growth of the Hilbert space. For this reason, in 1982, Feynman [4] suggested that the best way to simulate a quantum model is through a controllable experimental quantum device, which is able to mimic or emulate the degrees of freedom and dynamical laws of another system. In short, Feynman was the first physicist to put forward the idea of *quantum simulators*. These devices can either be a specialized machine, able to simulate a specific class of models or a universal machine that can simulate any model, i.e., a quantum computer.

What characterizes a gauge theory is the presence of local symmetries, which can be regarded as local constraints, that signal the presence of redundant degrees of freedom. In order to make them approachable via QS, they have to be reformulated on a lattice in a Hamiltonian framework. In this way, they can be fully treated as quantum many-body systems. However, the extensive number of local gauge constraints can complicate the implementation and simulation process. Some kind of scheme has to be employed in

order to either eliminate redundant degrees of freedom, or make unphysical configurations inaccessible.

Another point of debate regarding LGTs is the digitalization of gauge fields. In a typical gauge theory, like QED or QCD, the degrees of freedom live on a compact manifold (the gauge group manifold) making the number of states de facto infinite for each point in space. This is not compatible with a typical quantum simulator, where only a finite register of states is available, especially on a quantum computer. Therefore, some care has to be adopted in order to find a set of states and operators that can effectively reproduce a gauge theory in the continuum. There are many methods available: quantum link models, finite subgroups, representations truncations, etc.

In this work we focus on finite group gauge theories. We argue that choosing a finite subgroup of a Lie group (like U(1) or SU(N)) offers a more natural way of truncating the number of degrees of freedom, but while U(1) can be approximated with arbitrary precision with $\mathbb{Z}_N$ the same is not true for a general SU(N). The choice of finite groups preserves the unitarity of the parallel transporters, associated with the gauge fields. This property is lost, for example, if one chooses to truncate the irreducible representations of the Lie group instead. We focus on both Abelian [5] and non-Abelian [6] finite groups, and examine different aspects.

This manuscript is structured as follow:

Chap. 1 As a starting point, in the first part of the chapter we review Yang-Mills theory. It is a gauge field theory based on the compact Lie groups, like SU(N). They can be regarded as generalizations of QED and are the basis for theories like QCD. In order to create a clear context for LGTs, we also review Yang-Mills theory in Euclidean space-time and its Hamiltonian formulation.

In the second part of the chapter we move onto Wilson's lattice gauge formulation [2]. This is going to be useful in showcasing some fundamental concepts: the discretization on the lattice, how to construct interaction terms for the gauge fields, what kind of order parameters can be used.

Chap. 2 In this chapter, we change subject and introduce in more detail the topic of Quantum Simulation. After a general exposition and explanation of its context, we review the current landscape through the possible paths that can be taken in Quantum Simulation: digital, analog and quantum-inspired. Then, we focus more on the state of the art of Quantum Simulation of LGTs.

Chap. 3 The content of this chapter is based on [5]. We considered LGTs with gauge group $\mathbb{Z}_N$, in order to have a discretized $U(1)$ theory. Then, we formulated these models on a ladder geometry, because it is an almost one-dimensional lattice that allows for magnetic terms, which are not possible in a pure one-dimensional chain.

With QS in mind, we wanted to find an effective description of these models that was able to resolve all the gauge constraints. One of the main achievements of the work is the construction of a *duality map* between these $\mathbb{Z}_N$ models and *quantum clock models* (QCMs) [7]. Thanks to this duality, we were able to show that the super-selection sectors of the gauge model map to a different class of QCMs. This leads to the fact that each super-selection sector has its own distinguished phase diagram, in particular regarding deconfinement-confinement phase transitions.

Chap. 4 The content of this chapter is based on [6], where we consider lattice gauge theories with finite gauge group, focusing more on the non-Abelian case, inspired by the Hamiltonian formulation of Kogut and Susskind [8],

In the case of a Lie group, the electric Hamiltonian is given by the Casimir element of the Lie algebra, which can be reinterpreted as the Laplacian on the group manifold. In this chapter we show that in the case of a finite group, an analogous construction is possible, even though there is no equivalent of a Lie algebra for a finite group. In particular, we show that the electric Hamiltonian can still be written as a natural Laplacian, but, this time, on the *Cayley graph* of the finite group.

Another important result of this work is the full description of the physical, gauge-invariant Hilbert space, regardless of the choice of group or Hamiltonian. This was possible thanks to the use of *spin network states*, which exploits the subspace of invariant states of a vertex. Additionally, we show also how to compute the dimension of the physical Hilbert space for any lattice size.

chapter one

Introduction to Lattice Gauge Theories

One of the most important open questions in high-energy physics is *confinement* in Quantum Chromodynamics (QCD), or in general in a non-Abelian gauge theory. The best evidence for confinement comes from the Wilson formulation of gauge theories on a lattice [2], which, at first glance, can appear odd because the vacuum is not a crystal [9]. Indeed, there have not been experimental proofs so far that show any deviations from the symmetries of the Lorentz group.

From the point of view of particle physics, the lattice represents a mathematical trick. It provides a cutoff, which removes the ultraviolet infinities that often appear in Quantum Field Theories (QFTs). It is just a regulator and as such it must be removed after renormalization. Physical results can only be extracted in the continuum limit, where the lattice spacing goes to zero.

But why do we need such a regulator? Infinities have always been present in QFTs since its conception. Consider the case of Quantum Electrodynamics (QED). It had an immense success without ever using a discrete space-time, thanks to *perturbation theory*. The most conventional calculation schemes are based on Feynman expansions, where a given observable is expressed as a power series in the interaction coupling. The terms are computed until a divergence is met in a particular diagram. Then, these divergences can be removed using some regularization scheme or methods provided by the Renormalization Group [10].

The reason why this methodology may fail in non-Abelian theories lies in the fact that some phenomena, like confinement, are inherently *non-perturbative*. Roughly speaking, perturbation theory relies on the fact that the true interacting theory is just a slight modification of the free theory. In other words, it works only when the coupling constants are small. In the case of QCD, the free theory with vanishing coupling constant has no resemblance to the observed phenomenon.

In order to go beyond the diagrammatic approach of Feynman expansions, one needs a non-perturbative cutoff. This is the main strength of the lattice, it eliminates all the wavelengths smaller than the lattice spacing before any kind of expansions is done. Furthermore, on a lattice a field theory is *mathematically well-defined*, in contrast with many standard formulations of QFTs (like the path-integral approach).

Lattice Gauge Theories (LGTs) are just a reformulation of QFTs on a lattice, which exposes a close connection with *Statistical Mechanics (SM)*. For example, it can be showed that a path-integral in QFT is equivalent to a partition function in SM. Furthermore, it can be showed that the coupling constant in QFT corresponds directly to the temperature, and a strong coupling expansion becomes equivalent to a high temperature expansion. Thus, a lattice formulation of QFTs allows a particle physicist to use the full technology of SM and Condensed Matter (CM). Notice that this connection between QFT and SM does not require a lattice, but it is only made more transparent by it.

While in particle physics the lattice is a useful trick, this is not true in CM. Indeed, in this field a lattice structure can emerge naturally, or rather it can even be required. It is sufficient to think that many materials have a crystalline structure, hence the mathematical models describing these materials have to be formulated on a lattice. Then, field theories can be used for probing the physics at scale lengths much larger that the lattice spacing. Therefore, in CM the roles are reversed: continuous fields are "approximations" of what really happens on a lattice.

In this section we first briefly review Yang-Mills theory, which is the generalization of QED to any non-Abelian compact gauge group, like $SU(N)$. Then, we move onto the Wilson formulation of LGTs in the path-integral approach.

1.1   Review of Yang-Mills theory

A Yang-Mills (YM) theory is a gauge field theory on Minkowski space $\mathbb{R}^{1,d}$ coupled to matter. The gauge group G is usually chosen to be a compact Lie group like U(1) or SU(N) and the matter fields are defined by a representation of G. For example, QCD is an $SU(3)$ gauge theory with Dirac spinors in the fundamental representation. We choose to keep the dimension d of space completely general and to use D to denote the full dimension of space-time, i.e., $D = d + 1$.

We start from the Lagrangian. Considering that YM theory can be seen as the generalization of QED, a U(1) gauge theory, to any compact Lie group,

the Lagrangian looks exactly like the one from QED:

$$\mathcal{L}_{\mathrm{YM}} = -\frac{1}{2g^2}\,\mathrm{tr}(F_{\mu\nu}F^{\mu\nu}) + \overline{\psi}(i\gamma^\mu D_\mu - m)\psi, \qquad (1.1)$$

with some differences that will be explained later. Hereafter, the Einstein summation rule is implied. Notice that in (1.1) we have only considered one fermionic species. In more realistic cases we would have a some over the different fermion flavors but for simplicity and ease of exposition we will ignore flavors and consider only type of fermion.

Gauge fields   The symbol D_μ in (1.1) denote the *covariant derivative*:

$$D_\mu = \partial_\mu - iqA_\mu, \qquad (1.2)$$

where A_μ are the space-time components of the gauge fields. Each component is Lie algebra valued function of space-time:

$$A_\mu(x) = \sum_a A_\mu^a(x)T^a, \qquad (1.3)$$

where the sum is over the generators T^a of the Lie algebra $\mathfrak{g}$, corresponding to the group G. In the following, we will use Greek indices for space-time coordinates, and Latin indices for the algebra structure. We choose the convention where the generators T^a are Hermitian with

$$[T^a, T^b] = if^{abc}T^c \quad \text{and} \quad \mathrm{tr}\Big(T^aT^b\Big) = \frac{1}{2}\delta^{ab}, \qquad (1.4)$$

with real structure constants f^{abc}.

The dynamics of the gauge fields is given by $F_{\mu\nu}$, which is the *strength-field tensor* and defined as

$$F_{\mu\nu} = \partial_\mu A_\nu - \partial_\nu A_\mu - i[A_\mu, A_\nu]. \qquad (1.5)$$

and transforms in the adjoint representation of $SU(N)$. Notice that when $G = U(1)$, i.e. Abelian, the commutator term in (1.5) vanishes and we re-obtain the strength-field tensor of QED. Like the gauge field A_μ, also the tensor $F_{\mu\nu}$ lives in the Lie algebra $\mathfrak{g}$. Therefore, the product $F^{\mu\nu}F_{\mu\nu}$ is actually a matrix. Only scalar terms are allowed in the Lagrangian (1.1), hence we have to take the trace:

$$\mathrm{tr}\,F^{\mu\nu}F_{\mu\nu} = \sum_a F^{\mu\nu a}F_{\mu\nu}^a.$$

Fermions   Given the fact that we will not look at dynamical matter fields in this manuscript, we only give a very brief introduction to fermions. The fermion field $\psi(x)$ lives in the *fundamental representation* of G. The Lagrangian of a free fermion field ψ is

$$\mathcal{L}_\psi = \overline{\psi}(\partial_\mu \gamma^\mu - m). \tag{1.6}$$

The matrices γ^μ form a *Clifford algebra*, which is defined by the relations

$$\{\gamma^\mu, \gamma^\nu\} = 2\eta^{\mu\nu}, \tag{1.7}$$

where $\eta^{\mu\nu}$ is the space-time metric. For the latter we choose the convention $\eta^{\mu\nu} = \mathrm{diag}(+1, -1, -1, -1)$. The conjugate field $\overline{\psi}$ is defined as

$$\overline{\psi} = \psi^\dagger \gamma^0.$$

The interaction with the gauge field can be obtained with a simple minimal coupling, where the derivative ∂_μ is substituted with the covariant derivative D_μ in (1.2).

Gauge transformations   A gauge transformation is defined by a group valued function of space-time $g : \mathbb{R}^{1,d} \to G$. It transforms the fermion field as

$$\psi(x) \mapsto g(x)\psi(x). \tag{1.8}$$

Here we have been a bit sloppy with notation, by writing $g(x)\psi(x)$ in (1.8) we actually mean the action of the element $g(x) \in G$ in the same representation of $\psi(x)$.

   In order to have an invariant Lagrangian, the gauge fields A_μ have to undergo a transformation induced by the function g:

$$A_\mu(x) \mapsto g(x)A_\mu(x)g(x)^{-1} + ig(x)\partial_\mu g(x)^{-1}, \tag{1.9}$$

so that $D_\mu \psi(x) \mapsto g(x)D_\mu \psi(x)$, while

$$F_{\mu\nu} \mapsto g(x)F_{\mu\nu}g(x)^{-1}. \tag{1.10}$$

Path-integral   For a path integral formulation we need to first define the action. This is just the integral of the Lagrangian in (1.1), over the D-dimensional space-time:

$$\mathcal{S}[A, \psi, \overline{\psi}] = \int_{\mathbb{R}^{1,d}} \mathrm{d}^D x \mathcal{L}. \tag{1.11}$$

The action (1.11) defines the "weight" in the path-integral. Now we can write down the partition function for a YM theory:

$$\mathcal{Z} = \int \mathcal{D}A \, \mathcal{D}\overline{\psi} \, \mathcal{D}\psi \, e^{i\mathcal{S}[A,\psi,\overline{\psi}]}. \tag{1.12}$$

The measures in the path-integral can be physically interpreted as a measure over all the possible configurations of the fields A_μ, $\overline{\psi}$ and ψ, but are still lacking a rigorous mathematical definition [10]. We will not elaborate further on this topic.

1.1.1 Euclidean field theory

In the previous section we introduced YM theory in Minkowski space-time. We now need to move onto Euclidean space-time, which is the starting point for LGT. This is true for various reasons. As stated previously, Euclidean formulation allows to bridge into the territory of SM, meaning we can use its full technology. Second, there are also some advantages from the operational point of view. The weight in (1.12) is a complex phase, which can be problematic from the computational point of view because a priori convergence is not guaranteed. We will see that in Euclidean space-time the weight will become a positive-defined function, which makes it clear it is a probability distribution.

In order to pass to a Euclidean space-time $\mathbb{R}^{d+1}$, we need to perform a *Wick rotation*, where the time coordinate x_0 is mapped to a forth space coordinate x_4:

$$x_0 \mapsto -ix_4.$$

To distinguish quantities in Euclidean or Minkowski space-time we use the subscripts E and M, respectively. The rotation (1.1.1) affects both space-time measures,

$$\mathrm{d}^D x_M = \mathrm{d}x_0 \mathrm{d}^d x_i \quad \text{and} \quad \mathrm{d}^D x_E = \mathrm{d}^d x_i \mathrm{d}x_4,$$

and the time-components of the quantities that enters the Lagrangian, which leads to an overall effect

$$\mathcal{L}_E = -\mathcal{L}_M.$$

The action is defined in the same way in both types of space-time,

$$\mathcal{S}_M = \int \mathrm{d}^D x_M \mathcal{L}_M \quad \text{and} \quad \mathcal{S}_E = \int \mathrm{d}^D x_E \mathcal{L}_E,$$

and due to the Wick rotation (1.1.1), we obtain that they satisfy

$$i\mathcal{S}_M = -\mathcal{S}_E. \tag{1.13}$$

14

This leads to the following definition of the Euclidean path-integral:

$$\mathcal{Z}_E = \int \mathcal{D}A\, \mathcal{D}\overline{\psi}\, \mathcal{D}\psi\, e^{-\mathcal{S}_E[A,\overline{\psi},\psi]}. \tag{1.14}$$

Notice that the weight $e^{-\mathcal{S}_E}$ in (1.14) is now a positive-valued function, given that $\mathcal{S}_E$ is a real function, and has the form of a *Boltzmann weight*. In other words, following the spirit of SM, we have now a probability distribution $e^{-\mathcal{S}_E}$ over the configurations of the fields A_μ, ψ and $\overline{\psi}$.

Let's describe this procedure in more details. The Wick rotation does not change the aspect of the gauge kinetic term,

$$-\frac{1}{2g^2}\,\mathrm{tr}(F_{\mu\nu}F^{\mu\nu}), \tag{1.15}$$

but the sum is now a simple Euclidean sum, where there are minus signs appearing when raising or lowering indices, and $\mu = 1, \ldots, d+1$.

Considering now the fermionic part of the YM Lagrangian, we need to perform the Wick rotation on the Dirac fields ψ and $\overline{\psi}$. In Minkowski space-time

$$\overline{\psi}(i\gamma_M^\mu D_\mu - m)\psi = \overline{\psi}(i\gamma_M^\mu \partial_\mu + \gamma_M^\mu A_\mu - m)\psi, \tag{1.16}$$

where γ_M^μ denotes the gamma matrices in Minkowski space-time:

$$\{\gamma_M^\mu, \gamma_M^\nu\} = 2\eta^{\mu\nu}.$$

The Euclidean Clifford algebra instead uses gamma matrices γ_E^μ that instead satisfy

$$\{\gamma_E^\mu, \gamma_E^\nu\} = 2\delta^{\mu\nu}.$$

Given that we have $\partial_0 = i\partial_4$ and $A_0 = iA_4$, the correct form can only be achieved by putting $\gamma_M^0 = \gamma_E^4$. This procedure yields

$$\overline{\psi}(i\gamma_M^\mu \partial_\mu + \gamma_M^\mu A_\mu - m)\psi = -\overline{\psi}(\gamma_E^\mu \partial_\mu + i\gamma_E^\mu A_\mu + m)\psi. \tag{1.17}$$

Since $\mathcal{L}_E = -\mathcal{L}_M$, we can conclude

$$\mathcal{L}_E = \frac{1}{2g^2}\,\mathrm{tr}(F_{\mu\nu}F^{\mu\nu}) + \overline{\psi}(\gamma^\mu D_\mu + m)\psi, \tag{1.18}$$

where the indices are all Euclidean and $D_\mu = \partial_\mu + iA_\mu$.

1.1.2 Hamiltonian formulation

Even though Wilson's formulation [2] is in the path-integral and Lagrangian language, we will also review the Hamiltonian formulation of non-Abelian QFT because its connection to Quantum Simulation. Expressing a YM theory in

the Hamiltonian language can be tricky, especially in the presence of gauge symmetries. Usually, one has to procede by computing the conjugate momenta and perform a Legendre transform in order to obtain the Hamiltonian. In the presence of gauge symmetries, the time-component A_0 of the gauge fields does *not* have a conjugate momentum. Instead it leads to a *constraint*:

$$\frac{\partial \mathcal{L}}{\partial \dot{A}_0} = 0, \tag{1.19}$$

which means that the Legendre transform is not invertible.

The easiest remedy is to *fix the gauge* beforehand, by imposing $A_0 = 0$, which is called *canonical* or *temporal gauge*. With this condition, the gauge fields Lagrangian can be written as

$$-\frac{1}{2g^2} \operatorname{tr}(F_{\mu\nu}F^{\mu\nu}) = \frac{1}{g^2}\Big(\mathbf{E}^2 - \mathbf{B}^2\Big) = \frac{1}{g^2}(E_i^a E_i^a - B_i^a B_i^a), \tag{1.20}$$

where $\mathbf{E}$ and $\mathbf{B}$ are, respectively, the corresponding electric and magnetic fields for a non-Abelian theory. In the temporal gauge we only have the spatial components $\mathbf{A}$ of the gauge field A_μ. The electric field $\mathbf{E}$ is the time derivative of $\mathbf{A}$, i.e. $\mathbf{E} = \frac{\mathrm{d}\mathbf{A}}{\mathrm{d}t}$, which means that $\mathbf{E}$ is the conjugate momentum to $\mathbf{A}$. Meanwhile, the magnetic field $\mathbf{B}$ can be obtained from the spatial components of the strength-field tensor $F^{\mu\nu}$, with $B_i = -\frac{1}{2}\varepsilon_{ijk}F^{jk}$, where ε_{ijk} is the Levi-Civita symbol. Once the gauge is fixed, the Hamiltonian can be finally be obtained with a Legendre transform:

$$\mathcal{H} = \frac{1}{g^2}E_i^a \dot{A}_i^a - \frac{1}{2g^2}(E_i^a E_i^a - B_i^a B_i^a) = \frac{1}{2g^2}\operatorname{tr}\Big(\mathbf{E}^2 + \mathbf{B}^2\Big). \tag{1.21}$$

In the Hamiltonian formulation, the fields $\mathbf{A}$ and $\mathbf{E}$ have to be elevated to operators, by imposing the following commutation relations:

$$\begin{aligned}
\Big[A_i^a(x), E_j^b(y)\Big] &= ig^2\delta_{ij}\delta_{ab}\delta(x-y) \\
\Big[E_i^a(x), E_j^b(y)\Big] &= \Big[A_i^a(x), A_j^b(y)\Big] = 0.
\end{aligned} \tag{1.22}$$

A careful reader will notice that (1.22) are completely analogous to a position-momentum commutation relation, similar to $[x_i, p_j] = i\delta_{ij}$. In fact, like in the latter case, where the momentum p_i is the generator of translations of x_i, the electric field $\mathbf{E}$ is the generator of translation of $\mathbf{A}$. To be more precise, it is the canonical momentum $\mathbf{E}/g^2$ that generates translations of $\mathbf{A}$. In other words, $\mathbf{E}/g^2$ *generates infinitesimal gauge transformations*. This point of view will be rather useful when treating the gauge fields on a lattice.

In order to impose the canonical gauge $A_0 = 0$, the equation of motion for A_0 has to be satisfied:

$$\partial_\mu \left(\frac{\partial \mathcal{L}}{\partial(\partial_\mu A_0)}\right) - \frac{\partial \mathcal{L}}{\partial A_0} = 0. \tag{1.23}$$
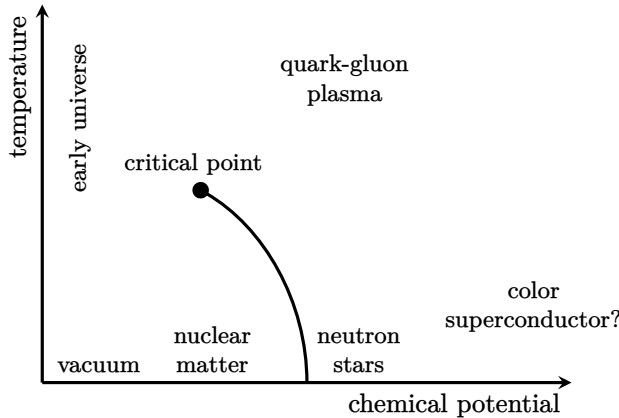
Figure 1.1. A (very) rough sketch of the phase diagram of QCD [11].

In the absence of sources, this leads to

$$D_i E_i = 0, \tag{1.24}$$

where D_i and E_i are the spatial components of the covariant derivative and electric field, respectively. What we obtained is basically the generalization of *Gauss law* to non-Abelian theories. In fact, the condition (1.24) for a $U(1)$ theory reduces to the well known $\nabla \cdot \mathbf{E} = 0$. Unfortunately, the equation (1.24) is inconsistent with the commutation relations (1.22), so it cannot be implemented as an operator equation. The easiest solution, or loophole, to this empasse is to impose to consider *physical* or *gauge-invariant* only states that satisfy

$$D_i E_i \left| \psi_{\text{phys}} \right\rangle = 0. \tag{1.25}$$

This constraint select a subspace of the overall Hilbert space $\mathcal{H}$, which will be labeled as the *physical Hilbert space* $\mathcal{H}_{\text{phys}}$.

1.1.3 The sign problem

A number of interesting phases have been predicted for QCD in the $\mu - T$ plane [11], where μ is the chemical potential and T the temperature, such as *quark-gluon plasma* [12] or *color superconductivity* [13] (see Fig. 1.1). Unfortunately, detailed quantitative analysis of QCD has been limited to the $\mu = 0$ region only [11]. This is mainly due to the difficulty of studying QCD in the low energy regime, where the perturbative approach fails [9, 10]. Moreover, even LGTs, at least in the path-integral formulation, is not applicable for $\mu \neq 0$ due to the infamous *sign problem*.

In the Hamiltonian formulation, the chemical potential in introduced in the same manner as standard SM. If H is the Hamiltonian density operator and

N a fermion density operator, then one can simply replace H with $H - \mu N$. In the case of a YM theory, the fermion density operator would correspond to the fermion number operator $N = \psi^\dagger \psi$.

In the path integral formalism, fermions are introduced as Grassmann variables. This means that they can easily be integrated out [10, 11]:

$$\int \mathcal{D}\overline{\psi}\, \mathcal{D}\psi \exp\left(-\int d^D x \overline{\psi} K \psi\right) = \det K, \qquad (1.26)$$

where K is the kinetic operator for the fermions. If the fermions are coupled to A_μ, as it happens in YM theory, then K has some complicated dependence on the fields A_μ. If one includes the chemical potential term $\mu \psi^\dagger \psi$ in the Lagrangian, then the fermion determinant $\det K$ turns out to be complex [11], with a non-trivial phase factor.

As a result, the integrand of the path-integral is no longer positive-definite, and it cannot be interpreted as a probability distribution. Furthermore, a complex weight in the path-integral makes the integrand oscillatory, which does not help with convergence. This is summarizes the so-called *sign problem*, which poses severe limitation to, for example, Monte Carlo (MC) simulations in the finite μ region.

1.2 Wilson approach to Lattice Gauge Theories

Starting from the path integral formulation, the first step in the formulation of a LGT is the discretization of space-time, where a discrete $d+1$-dimensional lattice substitutes the continuum space-time. The simplest choice in this regard is a hypercubic lattice with lattice spacing a, but in theory an LGT can be defined on any type of lattice. An immediate advantage of using a lattice instead of a continuum is the natural ultraviolet cutoff given by the inverse of the lattice spacing.

Formally, a lattice $\mathbb{L}$ is defined as

$$\mathbb{L} = \left\{ x \in \mathbb{R}^D : x = \sum_{\mu=1}^{D} a n_\mu \hat{\mu} \quad n_\mu \in \mathbb{Z} \right\}, \qquad (1.27)$$

where $\mu = 1, \ldots, D$, and $\hat{\mu}$ is the unit vector in the $\hat{\mu}$-th direction. The edges, or *links*, will be labeled by a pair $(x, \hat{\mu})$, meaning that we are referring to the link in the $\hat{\mu}$ direction from the vertex, or *site*, x. It is important to fix an orientation for each direction in the lattice. The most natural choice is to choose $+\hat{\mu}$ for each $\hat{\mu}$. So, even though $(x, \hat{\mu})$ and $(x + \hat{\mu}, -\hat{\mu})$ refers to the same link, the former is traversed in the positive direction while the latter in the negative direction.
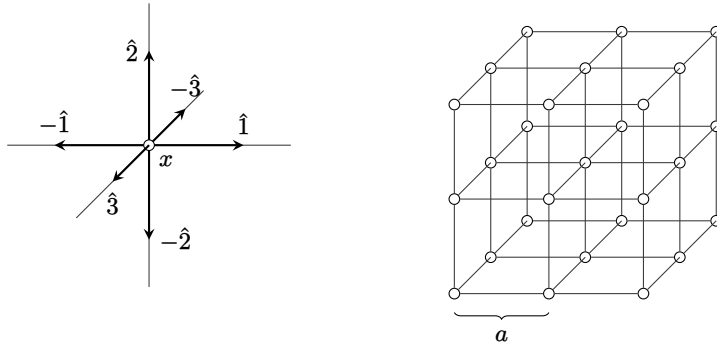
Figure 1.2. *Left.* Unit vectors $\hat{\mu}$ in three-dimensional lattice. *Right.* Example of a three-dimensional lattice.

In an LGT, both the sites and links host degrees of freedom (d.o.f). In particular, the matter fields lives on the sites while the gauge fields live on the links. The definition of these d.o.f will need some care, because we have two main requirements, especially if we are interested in YM theory:

- The lattice action should reduce to the continuum action in the continuum limit, i.e., $a \to 0$;

- The lattice action should respect the gauge symmetry.

Lorentz invariance is naturally broken on a lattice but we expect to recover it in the continuum limit.

1.2.1 Gauge fields on a lattice

The simplest way to define a YM action on a lattice would be to consider a continuum action, substitute finite-difference approximations for derivatives, and replace the space-time integral by a sum over the lattice sites. However, the result of this is an action which is not-gauge invariant for non-zero lattice spacing [2]. This is likely to mean that the theory would still lack gauge-invariance in the $a \to 0$ limit. The alternative, outlined in [2, 9], would be to formulate gauge invariance for a lattice theory then modify its action until it is gauge invariant for any a.

We start by considering a general group G. We associate an element $U_\mu(x) \in G$ to each link (x, μ). If one traverse the link in the opposite direction, one should consider the inverse element U^{-1}. In the case of SU(N), we take $U_\mu(x)$ to be the matrices in the fundamental representation and a vector potential can be obtained in the continuum limit by writing

$$U_\mu(x) = e^{iagA_\mu(x)}. \tag{1.28}$$
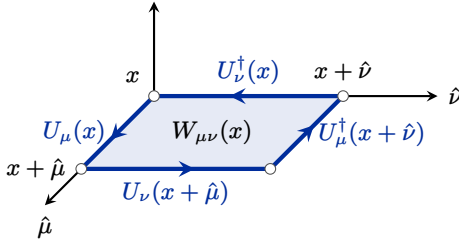
Figure 1.3. Single plaquette Wilson loop $W_{\mu\nu}(x)$, which is defined on the plaquette in the (μ, ν)–plane at x (highlighted in blue). For convenience we have set $a = 1$.

It is necessary to discuss about gauge invariance before moving to the dynamics of these gauge fields. A gauge transformation is described by a group-valued function $g(x)$ (in the appropriate representation), which acts on the vertices x. The variable $U_\mu(x)$ sits in the middle of the site x and $x + \hat{\mu}$, therefore it transforms as

$$U_\mu(x) \mapsto g(x)U_\mu(x)g(x + a\hat{\mu})^\dagger. \tag{1.29}$$

The action of the gauge fields $U_\mu(x)$ has to satisfy two requirements: it has to be *gauge-invariant* and reduce to the pure gauge YM action in the continuum limit. From (1.29), we can immediately deduce that taking the product of $U_\mu(x)$ along a closed curve will yield a gauge-invariant quantity. The simplest close curve we can consider is a *plaquette*, i.e., the smallest square face.

Consider a plaquette sitting in the (μ, ν)-plane at site x (see Fig. 1.3). We define the *single plaquette Wilson loop* $W_{\mu\nu}(x)$ as

$$W_{\mu\nu}(x) = U_\mu(x)U_\nu(x + a\hat{\mu})U_\mu(x + a\hat{\nu})^\dagger U_\nu(x)^\dagger. \tag{1.30}$$

Notice that we do not have any sum in the indices μ and ν because they are not Lorentz indices. Only scalar quantities are allowed in the action, so we need to take the trace of $W_{\mu\nu}$. Then, our lattice action will be defined as the sum over the plaquettes of $\operatorname{tr} W_{\mu\nu}$ (and its Hermitian conjugate):

$$\mathcal{S}_{\mathrm{W}} = -\frac{1}{g^2} \sum_x \sum_{\mu,\nu} \left(\operatorname{tr} W_{\mu\nu}(x) + \operatorname{tr} W_{\mu\nu}^\dagger(x) \right). \tag{1.31}$$

This is known as the *Wilson action* [2, 9]. The quantity $\operatorname{tr} W_{\mu\nu}$ behaves as expected in the continuum limit, where we have to work with the strength field $F^{\mu\nu}$:

$$\operatorname{tr} W_{\mu\nu} \approx N - \frac{a^4}{2} \operatorname{tr} F_{\mu\nu}F^{\mu\nu} + \mathcal{O}(a^6), \tag{1.32}$$

The lattice action is not unique. The Wilson action in (1.31) is the simplest choice that one can make that satisfies our requirement. Some other

modifications are possible, they can include other types of closed loops or other representations. These modification have their place, for example for improving the continuum limit or errors [14–16]. However, they will not be considered here.

Obviously, in a path-integral formulation of LGTs we need to define the path-integral in order to have a quantum theory:

$$Z = \int \prod_{(x,\hat{\mu})} \mathrm{d}U_\mu(x) e^{-\mathcal{S}_\mathrm{W}}. \tag{1.33}$$

Here we integrate over all possible values for the gauge variables. Due to the fact that U_μ are elements of a group G that for most physical applications is compact, the most natural choice is to the invariant group measure also known as *Haar measure* [9, Chap. 8]. Notice that (1.33) is now a well defined mathematical quantity, unlike the path-integral in continuum theory where a clear mathematical definition is still lacking. Now that the path-integral measure has been defined, we can compute the average of an observable $\mathcal{O}$ with

$$\langle \mathcal{O} \rangle = \frac{1}{Z} \int \prod_{(x,\hat{\mu})} \mathrm{d}U_\mu(x) \mathcal{O} e^{-\mathcal{S}_\mathrm{W}} \tag{1.34}$$

1.2.2 Order parameters and gauge invariance

The Wilson formulation of LGTs can resemble spin models studied in statistical mechanics. The link variables $U_\mu(x)$ can be thought as some sort of generalization of the spin d.o.f. They are distributed in a crystal-like structure and interact with their nearest neighbours, in this case through a four-body interaction (the plaquette action), instead of two-body interaction (like the Ising model). If one wants to pursue this analogy, then it is reasonable to look at order parameters that behaves like the spontaneous magnetization, where a non-vanishing expectation value signals a phase transition. The analogue of such an order parameter in LGT would be something like

$$\langle U_\mu(x) \rangle \neq 0, \tag{1.35}$$

but it has been shown that this is impossible in Wilson theory [17]. Let's argue why.

In standard spin models, a non-zero magnetization represents a spontaneous breaking of the global symmetry of the system. Consider the simplest case of the classical Ising model, where the d.o.f are binary variables $\sigma = \pm 1$. Without an external field, the energy is given by the interaction of nearest

neighbouring spins, i.e., $\sigma_i \sigma_j$. This system has an obvious global $\mathbb{Z}_2$ symmetry, that corresponds to the inversion $\sigma_i \mapsto -\sigma_i$ off all the spins. A ferromagnetic phase is, by definition, signaled by $\langle \sigma \rangle \neq 0$, which necessarily breaks the global $\mathbb{Z}_2$ symmetry of the model. Once a direction is selected by $\langle \sigma \rangle \neq 0$, it remains stable under thermal fluctuations because they cannot coherently shift the magnetization of a large (or infinite) number of spins.

In a LGT, an expectation value like (1.35) would *break gauge invariance*, which is a *local symmetry*, not a global one. As explained previously, gauge invariance means that the action is unchanged under local arbitrary "rotations" of the link variables $U_\mu(x)$ (see (1.29)). Hence, thermal fluctuations will induce such rotations and in the long rung it will average on all the possible gauges, which leads to

$$\langle U_\mu(x) \rangle = \int \mathrm{d}U_\mu(x) U_\mu(x) = 0 \tag{1.36}$$

if U_μ contains only non-trivial irreducible representations of the group (see Th. 5 in App. A). This means that "magnetization" is always vanishing in a LGT and gauge invariance cannot be spontaneously broken, which is the contents of the Elitzur theorem [17].

The conclusion of this brief discussion may seem rather grim, as magnetization in spin models is the most convenient and used order parameter. But this does not mean that there are no other order parameters in a LGT. We have just showed that the problem when considering something like $\langle U_\mu \rangle$ is gauge invariance. So, the most reasonable step forward is to consider *gauge-invariant quantities* as order parameters. We have already seen that tracing over a product of U_μ variables along a closed curve is a gauge-invariant quantity, called *Wilson loop (WL)*.

In so far, we have considered only single plaquette loops but nothing restraints us from considering arbitrary large loops, indeed it serves as a *confinement test* for pure gauge theories. It has been shown [2] that confinement is equivalent to the *area law* behaviour of WLs, i.e.,

$$\langle W(\mathcal{C}) \rangle \sim \exp(-\sigma A(\mathcal{C})), \tag{1.37}$$

where $A(\mathcal{C})$ is the minimal area inside the closed path $\mathcal{C}$ and σ the *string tension* (the coefficient of the linear potential between two quarks). On the other hand, in the absence of confinement one finds instead the *perimeter law*:

$$\langle W(\mathcal{C}) \rangle \sim \exp(-kP(\mathcal{C})), \tag{1.38}$$

where $P(\mathcal{C})$ is the perimeter of the curve $\mathcal{C}$ and k just some constant.
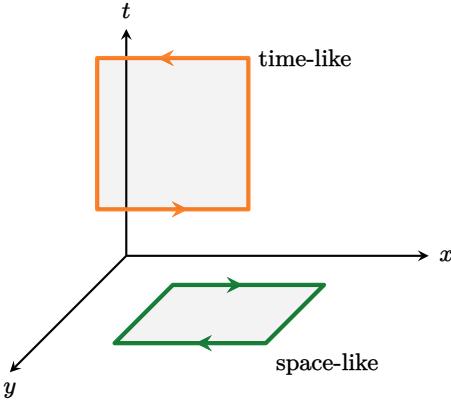
Figure 1.4. Space-like and time-like Wilson loop.
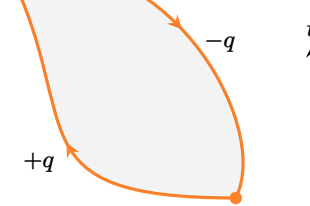
Figure 1.5. A time-like Wilson loop can be seen as a process where a quark-antiquark pair is created and then annihilated.
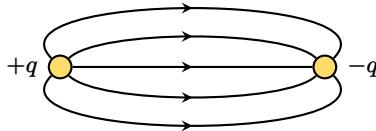
Figure 1.6. Example of a flux tube binding two charges, which gives rise to the quark binding mechanics

The reason behind this behaviour can be seen with a simple qualitative picture [2, 9]. A closed timelike WL basically represents a process in which a quark-antiquark pair is produced, moved along the sides of the loop and annihilated. If we are in a confining phase we can then expect a liner potential between the quark and antiquark. We can imagine a flux tube *binding* the two charges, which swoops the whole inside area of the loop. Then, it is easy to image that the energy of this whole process will necessarily depend on the area of the loop. On the other hand, if we are in a deconfined phase then there is no potential binding the two quarks. In this case the energy of the whole process depends only on the self-energy of quarks, which move along the sides of the loop. Therefore, the leading energy contribution of this process depends on the perimeter, instead of the area. Obviously, this picture is no longer valid when dynamical matter is involved, because in a confining phase pair production is always preferred when separating two quarks at large distances.

From (1.37) and (1.38), we can deduce that the string tension σ can be used as an order parameter. It is non-zero for a confining phase, while it vanishes for a deconfined phase. But it is *non-local* in nature, as it involves the asymptotic behaviour of potential, and therefore of the correlation functions of the theory.

1.2.3   Fermions on a lattice

The fermionic degrees of freedom lives on the sites of the lattice. So, for each site x of the lattice $\mathbb{L}$, we have a spinor variable ψ_x. Then, in order to build the lattice action, the derivative $\partial_\mu \psi(x)$ has to be substituted with a symmetric finite difference

$$\partial_\mu \psi(x) \quad \longrightarrow \quad \frac{1}{2a}(\psi_{x-\hat{\mu}} - \psi_{x+\hat{\mu}}).$$

One can suppose that this substitution, accompanied with the usual substitution of integrals with sums over the lattice will yield the correct lattice action for fermions. Unfortunately, this is not the whole story. Defining lattice fermions is not this straightforward due to the known *doubling problem* [18, 19]. In simple terms, when introducing fermions on a lattice, instead of a continuous space, it leads to an extra number of spurious fermions, which are just lattice artifacts.

In order to get an insight into the fermion doubling issue, consider the correlation function for a single fermionic species. If K is the kinetic matrix for the fermions, then $G = K^{-1}$ gives their correlation matrix. One finds that the correlation function between two sites x and y has the form [9]

$$(G)_{x,y} = \frac{1}{a^d L^d} \sum_k \tilde{G}_k e^{2\pi i k \cdot (x-y)/L}, \tag{1.39}$$

where a is the lattice spacing, L^d the total volume and $\tilde{G}_k$ the correlation function in momentum space:

$$\tilde{G}_k^{-1} = m + \frac{i}{a} \sum_\mu \gamma_\mu \sin(2\pi k_\mu / L). \tag{1.40}$$

It involves a simple trigonometric function because the derivative term involves nearest neighbouring sites. One can then take the model to a large lattice, which justifies in substituting the discrete sums with integrals:

$$\frac{2\pi k_\mu}{La} \to q_\mu \qquad \text{and} \qquad \frac{1}{a^d L^d} \sum_k \to \int \frac{dq^d}{(2\pi)^d}, \tag{1.41}$$

where the q_μ's are continuous momentum variables. This substitution maps (1.40) into

$$\tilde{G}_k^{-1} = m + \frac{i}{a} \sum_\mu \gamma_\mu \sin(aq_\mu). \tag{1.42}$$

One can naively think of taking the limit $a \to 0$ and expand $\sin(aq_\mu)$ around the zero and obtain something that look like the correct continuum limit:

$$\tilde{G}_\mu^{-1} = m + i\slashed{q} + \mathcal{O}(a^2). \tag{1.43}$$

But one should not be fooled by this sloppy procedure just because it appears to give the wanted result. Each component q_μ takes values in the region $[-\pi/a, +\pi/a]$, hence we have to integrate on the whole volume $[-\pi/a, +\pi/a]^d$. Looking at (1.42), it is clear that the major contributions to G in (1.39) comes from the zeros of $\tilde{G}_k^{-1}$. This, not only vanishes in the region $q_\mu \sim 0$ but also for large momentum $q_\mu \sim \pi/a$. The propagator has no suppression of momentum values near π/a. We can isolate the large momenta region by considering

$$\tilde{q}_\mu = q_\mu - \pi/a \qquad (1.44)$$

for each direction in space. In this way, we de facto half the integration region,

$$\int_{-\pi/a}^{\pi/a} \mathrm{d}q_\mu \;\to\; \int_{-\pi/2a}^{\pi/2a} (\mathrm{d}q_\mu + \mathrm{d}\tilde{q}_\mu) \qquad (1.45)$$

and now the limit $a \to 0$ can be taken safely, but it comes with a price to pay. For each direction in space, we have two independent regions that gives a free fermion contribution to the propagator in the continuum limit. We have effectively *doubled* the number of fermions for each direction. In a d-dimensional lattice we end up with 2^d independent fermions, even though we initially started with just one.

There are many solutions to this fermion doubling problem [19, 20], but we will focus only on one in this manuscript: *the staggered fermions* [8, 19]. We have seen that these fictitious fermions come from the large momenta regions, where $q_\mu \sim \pi/a$. Brutally cutting out this large momenta regions spoils the completeness of the Fourier transform, so it is not a solution, but a smarter solution can give out the same effect. The idea is to spread the fermionic d.o.f over multiple lattice sites, reducing effectively the momenta space. For example, in two dimensions it would correspond to placing the *particles* on *even* sites and the *antiparticles* on *odd* sites. A site is considered even or odd when $(-1)^x = (-1)^{x_1 + \cdots + x_d} = +1$ or -1.

To obtain a staggered fermion, we define a new fermionic species $\chi(x)$ such that

$$\psi(x) = \prod_\mu (\gamma^\mu)^{n_\mu} \chi(x), \qquad (1.46)$$

where $x_\mu = an_\mu$. Now, if we want to express the discretized covariant derivative, the term $\gamma^\mu \psi(x + an_\mu)$ have two extra powers of γ^μ compared to $\overline{\psi}$. Since $(\gamma^\mu)^2 = \pm 1$, we have therefore

$$\overline{\psi}(x)\gamma^\mu\psi(x) = (-1)^{\eta_\mu(x)} \chi(x)^\dagger \chi(x + an_\mu), \qquad (1.47)$$

where $\eta_\mu(x)$ is some sign function depending on the site x. This function can be obtained from the commutation relations of the gamma matrices. In

particular, in two dimensions we have

$$\eta_1(x) = 1 \quad \text{and} \quad \eta_2(x) = (-1)^{n_1}, \tag{1.48}$$

while in four (Euclidean) dimension we have instead [20]

$$\eta_1(x) = 1, \quad \eta_2(x) = (-1)^{n_1}, \quad \eta_3(x) = (-1)^{n_1+n_2}, \quad \eta_4(x) = (-1)^{n_1+n_2+n_3}. \tag{1.49}$$

A similar reasoning can be applied to the mass term $m\overline{\psi}(x)\psi(c)$, where it becomes

$$m\overline{\psi}(x)\psi(x) = (-1)^{\eta(x)}\chi(x)^\dagger\chi(x), \tag{1.50}$$

for some sign function $\eta(x)$ that can be obtained from the commutation relations of the gamma functions.

chapter two

Quantum Simulation of Lattice Gauge Theories

2.1 Quantum simulation

Simulating quantum mechanics is a very challenging task [4, 21], especially if one is interested in many-body systems. The description of a state requires a large number of variables, for keeping track of all the quantum amplitudes, which grows exponentially with the system size. Hence, one would have an *exponential explosion* in terms of *classical* resources (like for example computer memory), which clearly is not suitable.

If simulating a quantum system is not a task for classical machines, then it should be a task for *quantum machines* [3, 4, 22–25]. The possibility of using quantum devices for simulating physics was first envisioned by Feynman in his seminal talk [4]. The main idea is to encode the d.o.f of an ideal mathematical model of a physical system into a controllable and reliable quantum system. In other words, a *quantum simulator* is an experimental device that mimics a simple model, or a family of simple models [23]. Using quantum physics for simulating quantum physics itself may seem like fighting fire with fire, but it can actually be a powerful strategy. We will no longer need an exponentially large number of variables for describing the target system, because the d.o.f of the target system and the simulator would be in a one-to-one correspondence. Therefore, the size of a quantum computer would only be proportional to the size of the quantum system it intends to simulate, *without* an exponential explosion in *quantum* resources.

In this perspective, one would need a specific quantum simulator for simulating a specific class of models. This is not necessarily true with a *quantum computer* [26–29]. The idea for such a device was put forward in [4, 21, 26] and it would act as a *universal quantum simulator*, a statement proved by Lloyd in [30]. One caveat of the universal simulator is the need of *digitalization* of the target system d.o.f and its evolution, because a quantum com-
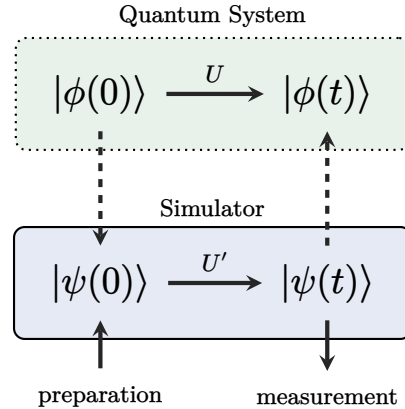
Figure 2.1. Schematic picture of a quantum simulator.

puter is essentially discrete, it is made up of *qubits*, so they are not suited for continuous-variable computation. This is in some sense analogous to classical computers, where real numbers have to be truncated and represented with a finite-size register of bits. On the other hand, a problem-specific simulator can potentially uses some kind of physical platform which allows for continuous d.o.f [24, 31].

In general, *Quantum Simulation (QS)* can be (loosely) defined as simulating a quantum system by quantum mechanical means, and by *quantum simulator* we mean a *controllable* quantum system used for simulating or emulating another quantum system. There are three paths that can be taken in this regard [22]:

- Digital Quantum Simulation

- Analog Quantum Simulation

- Quantum Information inspired algorithms for classical simulation

We will review each path in the following sections. Out of the three options, only the digital and analog QSs are actually based a some kind of quantum simulator. The last option uses methods inspired by quantum information for efficiently and faithfully approximates quantum states, which in turns makes classical simulations feasible for a large class of models.

2.1.1 Digital quantum simulations

The digital approach to QS employs the *circuit model* of quantum computation [27, 32]. This model is analogous to the circuit model of classical computation, where one works with *bits*, the smallest possible amount of information, an
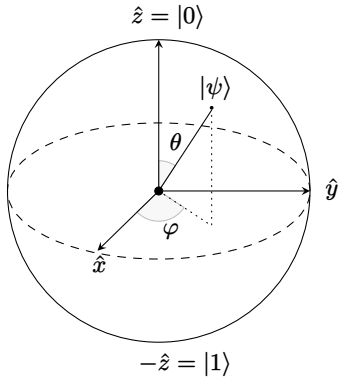
Figure 2.2. Picture of a Bloch sphere. A generic state of a qubit can be written as $|\psi\rangle = \cos\frac{\theta}{2}|0\rangle + e^{i\varphi}\sin\frac{\theta}{2}|1\rangle$, so it is fully described by a two angles θ and ϕ. For this reason, the Hilbert space of a qubit can be visualized as a two-dimensional sphere.

on–*or*–off state, and a minimal set of *logical operators* (like NOT, AND, OR, etc.). In quantum computation, the set up is the same but with some key differences: bits are substituted with *qubits* and the logical operators with *unitary operators*.

A bit can only have two values, either 0 or 1. In quantum computing these values are elevated to two *orthonormal* states $|0\rangle$ and $|1\rangle$. Therefore, the bits are substituted with *qubits*, which are two-levels quantum systems. A generic state of a qubit is $|\psi\rangle = \alpha|0\rangle + \beta|1\rangle$, with the normalization condition $\alpha^2 + \beta^2 = 1$, and the complex amplitudes α and β encodes the carried information. A visual representation of the Hilbert space of a qubit is given by the Bloch sphere (see Fig. 2.2). A set of qubits is called a *quantum register* and they encode the state of the quantum computational machine, the equivalent of the tape of a Turing machine.

The logical operators, or *gates*, of classical computation are single-bit or double-bit functions that have only a single-bit output. This makes classical computation *non-reversible*[1]. The idea behind quantum computing is to use the time-evolution of an ad-hoc quantum machine for performing computation. Time-evolution is a *unitary* process, which means that is reversible. Hence, the non-reversible model of classical computation is not suited for quantum computing. There is no one-to-one correspondence between the operations on a classical machine and those on a quantum machine. Logical operations on a quantum computer, also called *quantum gates*, have to implemented through *unitary operators* that act on the quantum register. A succession of logical operator, therefore, is equivalent to the product of these unitary operators. This makes the whole computation a unitary process, hence reversible.

It is known, in classical computing, that only a minimal set of logical gates

---

[1]There exist models of classical computation that are reversible, see [33], which will not be discussed here and are not very common in every-day applications. In [33] a universal *three-bits* gate is introduced that allows for reversible computation.

$$H \quad \frac{1}{\sqrt{2}} \begin{pmatrix} 1 & 1 \\ 1 & -1 \end{pmatrix}$$

$$R_k \quad \begin{pmatrix} 1 & 0 \\ 0 & e^{i2\pi/2^k} \end{pmatrix}$$

$$\begin{pmatrix} 1 & 0 & 0 & 0 \\ 0 & 1 & 0 & 0 \\ 0 & 0 & 0 & 1 \\ 0 & 0 & 1 & 0 \end{pmatrix}$$

Figure 2.3. Examples of quantum gates. From top to bottom: *(i)* Hadamard gate H; *(ii)* Phase gate R_k; *(iii)* `CNOT` (controlled `NOT`) gate.

are actually needed in order to perform any computation. For example, with a `NOT` gate and a `AND` gate is possible to implement every other possible logical function (actually only the `NAND` gate is necessary). A similar result is true also for quantum computing [34]. One only needs a minimal set of quantum gates in order to implement any unitary operators with arbitrary precision. Similar to the classical case, for quantum computing we only need single-qubit and two-qubits gates. The two-qubits gates have an important role, because they allow to introduce *entanglement*, which is the secret ingredient that makes quantum computing distinct from classical computing. This minimal set usually entails a set of single-qubit and one two-qubits entangling gate (like the `CNOT` gate). In Fig. 2.3 some example of quantum gates are shown, while in Fig. 2.4 an example of a quantum circuit can be found.

Even though it has been proven that "anything" can be simulated on a quantum computer [30], not all unitary operations can be simulated *efficiently*. The time-evolution of the target quantum system requires *digitalization*, which means that it has to be decomposed in smaller steps in order to be encodable as a sequence of quantum gates. This is possible to an arbitrary precision thanks to the Trotter-Suzuki product formula for the exponentiation of complex matrices:

$$e^{A+B} = \lim_{n \to \infty} \left(e^{A/n} e^{B/n} \right)^n. \tag{2.1}$$

In most physically interesting case, the Hamiltonian is a sum of non-commuting terms:

$$H = \sum_l H_l,$$

where $[H_l, H_{l'}] \neq 0$ for $l \neq l'$. In the case of a time-independent Hamiltonian, the time-evolution operator is given by

$$U(t) = e^{-it \sum_l H_l} \quad \text{such that} \quad U(t) \ket{\psi(0)} = \ket{\psi(t)}. \tag{2.2}$$

30

In order to implement (2.2) on a quantum operator, the time-evolution has to be divided in N steps of length Δt, such that $t = N\Delta t$ and $U(t) \simeq (U(\Delta t))^N$. For each single time step we can apply the first-order Trotter-Suzuki formula [27, 35] for the time-evolution operator:

$$U(\Delta t) = e^{-i\Delta t \sum_l H_l} = \prod_l e^{-i\Delta t H_l} + O(\Delta t^2). \qquad (2.3)$$

The drawback of Trotterization is that high accuracy comes at the cost of very small Δt and therefore a very large number of quantum gates. The scheme used in (2.3) has some shortcomings, that can be improved with higher order decompositions that will necessarily introduce more complexities in the quantum circuit. Moreover, some other types of methods have to be used in the case of time-dependent Hamiltonians [36].

It should be stressed that we are still far from perfect digital quantum computation. A typical quantum computer is affected by noise due to its interaction with the environment. The effect of noise can corrupt the state of the quantum register, by flipping or dephasing the qubits for example. Furthermore, interaction with an external environment will necessarily lead to *decoherence* where all the "quantumness" of the system is lost [37–39].

It becomes clear that error correction is a necessity for *fault-tolerant quantum computing* [40, 41] but it can greatly increase the number of qubits needed for useful computations. Indeed, it is said we are currently living in the *noisy intermediate-scale quantum* (NISQ) era of quantum computing [42]. The term refers to moderately sized quantum computers (around 50–100 qubits) whose gates are still affected by noise but are not large enough to fully implement error correction.

The typical setup for a digital simulation consists of three steps:

Initial-state preparation. The quantum register is prepared in the initial state $|\psi(0)\rangle$. This step can be difficult by itself, and it is not always guaranteed that an efficient algorithm may exist.

Unitary evolution. The circuit has to reproduce or simulate the action of a unitary operator U. This unitary operator is usually the time-evolution operator of the target system, which has to be decomposed in a sequence of smaller operation through trotterization, as explained before.

Final measurement. After obtaining the wanted state $|\psi(t)\rangle = U |\psi(0)\rangle$, a *measurement* is needed in order to extract relevant physical information. Instead of capturing the whole wave function $|\psi(t)\rangle$, with, for example, quantum tomography, one may proceed with the direct estimation of
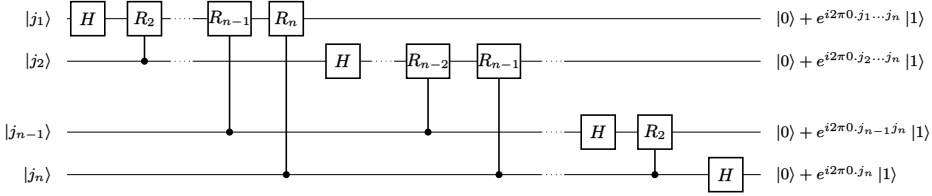
Figure 2.4. Example of a quantum circuit. In particular this circuit executes the quantum Fourier transform [27]. It uses some of the gates showed in Fig. 2.3.

certain physical quantities, such as correlation functions or spectra of operators.

2.1.2 Analog quantum simulations

Analog QS is another type of approach to QS, where one quantum system (the simulator) mimics or emulate another (the target) [25, 43–49]. This approach is not based on building a universal machine, like a quantum computer, that can emulate any other system. Instead, it focuses on recreating the features, or a subset of relevant features, of a chosen class of models in order to compute some physically relevant quantities.

Analog QS follows the idea of *analog computation*, where an experimental device is conceived for executing a specific algorithm, meaning that it is a specialized machine with some degree of controllability. Analog computation is not a new idea, rather it is the oldest type of computing devised by mankind, and analog machines are the earliest types of computers to ever be used [24]. Some historical examples can be the astrolabe for plotting the heavens (around 200 BC), the Antikythera mechanism for predicting astronomical routes (around 150 BC), or the mechanical differential analyser for integrating differential equations (around 1876) [50].

In an analog simulation, the Hamiltonian of the target H^{targ}, is directly mapped onto the Hamiltonian of the simulator, H^{sim}:

$$H^{\text{targ}} \longleftrightarrow H^{\text{sim}}.$$

Obviously, this is possible only if there is a mapping between the system and the simulator. If $|\phi(0)\rangle$ is the initial state of the target, then it can be mapped to the initial state $|\psi(0)\rangle$ of the simulator, via an operator $\mathcal{O}$, i.e. $|\psi(0)\rangle = \mathcal{O}|\phi(0)\rangle$. Next, the simulator would perform the desired time evolution $U(t)|\psi(0)\rangle = |\psi(t)\rangle$. The result then can be mapped back to a state of the target system via $\mathcal{O}^{-1}$, i.e. $\mathcal{O}^{-1}|\psi(t)\rangle = |\phi(t)\rangle$. In this case the Hamiltonians would be related by the mapping $\mathcal{O}$, $H^{\text{sim}} = \mathcal{O}H^{\text{targ}}\mathcal{O}^{-1}$. Note that the simulator may only partly reproduce the dynamics of the target, or

simulate some effective description of it. The choice of the mapping depends on what needs to be simulated and on the capabilities of the simulator [22]. Finding the mapping in an analog QS might look, at first, simpler than finding the most efficient gate decomposition of a Hamiltonian, but it is not always true and there are no recipes ready for constructing these mappings in a general case.

Initial state preparation is not such a topic in analog QS, as it is in digital QS. This is based on the assumption that the target system and the simulator are presumed to be very similar. It is expected that the preparation of the initial state can occur naturally in processes mimicking the natural relaxation of the simulated system to an equilibrium state. Moreover, analog QS has the natural advantage that physical quantities can be measured directly, without the need of special schemes like in digital QS, which can yield direct information about the target system [23].

One important advantage of analog QS is that fact that it does not require a fully fledged quantum computer. In fact, the simulator does not even need to be a quantum computer at all. This possibly makes analog QS much more achievable from the experimental point of view in the short term. Many different platforms are already available (see also Fig. 2.5):

- ultracold atoms and molecules [47, 49, 51];

- trapped ions [46];

- photons [45];

- polaritons [52];

- nuclear magnetic resonance systems [53];

- artificial lattices [54];

- superconducting qubits [48].

For more details see [22, 23, 25] and references therein.

Analog QS can be useful even in the presence of errors, up to a certain tolerance level, because it would still be able to give qualitative answers. Suppose one is interested in knowing if whether a certain set of physical conditions leads to a given quantum phase transition. Even without the full quantitative description or the perfect tuning of the control parameters, an analog simulator would, potentially, still be able to show the presence or not of a phase transition. Furthermore, due to the analog nature of these simulators, standard error correction and fault tolerance are not allowed [23], while the
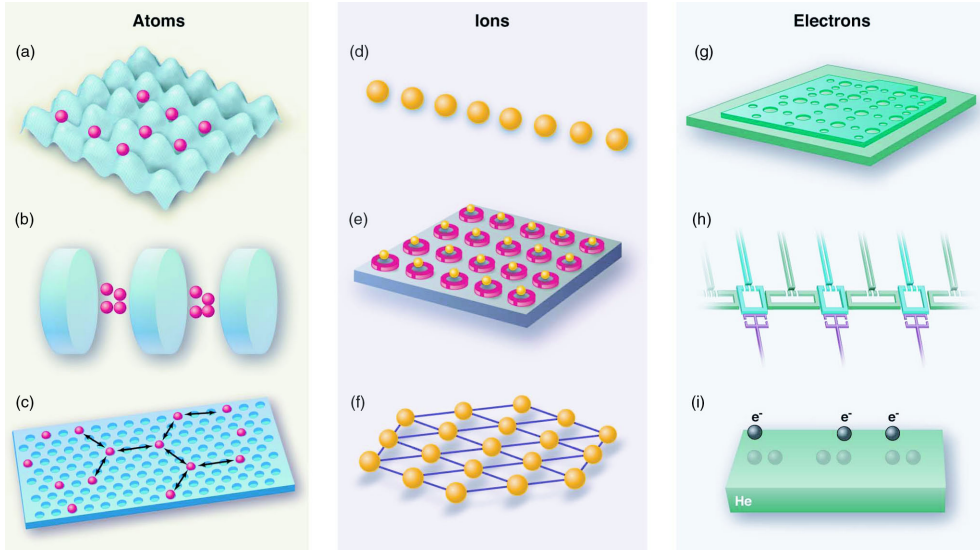
Figure 2.5. Picture from [25]. Examples of analog quantum simulators: *(a)* atoms in optical lattices, *(b)* one-dimensional or *(c)* two-dimensional arrays of cavities; *(d)* ions in linear chains, *(e)* two-dimensional arrays of planar traps, or *(f)* two-dimensional Coulomb crystal; *(g)* electrons in quantum dot arrays created by a mesh gate, *(h)* in arrays of superconducting circuits, or *(i)* trapped on the surface of liquid helium. For more details see [22, 25].

level of controllability depends on the type of platform used. For example, in the case of ultracold atoms in optical lattices the typical control parameters involve lattice parameters (laser wavelength, geometry, dimensionality, etc...), temperature and other thermodynamical control parameters, as well as atomic interaction strength [49].

2.1.3 Quantum-inspired algorithms

Traditionally, classical simulations of quantum systems have been done using one of the following methods [23]:

- Quantum Monte Carlo (MC).

- Systematic perturbation theory.

- Exact Diagonalization (ED).

- Density Matrix Renormalization Group (DMRG).

Each of these methods has its problems. Quantum MC methods can work with large systems but fails for fermionic systems due to the sign problem [55, 56]. Perturbation theory is applicable only when there is a small coupling constant, so it fails for strongly interacting systems. ED works only for rather small systems [55, 56]. DMRG is a variational method that has been proven

34

to be fully functional for strongly interacting systems [57–59]. Additionally, it has been proven to be of great success for one-dimensional systems, while for two-dimensional models it can be quite limited [60].

Thanks to the development of quantum information, new *classical algorithms* have been put forward for the simulation of quantum many-body systems, that much more exploit the quantum nature of these systems. One of the most groundbreaking example of quantum-inspired algorithms is the use of *Tensor Networks (TNs)* [61–66]. They make it possible to "compress" the information about a many-body wave function by expressing it as a *contraction* of a network of tensors (as suggested by the name). Additionally, TN also helped shining a light of the effectiveness of DMRG.

In a TN, to each physical site there is associate a tensor with a certain number of indices (or legs). One of these indices is called the *physical index* of the tensors, which runs over the basis of the local Hilbert space. The other indices are *auxiliary indices*, their dimension is governed by a parameter χ called the *bond dimension* and are "connected" to other sites. Roughly speaking, these auxiliary indices encodes the entanglement information between the connected sites.

To make it more clear, consider a one-dimensional open chain (with L sites), where each site has a d-dimensional local Hilbert space with basis $\{|i\rangle, i = 1, \ldots, d\}$. A general global state $|\Psi\rangle$ of the whole chain can be written as

$$|\Psi\rangle = \sum_{i_1,\ldots,i_L} C_{i_1,\ldots,i_L} |i_1 \cdots i_L\rangle. \tag{2.4}$$

The whole state is encoded in the tensor $C_{i_1,\ldots,i_L}$ of order L, which has a total of d^L entries. The indices i_n are physical indices of the tensor. Through Singular Value Decomposition, it is possible to factorize the tensor $C_{i_1,\ldots,i_L}$ into L tensors A^{i_n}, one for each site [57]:

$$C_{i_1,\ldots,i_L} = \sum_{\alpha_1,\ldots,\alpha_{L-1}} A^{i_1}_{\alpha_1} A^{i_2}_{\alpha_1,\alpha_2} \cdots A^{i_{L-1}}_{\alpha_{L-2},\alpha_{L-1}} A^{i_L}_{\alpha_{L-1}}. \tag{2.5}$$

We have introduced a set of indices α_n, the auxiliary indices, which are contracted (i.e. summed over). The example above is basically the essence of a *Matrix Product States (MPSs)*, a typical example of TN in one dimension.

The order of the indices α_n depends on the number of Schmidt eigenvalues of the bipartition that separates the first n sites from the rest. In other words, it depends on the entanglement entropy between the first n sites of the chain and the rest. Not all the Schmidt eigenvalues are of the same importance, therefore each tensor A^{i_n} can be optimized by discarding the Schmidt eigenvalues that are under a certain threshold. In this way we *compress* the

wave-function, by preserving the information that best represent the entanglement in the state. The order of the indices α_n after the optimization is the *bond-dimension*, and it is this parameter that fine tunes the amount of entanglement. Notice that with χ fixed, the right hand side of (2.5) has only around $Ld\chi^2$ entries, which scales better that d^L. If the system has a finite amount of entanglement, then there is an optimal value for the bond dimension χ. This would mean that we do not really need all the d^L entries of $C_{i_1,...,i_L}$. Only the $Ld\chi^2$ entries of the right hand side of (2.5) are sufficient to *faithfully* represent $|\Psi\rangle$.
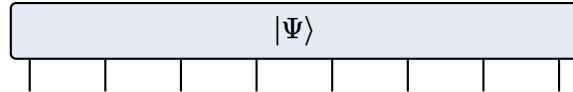
For a large class of physical models, the ground state is gapped and has a finite correlation length, which leads to a finite amount of entanglement. This fact is expressed by the so-called *area law*, where the entanglement between two partitions of the system grows with size of the boundary, the area between the two partitions, and not with the volume of the partition itself [67–71]. The main advantage of TN methods is their ability to capture this area law, which lead to an efficient computation of the ground states of these models.

TNs were first inspired by the ground state of the AKLT model [72], and from there different types TNs were developed. The paradigmatic example of TNs are the MPSs in one-dimension [57, 65], and the *Projected Entangled Pair States (PEPSs)* in two dimensions [62, 73]. Some other variants of TNs exists, like *Tree TNs* [74, 75] or *Multi-scale Entanglement Renormalization Ansatz (MERA)* [76–78]. An example of MPS, PEPS, and Tree TN are shown in Fig. 2.6.
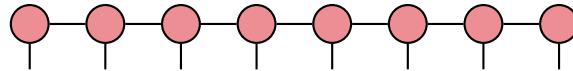
TN methods can still have some shortcomings. They work especially well for one-dimensional gapped systems, but it can become quite challenging to make them work efficiently in gapless systems or in higher dimensions. When a system is in a gapless phase, the correlation length diverges, which leads to drastic change in the entanglement structure. This is best captured by comparing the behaviour of entanglement entropy in massive (gapped) and massless (critical) one-dimensional models [68, 69]. In a massive theory the entanglement entropy is directly proportional to number of boundary points, regardless of the subsystem size (as long as it is larger then the correlation length). On the other hand, in a massless and critical phase the entanglement entropy has a direct dependence on the size of the subsystem.

Therefore, in a critical phases the bond-dimension would, potentially, need to increase with the system size in order to effectively capture the ground-state wave-function. Another shortcoming is the computational complexities of tensor contractions in dimensions higher than one. This is because the number of legs of a tensor increases with the dimensionality of the system, which lead to higher computational costs when performing calculations [61].
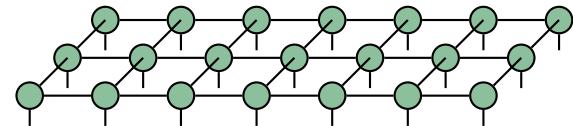
(a) Quantum state

$|\Psi\rangle$

(b) MPS

(c) PEPS

(d) TTN
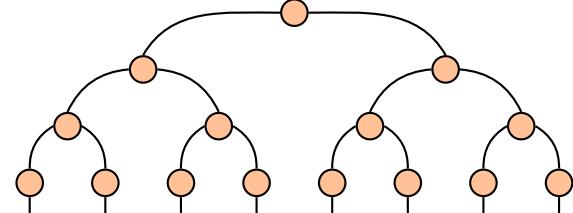
Figure 2.6. Examples of TNs. From top to bottom: *(a)* a generic quantum state can be represented as a unique tensor, with one index (or leg) for each site. *(b)* a MPS in one dimension; each site have one tensor with one physical leg and two auxiliary legs that connects with the neighbouring sites (only one leg at the boundary). *(c)* a PEPS in two dimensions on a square lattice; each site has an auxiliary legs going in each possible direction on the lattice. *(d)* a Tree TN state in one-dimension; each site has one tensor with one physical leg, but now these tensors are contracted in hierarchical structure, with intermediate tensors, that do not reflect the lattice geometry.

2.2   Simulating gauge theories

LGTs are arguably one of the most computationally intensive quantum many-body problem, due to the large numbers of d.o.f and, especially, the local gauge constraints. Typically, LGT computations uses the Quantum MC method in the Euclidean path integral formulation, due to the natural presence of a Boltzmann factor in the action, that act as a statistical weight. MC methods applied to QCD, which from here it will be referred as Lattice QCD, already yielded a number of very interesting results, that includes: calculations of fundamental properties of QCD (such as quark masses and the running coupling); masses of QCD bound states (such as protons, neutron, pions, etc.); structure of hadrons (for example how quarks and gluons interact with one another inside the proton); flavour physics (leading to constraints on the CKM matrix elements) and much more [79, 80].

However, MC methods suffer from some issues, mostly due to the Euclidean space-time formulation and the sign problem. The Euclidean space-time, due to its imaginary time, makes it impossible to compute observables that explicitly depend on real time. They are accessible only in Minkowski space-time, where time has a different signature. An example of these observables are light-cone correlations, in terms of which partonic properties are formulated and expressed [81]. As already mentioned, another severe shortcoming of Lattice QCD is posed by the sign problem, which has already been briefly discussed in Sec. 1.1.3. In summary, when chemical potential is introduced, the Boltzmann weight acquire a complex phase and can no longer be interpreted as a statistical weight. It should be noted that the sign problem in Lattice QCD is not strictly of fermionic origin, as it usually happens in quantum many-body physics, but is more fundamental and is due to the signature of space-time [80].

Furthermore, it has been proven that the sign problem is NP–hard[2] for the three-dimensional Ising spin glass [83], so, most probably, is also NP–hard for Lattice QCD. NP–hardness should not discourage a scientist from trying to solve a problem, rather it is what makes a problem interesting. NP–hardness only prevents a *generic* and *efficient* solution from existing (if NP $\neq$ P is in fact true). However, this does not mean that there are not ways to alleviate the hardness of a problem, in particular if one uses some physical insight.

---

[2]NP–hard problems are, informally, at least as hard as the hardest problem in NP. In very layman terms, NP is the class of problems that are *verifiable in polynomial time*, and is set against the P class where the problems are *solvable in polynomial time* [82]. If it is true that NP $\neq$ P, then NP problems would not admit an *efficient* algorithms for finding solution, "efficient" would mean in polynomial time. Although it is widely believed that NP $\neq$ P, this conjecture it is still yet not proven and it is one of the Millennium Prize Problems.

One way where physical insight has been used for classical simulation is represented by TNs methods, which completely avoids the sign problem for LGTs. They achieve such a result by not relying on MC methods and importance sampling, but by working directly in the Hilbert space of the model under investigation. As with every computational technique, it still has its shortcomings (see the discussion in Sec. 2.1.3).

On the other hand, one can try to avoid any computational complexity by means of QS, either digital or analog. Recently, different approaches have been proposed for the QS of LGTs, from different communities [1, 80, 84].

For analog QS, the options ranges from ultracold atoms in optical lattices [85–89], trapped ions [90, 91], or superconducting qubits [92–94]. The proposals have addressed LGTs of at different levels (Abelian or non-Abelian, with or without dynamical matter, etc.) For a complete review, see [1, 80, 84].

Regarding digital QS of LGT, some kind of *digitalization* of the fields is necessary. By digitalization, we mean the task of formulating, representing, and encoding QFT in ways that are useful for computations. The path-integral formulation, presented in Sec. 1.2, is the most straightforward digitalization scheme for non-perturbative field theory but it is not feasible for quantum computing. It relies on resources far beyond near-term quantum computers. For example, in gauge theories with Lie groups, like QCD or QED, the d.o.f lives on a compact manifold. This means that there an infinite number of states for each point in space-time (or lattice). In other terms, the bosons that represent the gauge fields have an infinite-dimensional Hilbert space. This is obviously not feasible on quantum computer with a finite quantum register, for the same reason that real numbers cannot be represented on a classical computers. Hence, some kind of truncation scheme is necessary. Additionally, in the path-integral formulation of LGT, fermionic fields are integrated out, leaving a non-local action. A direct application of this procedure to quantum computers would require a high connectivity between qubits[3], which again is not feasible for near-term quantum computers.

The starting point for the digital simulation of LGTs is the Hamiltonian formulation. This has been worked out by Kogut and Susskind in their seminal paper [8], but it has been done with compact Lie groups in mind, like $SU(N)$. So, some extra steps are necessary in order to have a formulation of LGTs that are implementable on a quantum computer. Several proposal for digitized LGTs have been put out [95–104] and different paths are possible. In the following list we highlight the main approaches for digitalized LGTs:

---

[3]One could work around this problem with suitable chains of 2-qubit gates.

Quantum Link Models   Essentially, this proposal digitizes U(N) and SU(N) gauge fields with spin operators in extra dimensions, while preserving gauge symmetry [102, 105]. This makes them suitable for digital simulations, because spins have finite d.o.f, while the continuum limit is reached with dimensional reduction techniques.

Dual variables   Many gauge theories have compact d.o.f. This compactness means that the lattice action admits a (possibly infinite) character expansion in the irreducible representations of the gauge group. These irreducible representations are the dual variables [106, 107]. The discreteness of these dual variables makes them adapt for QS. Then, the irreducible representations can be further truncated in order to have a finite number of d.o.f.

Finite subgroups   The simplest way to approximate a continuous group would be by substituting it with one of its discrete subgroup. This reduces the number of d.o.f to a finite number, one for each element of the subgroup. This can greatly simplifies theoretical analysis [108] and the development of algorithms [104]. On the other hand, it introduces issues when considering the continuum limit, due to a "freezing transition", that can be mitigated with the addition of some extra terms [109, 110].

In the works presented in this manuscript [5, 6] we chose to focus on finite groups, because they allow a formulation of LGTs where the unitarity of the gauge fields is preserved[4]. With digital QS as the main goal, unitarity is particularly convenient. In quantum computation only unitary operations are directly implementable as sequence of quantum gates. Hence, when a basis is fixed, the action of both the gauge fields and the electric fields will be translatable in terms of sequence of quantum gates. This greatly simplifies the development of quantum algorithms for LGTs.

However, this comes with a cost. The need to preserve unitarity may require the modification of the algebraic relations between the gauge fields and its conjugates. This is extremely relevant if one cares about the continuum limit, which is an important topic for someone that is interested in simulations of QCD for example. But if one is just interested in the theoretical exploration of finite group gauge theories, then this issue can be put aside, which is what we intend to do.

---

[4]To be more specific, the parallel transporters associated with the gauge fields and their conjugate operators are unitary.

Dualities in Abelian Models

In this chapter we present the findings of [5], where a duality transformation from the gauge-invariant subspace of a $\mathbb{Z}_N$ LGT on a ladder geometry to an N-clock model on a single chain. The main feature of this mapping is the emergence of a longitudinal field in the clock model, whose value depends on the super-selection sector of the gauge model. In order to investigate this and see if confined phases might emerge, we perform a numerical analysis for $N = 2, 3$, and 4, using Exact Diagonalization.

3.1 Toric Code and its features

The Toric Code (TC) is two-dimensional model of spin-$\frac{1}{2}$ d.o.f, which can be regarded as an example of a pure $\mathbb{Z}_2$ LGT. We consider the model on a $L \times L$ square lattice $\mathbb{L}$ with periodic boundary conditions. The d.o.f are defined on the links ℓ of the lattice and the link Hilbert space is $\mathbb{C}^2$. The main operators used for this model are the Pauli matrices

$$X_\ell = \begin{pmatrix} 0 & 1 \\ 1 & 0 \end{pmatrix} \quad \text{and} \quad Z_\ell = \begin{pmatrix} 1 & 0 \\ 0 & -1 \end{pmatrix}, \tag{3.1}$$

which here have been written in the computational basis $\{|0\rangle, |1\rangle\}$, where the Z-matrix is diagonal. It is important to note that these matrices X and Z *anticommutes* on the same link.

$$\{X_\ell, Z_\ell\} = 0, \tag{3.2}$$

while they commute with operators of other links.

The main *local* operators that enters the Hamiltonian are the *star operator* and *plaquette operator* of the lattice. The term *star* refers to the links attached to a common vertex v, while by *plaquette p* we mean the links around a face of the lattice. A *star operator* and a *plaquette operator* are respectively defined as

$$A_v = \prod_{\ell \in v} Z_\ell, \qquad B_p = \prod_{\ell \in p} X_\ell. \tag{3.3}$$
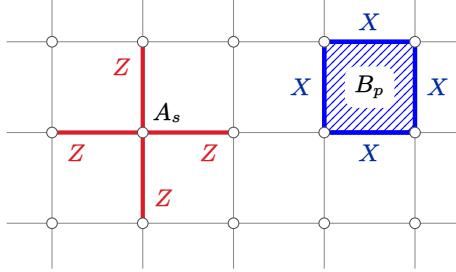
Figure 3.1. Graphical representation of the vertex operator A_v and plaquette operator B_p, defined in (3.3).

where v is a vertex and p a plaquette (see Fig. 3.1). One can easily see that

$$[A_v, A_{v'}] = 0 \quad \text{and} \quad [B_p, B_{p'}] = 0 \tag{3.4}$$

for all vertices v and v', and all plaquettes p and p'. But it is also true that

$$[A_v, B_p] = 0 \tag{3.5}$$

for all v and p. This is because a star and a plaquette share zero or two links, so the signs factors from the anticommutation of X and Z cancel out. The eigenvalues of the Pauli matrices are just ± 1, so the same holds true for A_s and B_p. Moreover, like the Pauli matrices, also $A_s^2 = \mathbb{1}$ and $B_p^2 = \mathbb{1}$.

Now, given the operators in (3.3), we can write down the Hamiltonian of the TC:

$$H^{\mathrm{TC}} = -\sum_v A_v - \sum_p B_p \tag{3.6}$$

which is *exactly solvable*, due to (3.4) and (3.5).

3.1.1 Topological Ground states

Given the commutation relations of the A_v and B_p operators in (3.4) and (3.5), one can find the ground state $|\Omega\rangle$ by simply imposing the constraints

$$A_v |\Omega\rangle = |\Omega\rangle \quad \text{and} \quad B_p |\Omega\rangle = |\Omega\rangle, \qquad \forall v, p. \tag{3.7}$$

From these constraints one can explicitly construct a ground state for the TC in the following way. Working in the Z-basis, we can start from

$$|0\rangle_{\mathrm{TC}} = \bigotimes_{\ell \in \mathbb{L}} |0\rangle_\ell, \tag{3.8}$$

which is the state where every link is in the $|0\rangle$, where $Z |0\rangle = |0\rangle$. This state obviously satisfy the first condition in (3.7).

Now, regarding the B_p's operators, consider a single plaquette in the state $|0\rangle_p$ where every link is in the $|0\rangle$ state. The action of B_p flips the state of

every link, from $|0\rangle$ to $|1\rangle$, obtaining $|1\rangle_p$. Therefore, a plaquette is in an eigenstate of B_p if is in an equal superposition of $|0\rangle_p$ and $|1\rangle_p$. Knowing this, it is straightforward to see that the operator $(\mathbb{1} + B_p)/\sqrt{2}$ generates an eigenstate of B_p from $|0\rangle_p$. In fact, a simple calculation

$$B_p \frac{\mathbb{1} + B_p}{\sqrt{2}} |0\rangle_p = \frac{B_p + \mathbb{1}}{\sqrt{2}} |0\rangle_p \tag{3.9}$$

shows that we obtain an eigenstate of B_p with eigenvalue $+1$, due to $B_p^2 = \mathbb{1}$.

Therefore, we can obtain a ground state for the TC Hamiltonian

$$|\Omega\rangle = \prod_p \frac{\mathbb{1} + B_p}{\sqrt{2}} |0\rangle_{\text{TC}}. \tag{3.10}$$

More generally, we can define the space of ground states

$$\mathcal{G} = \{|\Omega\rangle : A_s |\Omega\rangle = |\Omega\rangle, \quad B_p |\Omega\rangle = |\Omega\rangle \quad \forall s, p\}, \tag{3.11}$$

whose content *depends on the topology of the lattice*. For example, we will show that with *periodic boundary conditions* then there are *four degenerate ground states*.

Consider a lattice $\mathbb{L}$ of size $L \times L$ with periodic boundary conditions in both directions, i.e. a torus. From (3.7), we have $2L^2$ constraints. These are not all independent because if we multiply them all, we obtain

$$\prod_v A_v = \mathbb{1} \quad \text{and} \quad \prod_p B_p = \mathbb{1}, \tag{3.12}$$

which actually means that there are $2L^2 - 2$ independent conditions. The total Hilbert space has dimension 2^{2L^2}. Combined with $2L^2 - 2$ independent conditions we obtain $2^{2L^2 - 2L^2 + 2} = 4$ independent states. Therefore, $\dim \mathcal{G} = 4$ because we have four degenerate distinct ground states. These are eigenstates of all A_v and B_p, with all the same eigenvalues. Any other that commutes with the Hamiltonian is given by a product of A_v and B_p, so it cannot distinguish the different ground states.

The only way to distinguish these ground states is through *non-local operators* that commute with the Hamiltonian in (3.6). Non-local in this instance means not expressible as a product or sum of vertex and plaquette operators. But first let look more closely at *local operators*.

Consider any region $\mathcal{R}$ on the lattice $\mathbb{L}$. Without loss of generality, let $\mathcal{R}$ be a connected region, which means it is just a set of jointed plaquettes. On this region $\mathcal{R}$ we can define a local operator W as a product of B_p operators:

$$W = \prod_{p \in \mathcal{R}} B_p. \tag{3.13}$$

This operator commutes will the terms of the Hamiltonian (3.6). Due to $X_\ell^2 = \mathbb{1}$, the previous equation can be rewritten as

$$W = \prod_{\ell \in \partial \mathcal{R}} X_\ell. \tag{3.14}$$

In other words, W is equivalent to the product of X's along the closed curve given by the boundary $\partial \mathcal{R}$ of $\mathcal{R}$. In fact, the B_p themselves are defined as product of X's along a closed curve, the plaquette. In a sense, they are all *string operators* on closed curves.

The same argument can be repeated for A_v with the minor caveat that the dual lattice have to considered. In the dual lattice $\mathbb{L}^*$, to each plaquette p of $\mathbb{L}$ corresponds a vertex v^* on the dual lattice. Then, to each link ℓ in $\mathbb{L}$ corresponds a link ℓ^* in $\mathbb{L}^*$ in the perpendicular direction. In this way, a star becomes a plaquette in the dual lattice and we can repeat the same argument. Consider a region $\mathcal{R}^*$ a local operator S such that

$$S = \prod_{v \in \mathcal{R}^*} A_v, \tag{3.15}$$

and, due to $Z_\ell^2 = \mathbb{1}$, this is equal to

$$S = \prod_{\ell \in \partial \mathcal{R}^*} Z_\ell. \tag{3.16}$$

The local operator S is a string of Z's operators along the closed curve given by the boundary $\partial \mathcal{R}$ in $\mathbb{L}^*$. The same can be said for A_v, it is a string operator around the smallest possible curve in $\mathbb{L}^*$. We can conclude that all the local operators that commutes with Hamiltonian are just string operators over closed curve in either $\mathbb{L}$ or $\mathbb{L}^*$. But, these operators have all a common feature, they are defined on *contractible* curves. Meaning that they can be "continuously" deformed to a single point.

String operators on non-contractible curves, either on the direct or dual lattice, are the non-local operators we have been looking for distinguish the states in $\mathcal{G}$. Consider two non-contractible loops $\mathcal{L}_1$ and $\mathcal{L}_2$ on $\mathbb{L}$ along the $\hat{1}$ and $\hat{2}$ direction respectively, like in Fig. 3.2. On these paths we can define the string operators $\overline{W}_1$ and $\overline{W}_2$ as

$$\overline{W}_1 = \prod_{\ell \in \mathcal{L}_1} X_\ell, \qquad \overline{W}_2 = \prod_{\ell \in \mathcal{L}_2} X_\ell. \tag{3.17}$$

It can be proved that they commute with all the terms of the Hamiltonian, even though they cannot be expressed as a product of them. The same can
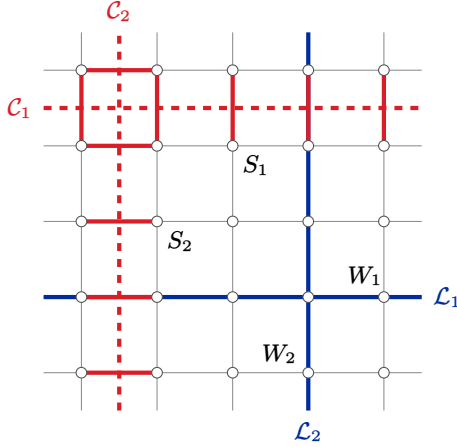
Figure 3.2. Graphical representation of the different types of non-local operators. On the non-contractible loops $\mathcal{L}_1$ and $\mathcal{L}_2$ (in the direct lattice) we have defined $\overline{W}_1$ and $\overline{W}_2$ (see (3.17)). While on the non-contractible cuts $\mathcal{C}_1$ and $\mathcal{C}_2$ (in the dual lattice) we have the operators $\overline{S}_1$ and $\overline{S}_2$.

be repeated on the dual lattice $\mathbb{L}^*$, by considering two non-contractible cuts $\mathcal{C}_1$ and $\mathcal{C}_2$ and defining $\overline{S}_1$ and $\overline{S}_2$ as

$$\overline{S}_1 = \prod_{\ell \in \mathcal{C}_1} Z_\ell, \qquad \overline{S}_2 = \prod_{\ell \in \mathcal{C}_2} Z_\ell. \tag{3.18}$$

Likewise, the operators in (3.18) commutes with all the vertex and plaquettes operators but they do not commute with the operators in (3.17).

In fact, (3.17) and (3.18) anticommutes,

$$\{\overline{W}_1, \overline{S}_2\} = 0 \quad \text{and} \quad \{\overline{W}_2, \overline{S}_1\} = 0, \tag{3.19}$$

while

$$\left[\overline{W}_1, \overline{W}_2\right] = 0 \quad \text{and} \quad \left[\overline{S}_1, \overline{S}_2\right] = 0. \tag{3.20}$$

These relations can be thought as the same commutation relations of the X and Z gates of two qubits.

Therefore, the TC (on a torus) has a protected subspace $\mathcal{G}$, see (3.11), that behaves like the Hilbert space of two qubits and the operators (3.17) and (3.18) acts like unitary gates on this space. Unfortunately, we cannot do quantum computation with these topological qubits because there is no entangling gates. Nonetheless they can be used for storing information in a fault-tolerant way, because in order to flip a topological qubit you would need to act with a non-local operator that involves a large amount of links.

3.1.2 Toric Code as a $\mathbb{Z}_2$ LGT

The TC was formulated as a type of error-correcting code for quantum computing, but it can be reinterpreted as a pure $\mathbb{Z}_2$ LGT. This is a type of LGT where we allow only two possible states for the gauge field.
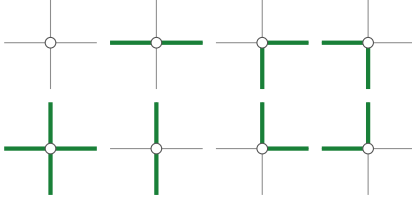
Figure 3.3. Gauge-invariant vertex states for the $\mathbb{Z}_2$ LGT. Green lines represent the $|1\rangle$ link state.

On a single link ℓ, we consider the X_ℓ as the gauge field operator, while Z_ℓ the electric field operator. In this way, we can automatically see that the term B_p is the magnetic energy because it has the same form of single-plaquette WL. Furthermore, the vertex operator A_v can be read as a gauge transformation on the vertex v, because the Z's operators flips the states in the X-basis, which would corresponds to gauge field configurations.

Now that we know the form of gauge transformations, we call a state *physical* or *gauge-invariant* if

$$A_v |\phi\rangle = |\phi\rangle \quad \forall v \in \mathbb{L}, \tag{3.21}$$

which leads to the definition of the *physical Hilbert space*:

$$\mathcal{H}_{\text{phys}} = \{|\phi\rangle \text{ s.t. } A_v |\phi\rangle = |\phi\rangle \quad \forall v \in \mathbb{L}\}. \tag{3.22}$$

For greater clarity, lets work in the *electric basis*, which is just the Z-basis where the electric field is diagonal. The electric field operator Z has eigenvalue $+1$ and -1, corresponding respectively to the states $|0\rangle$ and $|1\rangle$. In order to meet the condition in (3.21), a vertex configuration must have an even number of links in the $|1\rangle$ state (examples can be seen in Fig. 3.3).

We have already argued that the B_p's give the magnetic energy, and obviously the Z's give the electric energy. Hence, the pure gauge theory Hamiltonian is just

$$H^{\mathbb{Z}_2} = -\sum_p B_p - \lambda \sum_\ell Z_\ell, \tag{3.23}$$

where λ is a generic coupling that tunes the strength of the electric field with respect to the magnetic field. Notice that we no longer have a dynamical vertex term in (3.23) because we have imposed the condition (3.21) on the physical states.

In order to better explain the different phases we can have by varying the coupling λ in (3.23), we want to have a closer look at the physical states. We have already seen that the condition (3.21) constraints the types of vertex configurations. From the allowed configuration, we can see that the only possible lattice states (in the electric basis) are states made of *closed electric loops*. An example of such state can be seen in Fig. 3.4.
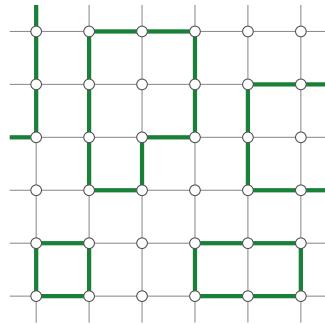
Figure 3.4. Physical states in the $\mathbb{Z}_2$ LGT are made of closed electric loops.

For $\lambda = 0$ we recover the TC and its ground state can be reinterpreted as an equal superposition of all the possible configuration of closed electric loops. This kind of phase is also called a *loop condensate*. For large λ the electric term dominates over the magnetic term, hence all the links will favor the state $|0\rangle$. So in the regime of strong coupling we expect to be in a *polarized phase*, where the presence of electric loops is suppressed. Therefore, there is a critical coupling λ_c for which we have a *phase transition*. In the language of gauge theories, the loop condensate corresponds to a *deconfined phase* while the polarized one is a *confined phase*. Hence, for λ_c we have a deconfined-confined phase transition.

3.1.3 Super-selection sectors

We have already seen in Sec. 3.1.1 the non-local operators $\overline{W}_{1,2}$ and $\overline{S}_{1,2}$ that can classify the topological ground states. They can be treated on equal footing in the pure TC, because they both commutes with all the terms of the Hamiltonian (3.6). This is no longer true in (3.23), when the electric term is present. Both kind of operators are gauge-invariant, in the sense that they commute with the gauge transformations A_v, i.e.

$$\left[\overline{W}_{1,2}, A_v\right] = 0 \quad \text{and} \quad \left[\overline{S}_{1,2}, A_v\right] = 0, \quad \text{for all } v \in \mathbb{L} \qquad (3.24)$$

but only the $\overline{S}_{1,2}$ string operator commute with the electric field Z_ℓ.

This means, that we can classify all the state of $\mathcal{H}_{\text{phys}}$ (see (3.22)) through their $\overline{S}_1$ and $\overline{S}_2$ eigenvalues, because they commute with the Hamiltonian. Therefore, we obtain a decomposition of the physical Hilbert space in super-selection sectors

$$\mathcal{H}_{\text{phys}} = \mathcal{H}_{\text{phys}}^{(0,0)} \oplus \mathcal{H}_{\text{phys}}^{(0,1)} \oplus \mathcal{H}_{\text{phys}}^{(1,0)} \oplus \mathcal{H}_{\text{phys}}^{(1,1)}, \qquad (3.25)$$

where for each $|\phi\rangle \in \mathcal{H}_{\text{phys}}^{(n,m)}$ we have

$$S_1 |\phi\rangle = (-1)^m |\phi\rangle \quad \text{and} \quad S_2 |\phi\rangle = (-1)^n |\phi\rangle, \qquad (3.26)$$
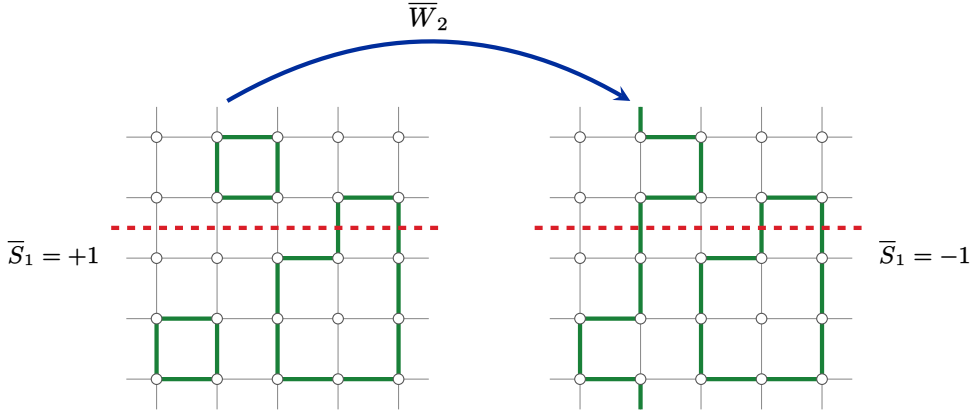
Figure 3.5. Pictorial representation of states of different super-selection sector and the action of the string operator W_2. Notice that the action $\overline{W}_2$ introduces a non-contractible electric loop in the state, which modifies the value of $\overline{S}_1$, which, in a sense, measure the presence of non-contractible electric loops in the orthogonal direction $\hat{2}$.

where $n, m = 0, 1$.

The string operators $\overline{W}_{1,2}$ do not commute with the Hamiltonian (3.23), hence they cannot be used to classify the states in $\mathcal{H}_{\text{phys}}$. On the other hand, given the algebraic relations (3.19), they are able to modify the effect of $\overline{S}_{1,2}$. In fact, $\overline{W}_{1,2}$ can change the super-selection sectors:

$$W_1 : \mathcal{H}_{\text{phys}}^{(n,m)} \mapsto \mathcal{H}_{\text{phys}}^{(n+1,m)} \quad \text{and} \quad W_2 : \mathcal{H}_{\text{phys}}^{(n,m)} \mapsto \mathcal{H}_{\text{phys}}^{(n,m+1)}, \tag{3.27}$$

where the $n, m = 0, 1$ and the addition is taken modulus 2.

From a more physical point of view, the operator $\overline{S}_i$ (with $i = 1, 2$) measures the presence non-contractible electric loops in the state in the direction orthogonal to $\hat{i}$. Therefore, the decomposition in (3.25) divides the physical Hilbert space by the number of non-contractible electric loops in each direction. On the other hand, the operators $\overline{W}_i$ introduces a non-contractible electric loop in the $\hat{i}$ direction, which explains (3.27). This can be seen in Fig. 3.5. Notice that in the case of $\mathbb{Z}_2$ LGT we can have at most one non-trivial electric loops. For examples, two parallels electric loops can be obtained by a strip of B_p operators, without requiring the $\overline{W}$ string operators.

3.2 Generalization to $\mathbb{Z}_N$

In this section we are going to generalize the $\mathbb{Z}_2$ LGT to a class of Abelian LGT with discrete symmetry $\mathbb{Z}_N$. This class is of particular interest because they approximate a $U(1)$ gauge theory in the limit $N \to \infty$.
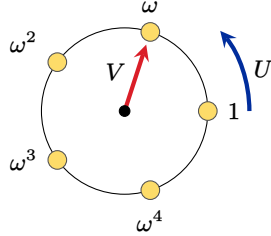
Figure 3.6. The operators U and V of a single link, in the $\mathbb{Z}_5$ case. The V plays the role of a position operator, while U that of a shift operator.

3.2.1 Schwinger-Weyl algebra

According to Wilson's Hamiltonian approach to LGTs [2], $U(1)$ gauge fields are defined on the links of a lattice $\mathbb{L}$ either in a pair of conjugate variables, the electric field E_ℓ and either the vector potential A_ℓ, satisfying

$$[E_\ell, A_{\ell'}] = i\delta_{\ell,\ell'}, \tag{3.28}$$

or equivalently the *magnetic operator*, also called *comparator*, $U_\ell = e^{-iA_\ell}$, such that

$$[E_\ell, U_{\ell'}] = \delta_{\ell,\ell'} U_\ell, \tag{3.29}$$

all acting on an infinite dimensional Hilbert space defined on each link $\ell \in \mathbb{L}$. This form of the canonical commutation relations represents the infinitesimal version of the relations:

$$e^{i\xi E} e^{-i\eta A} e^{-i\xi E} = e^{i\xi\eta} e^{-i\eta A}, \tag{3.30}$$

for any $\xi, \eta \in \mathbb{R}$, that define the Schwinger-Weyl group [111–113].

For a discrete group like $\mathbb{Z}_N$, the notion of infinitesimal generators loses any meaning and we are led to directly consider, for each link $\ell \in \mathbb{L}$, two unitary operators V_ℓ, U_ℓ, such that [113, 114]

$$V_\ell U_\ell V_\ell^\dagger = e^{2\pi i/N} U_\ell, \qquad U_\ell^N = \mathbb{1}_N, \qquad V_\ell^N = \mathbb{1}_N. \tag{3.31}$$

while they commute on different links. Thus, by representing $\mathbb{Z}_N$ with the set of the N roots of unity $e^{i2\pi k/N}$ $(k = 1, \cdots, N)$, commonly referred to as the discretized circle, we see that V plays the role of a "position operator" on the discretized circle, while U that of a "momentum operator".

These algebraic relations admit a faithful finite-dimensional representation of dimension N [115], for any integer N, which is obtained as follows. To each link ℓ, we can associate an N-dimensional Hilbert space $\mathcal{H}_\ell \simeq \mathbb{C}^N$. As an orthonormal basis for $\mathcal{H}_\ell$ we choose the *electric basis* $\{|v_{k,\ell}\rangle, k = 1, \ldots, N\}$, that diagonalizes the operator V_ℓ. With this choice, we can promptly write the actions of U_ℓ and V_ℓ:

$$\begin{aligned} U_\ell |v_{k,\ell}\rangle &= |v_{k+1,\ell}\rangle, \qquad (\text{mod } N) \\ V_\ell |v_{k,\ell}\rangle &= \omega^k |v_{k,\ell}\rangle, \end{aligned} \tag{3.32}$$
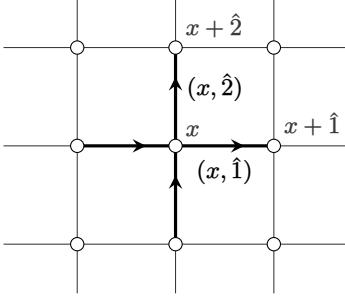
Figure 3.7. Labelling of the sites and the links in the two dimensional lattice. A site is labeled simply with $x = (x_1, x_2)$, while $\hat{1} = (1,0)$ and $\hat{2} = (0,1)$ stand for the unit vectors of the lattice. A link ℓ is denoted with a pair $(x, \pm\hat{i})$, with $\hat{i} = \hat{1}, \hat{2}$.

where $\omega = e^{2\pi i/N}$ and $k = 0, \ldots, N-1$. It is immediate to find the action for the Hermitian conjugates $U_\ell^\dagger$ and $V_\ell^\dagger$:

$$
\begin{aligned}
U_\ell^\dagger \left| v_{k,\ell} \right\rangle &= \left| v_{k-1,\ell} \right\rangle, \qquad (\text{mod } N) \\
V_\ell^\dagger \left| v_{k,\ell} \right\rangle &= \omega^{-k} \left| v_{k,\ell} \right\rangle.
\end{aligned}
\tag{3.33}
$$

With this choice, U_ℓ and V_ℓ in matrix form are written as

$$
U_\ell = \begin{pmatrix} 0 & 0 & \cdots & \cdots & 1 \\ 1 & 0 & \cdots & \cdots & 0 \\ 0 & 1 & \ddots & & \vdots \\ \vdots & \vdots & \ddots & \ddots & \vdots \\ 0 & 0 & \cdots & 1 & 0 \end{pmatrix} \quad \text{and} \quad V_\ell = \begin{pmatrix} 1 & & & & \\ & \omega & & & \\ & & \omega^2 & & \\ & & & \ddots & \\ & & & & \omega^{N-1} \end{pmatrix}.
\tag{3.34}
$$

We choose to work in this particular basis and the various k can be interpreted as the quantized values of the electric field on the links.

In the $\mathbb{Z}_N$ case it is important to fix the orientation of the lattice $\mathbb{L}$, because for $N \geq 3$ we have $U^\dagger \neq U$ and $V^\dagger \neq V$. We choose the orientation shown in Fig. 3.7. On a two-dimensional square lattice of size $L \times L$, the links ℓ of the lattice can also be labeled with $(x, \pm\hat{i})$, where $x \in \mathbb{L}$ is a site and $\hat{i} = \hat{1}, \hat{2}$ the two independent unit vectors. In this way, $(x, \pm\hat{i})$ will refer to the link that start in x and goes in the positive (negative) direction $\hat{i}$. As we will see later, the choice of the orientation affects the definition of any string operator. The general rule for when defining a string operator as a product of $\mathcal{O}$ operators, where $\mathcal{O}$ is either U or V for example, is to use $\mathcal{O}$ when going in the positive direction or $\mathcal{O}^\dagger$ otherwise.

3.2.2 Gauge invariance and Hamiltonian

Gauge transformations transforms the vector potential while preserving the electric field. For a $U(1)$ gauge theory, a local phase transformation is induced by a real function α_x defined on the vertices $x \in \mathbb{L}$, such that $A_\ell \mapsto A_\ell + (\alpha_{x_2} - \alpha_{x_1})$ or equivalently

$$
U_\ell \mapsto e^{i(\alpha_{x_2} - \alpha_{x_1})E_\ell} U_\ell e^{-i(\alpha_{x_2} - \alpha_{x_1})E_\ell},
\tag{3.35}
$$
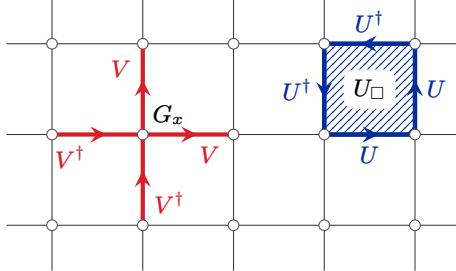
Figure 3.8. Pictorial representation of the Gauss operators G_x in (3.36) (*left*) and plaquette operator $U_\square$ in (3.37) (*right*).

where x_1, x_2 are the initial and final vertices of the (directed) link ℓ. In the case of a discrete symmetry, a gauge transformation at a site $x \in \mathbb{L}$ is a product of V's (and $V^\dagger$'s) defined on the links which comes out (and enters) the vertex. More specifically, for a two dimensional lattice, if the link ℓ at site x is oriented in the positive direction, i.e. either $(x, +\hat{1})$ or $(x, +\hat{2})$, then V is used, otherwise $V^\dagger$. Thus, the single local gauge transformation at the site x is enforced by the operator:

$$G_x = V_{(x,\hat{1})} V_{(x,\hat{2})} V^\dagger_{(x,-\hat{1})} V^\dagger_{(x,-\hat{2})}, \tag{3.36}$$

as shown in the left part in Fig. 3.8.

The operators that enters the Hamiltonian have to be gauge invariant, i.e. commute with all the operators G_x. Using (3.36) and recalling (3.31), it is possible to see that the V_ℓ's commute with G_x (as expected), while the U_ℓ's do not. In spite of that, we can build gauge-invariant operators out of the comparators U_ℓ. Generalizing directly from TC case, one another gauge-invariant operator is the *plaquette operator*, which we will denote with $U_\square$, that will play the role of the magnetic operator. A plaquette now has an orientation. Given a plaquette $\square$ with vertices $\{x, x + \hat{1}, x + \hat{1} + \hat{2}, x + \hat{2}\}$, we consider the path that start from x and goes in the counterclockwise direction. On this plaquette, the operator $U_\square$ is defined as follows:

$$U_\square = U_{(x,\hat{1})} U_{(x+\hat{1},\hat{2})} U^\dagger_{(x+\hat{1}+\hat{2},-\hat{1})} U^\dagger_{(x+\hat{2},-\hat{2})}, \tag{3.37}$$

which can be seen on the right in Fig. 3.8.

The whole operator algebra $\mathcal{A}$ of the theory is generated by the set of all U_ℓ and V_ℓ (and their Hermitian conjugates) of all the links of the lattice $\mathbb{L}$, while the *gauge-invariant subalgebra* $\mathcal{A}_{\text{gi}}$ consists of operators that commutes with all the G_x:

$$\mathcal{A}_{\text{gi}} = \{O_{\text{gi}} \in \mathcal{A} \,:\, [O_{\text{gi}}, G_x] = 0 \quad \forall x \in \mathbb{L}\}. \tag{3.38}$$

Guided by the TC, we already know that the set $\{U_\square, V_\ell\}$ (for all plaquettes $\square$ and all links ℓ) does not generate the whole algebra $\mathcal{A}_{\text{gi}}$, in the case of
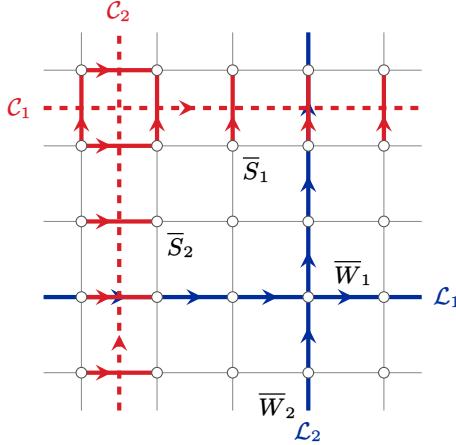
Figure 3.9. Graphical representation of the non-local operators $\overline{W}_{1,2}$ (in blue) and $\overline{S}_{1,2}$ (in red) and their respective paths $\mathcal{L}_{1,2}$ and $\mathcal{C}_{1,2}$.

periodic boundary conditions. Indeed, we have yet to add string operators on non-contractible loops.

In Sec. 3.1.1 we have already introduced the non-local operators $\overline{W}_i$ and $\overline{S}_i$, with $i = 1, 2$. These can readily be generalized to the $\mathbb{Z}_N$ case, by replacing X_ℓ and Z_ℓ with U_ℓ and V_ℓ respectively. More precisely, consider direct non-contractible loops $\mathcal{L}_i$ and cuts $\mathcal{C}_i$ (in the i-th direction). Then $\overline{W}_i$ and $\overline{S}_i$ operators are defined as

$$\overline{W}_i = \prod_{\ell \in \mathcal{L}_i} U_\ell \quad \text{and} \quad \overline{S}_i = \prod_{\ell \in \mathcal{C}_i} V_\ell, \tag{3.39}$$

with the caveat that when going in the negative direction, $U^\dagger$ and $V^\dagger$ have to be used. Operators $\overline{W}_i$ will also be called *Wilson loops*, while the $\overline{S}_i$ will be called *'t Hooft strings* (tHS). These operators are pictured in Fig. 3.9.

Both sets of operators, $\overline{W}_i$ and $\overline{S}$, are gauge invariant but only the WLs cannot be expressed as product of neither $U_\square$ and V_ℓ. Therefore, they have to be added explicitly to the set of generators of $\mathcal{A}_{\text{gi}}$ in order to obtain the whole algebra. Similar to the TC, these non-local operators will play a fundamental role in defining the super-selection sectors of the theory.

The class of models we consider are described by the Hamiltonian [116–118]:

$$H_{\mathbb{Z}_N}(\lambda) = -\sum_\square U_\square - \lambda \sum_\ell V_\ell + \text{h.c.}, \tag{3.40}$$

where the first sum is over the plaquettes $\square$ of the lattice while the second sum is over the links ℓ. As stated before, the operators $U_\square$ plays the role of a *magnetic* term, to be more precise it is the magnetic flux inside the plaquette $\square$, while V is the *electric* term. The coupling λ tunes the relative strength of the electric and magnetic energy contribution.

3.2.3 Physical Hilbert space and super-selection sectors

The total Hilbert space $\mathcal{H}_{\text{tot}}$ is given by

$$\mathcal{H}_{\text{tot}} = \bigotimes_{\ell \in \mathbb{L}} \mathcal{H}_\ell, \tag{3.41}$$

where $\mathcal{H}_\ell \simeq \mathbb{C}^N$ in the case of $\mathbb{Z}_N$ theory. A state of the whole lattice $|\phi_{\text{phys}}\rangle \in \mathcal{H}_{\text{tot}}$ is said to be *physical* if it is a *gauge-invariant state*:

$$G_x |\phi_{\text{phys}}\rangle = |\phi_{\text{phys}}\rangle, \qquad \forall\, x \in \mathbb{L}. \tag{3.42}$$

This condition can be translated into a constraint on the eigenvalues v_ℓ of the electric operators V_ℓ. Given that a link ℓ can be referred to as $(x, \hat{i})$, then the constraint (3.42) can be translated to

$$v_{(x,\hat{1})} v_{(x,\hat{2})} v^*_{(x,-\hat{1})} v^*_{(x,-\hat{2})} = 1. \tag{3.43}$$

For a $\mathbb{Z}_N$ theory we have $v_\ell = \omega^{k_\ell}$, where $\omega = e^{i2\pi/N}$, which leads to

$$\sum_{i=1,2} \left(k_{(x,\hat{i})} - k_{(x,-\hat{i})} \right) = 0 \mod N. \tag{3.44}$$

for (3.42). Given the fact that the k in (3.31) represent the values of the electric field, one can see that (3.44) can be interpreted as a discretized version of the Gauss law $\nabla \cdot \vec{E} = 0$ in two dimensions, for a pure gauge theory.

Consider now the *physical Hilbert space* for a $\mathbb{Z}_N$ theory:

$$\mathcal{H}_{\text{phys}} = \{ |\phi_{\text{phys}}\rangle : G_x |\phi_{\text{phys}}\rangle = |\phi_{\text{phys}}\rangle \quad \forall\, x \in \mathbb{L} \}. \tag{3.45}$$

This space can be decomposed into super-selection sectors, like it has been done for the $\mathbb{Z}_2$ theory in Sec. 3.1.3. In fact, it can be generalized in a straightforward way, using the string operators in (3.39) (showed in Fig. 3.9). The physical Hilbert space $\mathcal{H}_{\text{phys}}$ decomposes as

$$\mathcal{H}_{\text{phys}} = \bigoplus_{n,m=0}^{N-1} \mathcal{H}_{\text{phys}}^{(n,m)}, \tag{3.46}$$

where each sector (n, m) satisfy

$$S_1 |\phi\rangle = \omega^m |\phi\rangle \quad \text{and} \quad S_2 |\phi\rangle = \omega^n |\phi\rangle \tag{3.47}$$

for $|\phi\rangle \in \mathcal{H}_{\text{phys}}^{(n,m)}$. This is possible because the tHSs $\overline{S}$ commutes with all the terms of the Hamiltonian.

On the other hand, the $\overline{W}_i$ do not commute with all the terms in the Hamiltonian (3.40), in particular with the electric operators V_ℓ, but are still

gauge-invariant. Nonetheless, we are interested in the commutation relation between the WLs and tHSs:

$$\overline{W}_1\overline{S}_2 = \omega\overline{S}_2\overline{W}_1 \quad \text{and} \quad \overline{W}_2\overline{S}_1 = \omega\overline{S}_1\overline{W}_2. \tag{3.48}$$

It is a direct generalization of the relations (3.19) of the TC, where the sign -1 is upgraded to a characteristic phase ω. Given (3.48), it is easy to see that the WLs have the ability to change the super-selection sectors:

$$W_1 : \mathcal{H}_{\text{phys}}^{(n,m)} \to \mathcal{H}_{\text{phys}}^{(n+1,m)} \quad \text{and} \quad W_2 : \mathcal{H}_{\text{phys}}^{(n,m)} \to \mathcal{H}_{\text{phys}}^{(n,m+1)}, \tag{3.49}$$

where the addition is taken modulus N.

From a physical point of view, the WLs operators create non-contractible electric loops around the lattice, while the tHSs detect the presence and the strength of these electric loops, by traversing it in the orthogonal direction. Exactly like in the case of the $\mathbb{Z}_2$ LGT, but the difference that now the non-contractible electric strings can have different "strengths", given by the different eigenvalues of $\overline{S}_i$. Therefore, it is clear that the Hilbert subspace $\mathcal{H}_{\text{phys}}^{(n,m)}$ is the subspace of all the states that contains an electric loop of strength ω^n and ω^m along the $\hat{1}$ and $\hat{2}$ direction, respectively.

Furthermore, the evolution of a state in $\mathcal{H}_{\text{phys}}^{(n,m)}$ with the Hamiltonian in (3.40) is confined in $\mathcal{H}_{\text{phys}}^{(n,m)}$. This is because none of the local terms in the Hamiltonian can change the super-selection sector, only the non-local WLs. In this chapter we will see how this fact can have major consequences when considering $\mathbb{Z}_N$ models on particular lattice geometries, in particular on the *ladder*.

3.3 Abelian models on the ladder

In this short chapter we will introduce $\mathbb{Z}_N$ LGT on a *ladder geometry*. This type of lattice can be considered as a strip of a two-dimensional square lattice. The peculiarity of this geometry is that it allows the existence of magnetic terms in a quasi one-dimensional lattice, which usually are not possible in a pure one-dimensional systems. Moreover, since the Hilbert space is highly constrained, it allows the possibility to study systems of moderate size through exact diagonalization. The latter will be analyzed in the last section.

A *ladder* is a lattice $\mathbb{L}$ made of two parallels chains, the *legs*, coupled to each other by the *rungs* to form square plaquettes. On the ladder, each rung is identified by a coordinate $i = 1, \ldots, L$, where L is the length of the ladder, and the two vertices on the rung are denoted with $i^\uparrow$ and $i^\downarrow$ in the upper and lower leg, respectively (see Fig. 3.10). Links, as usual, will be denoted by ℓ.
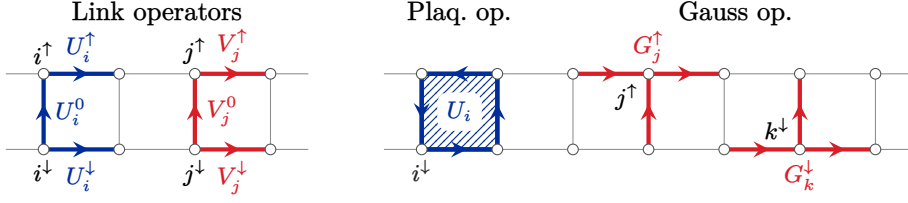
Figure 3.10. Picture of the different ladder operators. *Left*: the magnetic and electric link operators. *Right*: plaquette operator U_i and the Gauss operators $G_j^\uparrow$ and $G_k^\downarrow$. Notice that operators and sites on the upper leg are indicated with an up arrow, on the lower leg with a down arrow and on the rungs with a superscript 0.

On the legs they are labelled as $\ell_i^\uparrow$ (upper leg) or $\ell_i^\downarrow$ (lower leg), while on the rungs they are labelled ℓ_i^0.

We preserve the same formulation of $\mathbb{Z}_N$ LGT but in order to lighten our notation, we use the symbols V_i^0, U_i^0 for the operators defined on the rung i, and V_i^ρ, U_i^ρ with $\rho = \uparrow, \downarrow$ for the operators on the horizontal links of the upper and lower leg, respectively, to the right of the rung. In synthesis:

$$U_{\ell_i^0} \equiv U_i^0, \quad U_{\ell_i^\downarrow} \equiv U_i^\downarrow, \quad U_{\ell_i^\uparrow} \equiv U_i^\uparrow$$
$$V_{\ell_i^0} \equiv V_i^0, \quad V_{\ell_i^\downarrow} \equiv V_i^\downarrow, \quad V_{\ell_i^\uparrow} \equiv V_i^\uparrow. \tag{3.50}$$

The plaquette operator on the right of the rung i will be labeled as U_i:

$$U_i = U_i^\downarrow U_{i+1}^0 (U_i^\uparrow)^\dagger (U_i^0)^\dagger. \tag{3.51}$$

Moreover, on a ladder the vertices are three-legged, so the Gauss operators are slightly modified:

$$G_i^\uparrow = V_i^\uparrow (V_{i-1}^\uparrow)^\dagger (V_i^0)^\dagger \text{ and } G_i^\downarrow = V_i^\downarrow V_i^0 (V_{i-1}^\downarrow)^\dagger, \tag{3.52}$$

where $G_i^\uparrow$ and $G_i^\downarrow$ refers, respectively, to the Gauss operators on the vertices $i^\uparrow$ and $i^\downarrow$. As a reference see Fig. 3.10.

Finally, we write explicitly the Hamiltonian for a $\mathbb{Z}_N$ LGT on a ladder:

$$H^{N\text{-lad}}(\lambda) = -\sum_i \left[U_i + \lambda \left(V_i^\uparrow + V_i^\downarrow + V_i^0 \right) + \text{h.c.} \right]. \tag{3.53}$$

For what concerns the super-selection sectors of the theory, non-contractible loops are possible now only in the $\hat{2}$ direction. Therefore, out of the WL operators in (3.39) only $\overline{W}_1$ is well defined, meaning that we can create non-contractible electric loops along the $\hat{1}$. Hence, only $\overline{S}_2$ in (3.39) (the tHS conjugate to W_1) can be used as a mean for distinguishing these different sectors. Explicitly, the WL $\overline{W}_1$ and $\overline{S}_2$ can be written as

$$\overline{W}_1 = \prod_i U_i^\downarrow \quad \text{and} \quad \overline{S}_2 = V_{i_0}^\uparrow V_{i_0}^\downarrow, \tag{3.54}$$

$$\overline{S}_2 = V_{i_0}^\uparrow V_{i_0}^\downarrow$$

$$\overline{W}_1 = \prod_i U_i^\downarrow$$
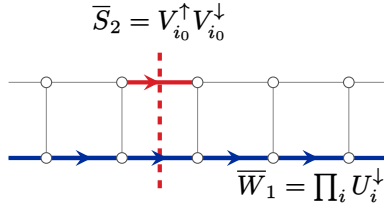
Figure 3.11. Picture of the non-local string operators $\overline{W}_1$ and $\overline{S}_2$ on the ladder.

$\mathbb{Z}_2$ sector $n = 0$

$\mathbb{Z}_2$ sector $n = 1$
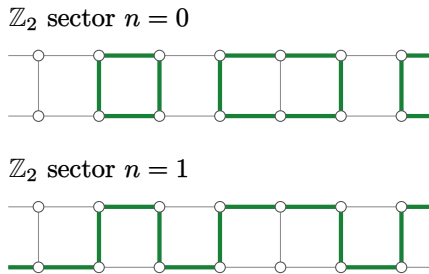
Figure 3.12. Example of two physical configurations (in the electric basis) in a $\mathbb{Z}_2$ theory in the two different super-selection sectors. This shows that states belonging to two different sectors can be quite different.

where i_0 is any chosen rung (see Fig. 3.11). Furthermore, it does not make sense to consider the tHS S_1 because it is equal to the product of all the Gauss operators on either one of the legs,

$$\overline{S}_1 = \prod_i G_i^\downarrow = \prod_i G_i^\uparrow, \tag{3.55}$$

so it always equal to the identity on physical states, signaling the obvious fact that we do not have non-contractible electric loops around the $\hat{2}$ direction. We can conclude that the physical Hilbert space can be decomposed in only N sectors as

$$\mathcal{H}_{\text{phys}} = \mathcal{H}_{\text{phys}}^{(0)} \oplus \mathcal{H}_{\text{phys}}^{(1)} \oplus \cdots \oplus \mathcal{H}_{\text{phys}}^{(N-1)}, \tag{3.56}$$

and in each sector we have that

$$S |\phi\rangle = \omega^n |\phi\rangle \quad \text{if} \quad |\phi\rangle \in \mathcal{H}_{\text{phys}}^{(n)}. \tag{3.57}$$

Due to the fact that the ladder is quasi one-dimensional, the presence of non-contractible electric loops can highly affects the physical states. Take the case of a $\mathbb{Z}_2$ theory, which is pictured in Fig. 3.12. It has just two sectors: $n = 0$ and $n = 1$. In the former all the physical configuration are made of closed loop, distributed along the $\hat{1}$ direction. While in the latter, the physical configurations are just deformations of of one single electric loop that goes around the ladder. This can make us reasonably believe that the two sectors might have completely different physical content.

Like in the two-dimensional case, the Hamiltonian can be reduced to a single super-selection sector. One of the main features of this is that once the sector is fixed, it is possible to write a duality transformation of the Hamiltonian to a pure one-dimensional *quantum clock model*, resolving entirely the

gauge symmetries. Thanks to this duality map, we will see how that the different sectors have very different behaviour and each can have its own unique phase diagram. The latter is the object of discussion of the second part of this chapter, but before doing so we need to introduce the notion of *dualities* and, in particular, *the bond-algebraic approach to dualities.*

3.4 Dualities in physics

Duality is a simple yet powerful idea in physics. They can be intended as specific mathematical transformations connecting seemingly unrelated physical phenomena. They have been know for a long time, indeed a first example would be the duality of the electromagnetic field in the absence of sources, noticed by Heaviside in 1884. Generally in physics, the concept of duality is connected to ideas, like symmetries, mappings between different coupling regimes, perturbative expansions for strongly correlated systems, and the wave-particle duality of quantum mechanics [106, 119].

They play a major role in statistical physics and condensed matter. In statistical mechanics, dualities were introduced for the first time by Kramers and Wannier [120], who found a relation between the high temperature and low temperature regimes of the two-dimensional Ising mode. In this way, they were able to find the critical temperature years before Onsager solution [121]. In this case we speak of self-dualities, where the same model is mapped onto itself but in a different coupling regime. The essential legacy of Kramers and Wannier is the fact that self-dualities can put constraints on the phase boundaries and the exact location of critical points.

Not all dualities are self-dualities. In fact, it also possible to relate two apparently different physical models with a duality transformation. A known example is the Jordan-Wigner transformation [122, 123], where spin d.o.f (which are bosonic in nature) are mapped onto fermionic d.o.f in one-dimension. This duality shows that, in fact, there is not much difference between bosonic and fermionic d.o.f in one dimension.

3.4.1 The bond-algebraic approach

In the following section we will quickly review the bond-algebraic approach to dualities [119, 124], because it offers a powerful and convenient way for dealing with duality transformations, in particular when gauge symmetries are involved. The concept of *bond-algebra* was first introduced in [125] and it exploits the fact that most *Hamiltonian are a sum of simple and (quasi)local*

terms:

$$H = \sum_\Gamma \lambda_\Gamma h_\Gamma, \tag{3.58}$$

where Γ is a set of indices (e.g. the lattice sites but can be completely general) and λ_Γ are numbers (usually the couplings). Roughly speaking, by quasi-local we mean that a operator h_Γ involves a small number of d.o.f that are spatially near each other (for example nearest neighbour). The terms h_Γ are called *bond operators* (or simply *bonds*). From the bonds h_Γ we obtain a *bond algebra* $\mathcal{A}\{h_\Gamma\}$, which is the algebra of all the operators generated by all the possible products and sums of the bonds h_Γ and their Hermitian conjugates. In practical terms, given a set of bonds $\{h_\Gamma\}$, the bond-algebra $\mathcal{A}\{h_\Gamma\}$ is the algebra spanned by

$$\{\mathbb{1}, h_\Gamma, h_\Gamma^\dagger, h_\Gamma h_{\Gamma'}, h_\Gamma^\dagger h_{\Gamma'}, h_\Gamma h_{\Gamma'}^\dagger, h_\Gamma^\dagger h_{\Gamma'}^\dagger, h_\Gamma h_{\Gamma'} h_{\Gamma''}, \dots\}$$

By construction, $\mathcal{A}\{h_\Gamma\}$ is closed under the operation Hermitian conjugation, but since an Hamiltonian H is Hermitian then $h_\Gamma^\dagger = h_{\Gamma'}$ for some Γ'. Therefore, $\mathcal{A}\{h_\Gamma\}$ is simply spanned by

$$\{\mathbb{1}, h_\Gamma, h_\Gamma h_{\Gamma'}, h_\Gamma h_{\Gamma'} h_{\Gamma''}, \dots\}$$

Notice that the bonds h_Γ that generate $\mathcal{A}\{h_\Gamma\}$ do not need to be independent.

It is important to point out that a single Hamiltonian H can have different bond algebras associated to it. In fact, a bond algebra is determined by the partitioning of the bonds in H. In principle, given any two decomposition of the same Hamiltonian,

$$H = \sum_\Gamma \lambda_\Gamma h_\Gamma = \sum_\Sigma \lambda'_\Sigma h'_\Sigma,$$

one should expect $\mathcal{A}\{h_\Gamma\} \neq \mathcal{A}\{h'_\Sigma\}$ in general (see [119]). To make an example, consider the Hamiltonian

$$H = \sum_i \left(h_x \sigma_i^x + h_y \sigma_i^z\right).$$

We can either partition the bonds by taking σ_i^x and σ_i^z as generators separately or by taking $h_x \sigma_i^x + h_z \sigma_i^z$ as a single bond. In the former case we would obtain $\mathcal{A}\{\sigma^x, \sigma^z\}$, while in the latter we would have $\mathcal{A}\{h_x \sigma_i^x + h_z \sigma_i^z\}$. These two algebras are clearly different,

$$\mathcal{A}\{\sigma^x, \sigma^z\} \neq \mathcal{A}\{h_x \sigma_i^x + h_z \sigma_i^z\},$$

because $\mathcal{A}\{h_x \sigma_i^x + h_z \sigma_i^z\}$ is commutative, while $\mathcal{A}\{\sigma^x, \sigma^z\}$ is not.

In the framework of bond-algebra, quantum dualities can be formulated as *homomorphisms of bonds-algebras*. By homomorphism we intend a map Φ between two algebras $\mathcal{A}_1$ and $\mathcal{A}_2$ that preserves the linear and multiplicative structure of the algebras. In mathematical terms, given any $u, v \in \mathcal{A}_1$ and any complex number λ we have

$$\Phi(u + \lambda v) = \Phi(u) + \lambda \Phi(v) \quad \text{and} \quad \Phi(uv) = \Phi(u)\Phi(v).$$

To be more precise with our definition of quantum duality, consider two Hamiltonians H_1 and H_2 that act on Hilbert spaces of the same dimensions. They are said to be *dual* if there is some bond-algebra $\mathcal{A}_{H_1}$ of H_1 that is homomorphic to some bond-algebra $\mathcal{A}_{H_2}$ of H_2 and if the homomorphism $\Phi : \mathcal{A}_{H_1} \rightarrow \mathcal{A}_{H_2}$ maps H_1 onto H_2, $\Phi(H_1) = H_2$. These mappings do not need to be isomorphisms (i.e. invertible), especially when gauge symmetries are involved, and we will explain why later.

In a traditional approach to quantum dualities, one tries to map each degree of freedom of H_1 onto a degree of freedom of H_2. This can be rather cumbersome, because in this way most duality transformations appear to be non-local. In other words, one degree of freedom on one side may correspond to a large number of d.o.f on the other side. This is apparent, for example, with the Jordan-Wigner transformation, where a single spin is dual to a whole chain of fermions.

Quantum dualities in the bond-algebraic approach are instead *local*, meaning that each single *bond* h_{Γ_1} of H_1 is mapped onto a single bond h_{Γ_2} of H_2. This may translates in non-locality when treating elementary d.o.f and this is due to the fact that the generators of a bond algebra are usually two- (or more) body operators and expressing the elementary d.o.f with these operators may require large (if not infinite) products.

An isomorphism like Φ is physically sound if it is *unitarily implementable* [119], which means that there is a unitary matrix $\mathcal{U}$ such that the duality isomorphism reads

$$\Phi(\mathcal{O}) = \mathcal{U}\mathcal{O}\mathcal{U}^\dagger, \quad \forall \mathcal{O} \in \mathcal{A}, \tag{3.59}$$

where $\mathcal{A}$ is the operator algebra of the model under investigation [119].

To make the bond-algebraic approach more clear we will consider one example: the *Quantum Ising Model (QIM)*. In this model we will see an example of self-duality through the use of disorder variables. Our intent is not to shine new physics but to show how the use of bond-algebras offers a clear *formalism* for treating dualities.

3.4.2 The quantum Ising model

The Quantum Ising Model with a transverse field is a chain of spin-$\frac{1}{2}$ described by the Hamiltonian

$$H^{\text{Ising}}(h) = \sum_i \left(\sigma_i^z \sigma_{i+1}^z + h\sigma_i^x \right), \qquad (3.60)$$

where the sums runs over the sites of the chain and h is the transverse field strength. Notice that the Hamiltonian H^{Ising} is indeed a sum of quasi-local terms. In particular we have two types of terms: the interaction term $\sigma_i^z \sigma_{i+1}^z$ and the transverse field σ_i^x. They are local or quasi-local because they involve at most two neighbouring sites. These two sets of terms are the bonds of the Hamiltonian H^{Ising}, therefore bond-algebra $\mathcal{A}\{\sigma_i^z \sigma_{i+1}^z, \sigma_i^x\}$ is spanned by:

$$\left\{ \mathbb{1}, \ \sigma_i^z \sigma_{i+1}^z, \ \sigma_i^z \sigma_{i+1}^z \sigma_j^z \sigma_{j+1}^z, \ \ldots, \ \sigma_i^x, \ \sigma_i^x \sigma_j^x, \ \ldots, \ \sigma_i^z \sigma_{i+1}^z \sigma_i^x, \ \ldots \right\}.$$

We consider an infinite chain in order to avoid subtleties with the boundaries conditions, which can have major effects on a duality transformation.

The algebraic relations that defines the generators of $\mathcal{A}^{\text{Ising}}$ can be summarized as follows:

1. each bonds square to the identity operator,

$$(\sigma_i^z \sigma_{i+1}^z)^2 = (\sigma_i^x)^2 = \mathbb{1}.$$

2. the bonds σ_i^x anticommutes with $\sigma_i^z \sigma_{i+1}^z$ and $\sigma_{i-1}^z \sigma_i^z$ while commuting with the others,

$$\left\{ \sigma_i^x, \sigma_i^z \sigma_{i+1}^z \right\} = \left\{ \sigma_i^x, \sigma_{i-1}^z \sigma_i^z \right\} = 0.$$

3. the bonds $\sigma_i^z \sigma_{i+1}^z$ anticommutes with σ_i^x and σ_{i+1}^x while commuting with the others,

$$\left\{ \sigma_i^z \sigma_{i+1}^z, \sigma_i^x \right\} = \left\{ \sigma_i^z \sigma_{i+1}^z, \sigma_{i+1}^x \right\} = 0.$$

Given the symmetric roles that the basic bonds σ_i^x and $\sigma_i^z \sigma_{i+1}^z$ play with each other, we can set up a mapping Φ^{Ising} that exchange their roles:

$$\Phi^{\text{Ising}}(\sigma_i^z \sigma_{i+1}^z) = \sigma_i^x, \qquad \Phi^{\text{Ising}}(\sigma_i^x) = \sigma_{i-1}^z \sigma_i^z. \qquad (3.61)$$

This transformation can be extended to the whole $\mathcal{A}^{\text{Ising}}$ through the homomorphic property of Φ^{Ising}. It preserves all the important algebraic relationship and is one-to-one, hence it is an *isomorphism* of $\mathcal{A}^{\text{Ising}}$ onto itself. The
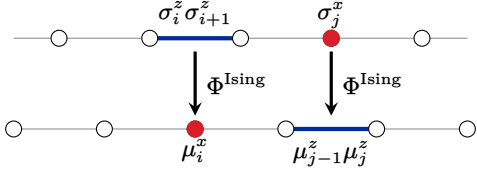
Figure 3.13. Pictorial representation of the duality map Φ^{Ising}, that maps the QIM on the same model on the dual lattice

Hamiltonian H^{Ising} is just an element of $\mathcal{A}^{\text{Ising}}$. We can apply Φ^{Ising} to H^{Ising} and use its homomorphic property, which yields

$$
\begin{aligned}
\Phi^{\text{Ising}}(H^{\text{Ising}}(h)) &= \sum_i \left(\Phi^{\text{Ising}}(\sigma_i^z \sigma_{i+1}^z) + h\Phi^{\text{Ising}}(\sigma_i^x) \right) \\
&= \sum_i \left(\sigma_i^x + h\sigma_{i-1}^z \sigma_i^z \right) \\
&= h\sum_i \left(\sigma_i^z \sigma_{i+1}^z + h^{-1}\sigma_i^x \right).
\end{aligned}
\tag{3.62}
$$

Notice that the indices in the sum can be freely shifted because we are working with an infinite number of sites. We have thus obtained

$$
\Phi^{\text{Ising}}(H^{\text{Ising}}(h)) = hH^{\text{Ising}}(h^{-1}),
\tag{3.63}
$$

henceforth Φ^{Ising} is a *self-duality* of (3.60). Notice that $H^{\text{Ising}}(h)$ is mapped onto itself but with the inverted coupling, $h \mapsto h^{-1}$, meaning that we can map the strongly coupled phase $h \gg 1$ into the weakly coupled phase $h \ll 1$, and vice versa. This is basically the quantum version the *Kramers-Wannier duality* [120, 126].

If we think of the term σ_i^x as living on the site i and of $\sigma_i^z \sigma_{i+1}^z$ as of living on the *link* between the site i and $i+1$, then we can think of Φ^{Ising} as mapping (3.60) onto the *dual lattice*. In fact, the dual lattice of a chain is still a chain and the site term σ_i^x is mapped onto a link term $\sigma_i^z \sigma_{i+1}^z$, and vice versa.

We want to have a clearer physical picture of the duality map Φ^{Ising} and build a bridge with the traditional approach to dualities for the QIM. For this reason we want to find the *elementary d.o.f of the dual model*. The d.o.f of the dual model lives on the sites of the dual lattice, which corresponds to the links of the original lattice. On these dual sites we again have spin-$\frac{1}{2}$d.o.f and, for more clarity, we use μ^x and μ^z for referring to the Pauli matrices acting on these new spins. The dual site i corresponds to the link $(i, i+1)$, while the dual link $(i-1, i)$ corresponds to the site i.

From (3.61), we already know that

$$
\sigma_i^z \sigma_{i+1}^z = \mu_i^x \quad \text{and} \quad \sigma_i^x = \mu_{i-1}^z \mu_i^z.
\tag{3.64}
$$

The role of μ_i^x is evident, it measure the alignment of two neighbouring spins on the sites i and $i+1$, while the meaning of μ_i^z is still opaque. We can arrive at
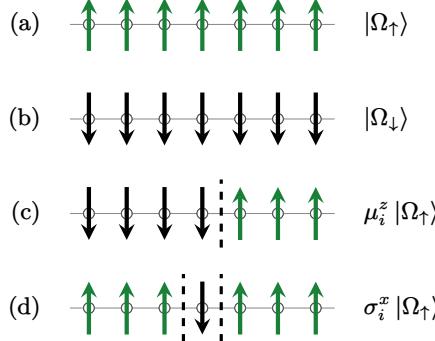
Figure 3.14. *(a)* and *(b)* ferromagnetic ground states $|\Omega_\uparrow\rangle$ and $||\Omega_\downarrow\rangle\rangle$. *(c)* kink created on the link between site i and $i+1$ by the operator μ_i^z. *(d)* kink-antikink pairs created around the site i by the spin flip σ_i^x.

the definition of μ_i^z by exploiting the map Φ^{Ising}. The bond $\mu_{i-1}^z \mu_i^z$ corresponds to the image of σ_i^x through Φ^{Ising}, so we know how they are mapped. If we isolate μ_i^z with an *infinite product*, we then obtain

$$\mu_i^z = \prod_{j=-\infty}^{i} \mu_{j-1}^z \mu_j^z = \prod_{j=-\infty}^{i} \sigma_j^x. \tag{3.65}$$

We see that μ_i^z flips all the spins before the i-th site. From (3.65), we can see the *non-local* origin of the dual d.o.f in traditional dualities. When working with two, or more, body terms, in order to isolate a single body term the use of large (or even infinite) product is necessary.

To understand the role of μ_i^x and μ_i^z, consider now the ferromagnetic ground states $|\Omega_\rho\rangle$ of (3.60), where $\rho = \uparrow, \downarrow$. Say we start from $|\Omega_\uparrow\rangle$, without loss of generality. The action of μ_i^z on $|\Omega_\rho\rangle$ is to create a *kink*, which is a domain wall between two ordered regions. From this point of view, a single spin-flip $\sigma_i^x |\Omega_\uparrow\rangle$ creates a *kink-antikink pair*.

3.4.3 Gauge-reducing dualities

In this section we will review the notion of *gauge-reducing dualities*, In order to do so we start by highlighting the difference between ordinary symmetries and quantum symmetries.

Following the statement of Wigner's theorem [127], a quantum symmetry is a unitary or anti-unitary mapping that commute with the Hamiltonian. This does not mean that all symmetries have the same physical meaning or mathematical consequences. By the term "*ordinary symmetries*" we refer to the most common types of symmetry that we encounter in physical systems that usually correspond to *global transformation* of the physical apparatus or system, like for example rotational invariance. These symmetries have a direct physical impact, since they can influence the level degeneracy of an Hamiltonian and force strict selection rules.

On the other hand, gauge symmetries are *local symmetries* of the model that signal the presence of *redundant d.o.f.* In fact, it is better to think of gauge symmetries as *local constraints* on the elementary d.o.f of the gauge model. As a result, the state space of a gauge model is larger than the set of physical states, which are exactly the states that are invariant under the action of the gauge symmetries. The same reasoning applies to the observables of the gauge model. An observables is represented by an Hermitian operator and a *physical observable* is represented by an Hermitian operator that commutes with gauge symmetries.

So, if physical states and physical observables already satisfies the local constraints of the gauge symmetries, this means that the physical impact of the latter is already encoded in the former. It is clear that the ordinary symmetries and gauge symmetries are very different and is better to put them conceptually far apart as possible [119].

When dealing with a gauge model, it would be natural to assume that, in order to establish a duality, the gauge symmetries have to be eliminated *first* from the gauge model. In other terms, that it would be necessary to proceed with gauge-fixing [106]. By gauge-fixing we mean the process of "turning off" *some* d.o.f, by means of gauge transformations. A popular example of gauge-fixing in $\mathbb{Z}_2$ or $\mathbb{Z}_N$ LGTs is the axial gauge, where all the gauge d.o.f along a specified direction are fixed [106] (i.e. turned off). A global gauge-fixing is not always possible and it may depends, for example, on the geometry of system or its boundary conditions.

Although gauge-fixing is common in traditional approach to dualities in gauge models, it is not strictly necessary with bond-algebras. As stated in [119], with the bond-algebraic approach one can find mappings to models without any gauge symmetry, that preserve all the important algebraic properties without the need of gauge-fixing. Later in the chapters, we will see some examples of gauge-reducing dualities that do not need require gauge-fixing first.

The procedure goes as follows: consider a gauge model and let H^{G} be its Hamiltonian and G_Γ its gauge symmetries. An operator $\mathcal{O}$ is gauge-invariant if and only if it commutes with all the G_Γ:

$$\mathcal{O} \text{ physical} \quad \Longleftrightarrow \quad [\mathcal{O}, G_\Gamma] = 0 \quad \forall \Gamma.$$

Clearly, the Hamiltonian has to be gauge-invariant, hence $[H^{\mathrm{GR}}, G_\Gamma] = 0$. Now let H^{GR} be the dual Hamiltonian of a non-gauge, or gauge-reduced, model. Furthermore, let $\mathcal{A}^{\mathrm{G}}$ and $\mathcal{A}^{\mathrm{GR}}$ be the bond-algebra of the gauge and gauge-reduced models, respectively. A *gauge-reducing duality* is a map

$$\Phi^{\mathrm{GR}} : \mathcal{A}^{\mathrm{G}} \to \mathcal{A}^{\mathrm{GR}}$$

such that H^{G} is mapped onto H^{GR} while making all the gauge symmetries of the gauge model trivial:

$$\Phi^{\mathrm{GR}}(H^{\mathrm{G}}) = H^{\mathrm{GR}} \quad \text{and} \quad \Phi^{\mathrm{GR}}(G_\Gamma) = \mathbb{1} \quad \forall \Gamma. \tag{3.66}$$

Unlike the dualities in Sec. 3.4.1, a gauge-reducing duality like Φ_{GR} has to be implementable as a *projective unitary operator* $\mathcal{U}$. Formally, this can be written as

$$\Phi^{\mathrm{GR}}(\mathcal{O}) = \mathcal{U}\mathcal{O}\mathcal{U}^\dagger, \quad \mathcal{U}\mathcal{U}^\dagger = \mathbb{1}, \quad \mathcal{U}^\dagger\mathcal{U} = P_{\mathrm{GI}} \tag{3.67}$$

where P_{GI} is the projector of the subspace of gauge-invariant states, i.e. $G_\Gamma \left|\psi\right\rangle = \left|\psi\right\rangle$ for all Γ. Roughly speaking, this projective unitary operator can be represented as rectangular matrix that preserves the norm of gauge-invariant states while projecting out all the other states.

In the next section we will use an example of gauge-reducing duality, which will be instrumental for the rest of the chapter.

3.4.4 Dualities in two dimensions

As an example of gauge-reducing duality, we will apply the technology introduced in Sec. 3.4.3 to the $\mathbb{Z}_2$ LGT in two-dimensions. We resume the Hamiltonian (3.23)

$$H^{\mathbb{Z}_2} = -\sum_p B_p - \lambda \sum_\ell Z_\ell = -\sum_p B_p - \lambda \sum_x \left(Z_{(x,+\hat{1})} + Z_{(x,+\hat{2})} \right), \tag{3.68}$$

and its Gauss (or vertex) operators

$$A_v = \prod_{\ell \in v} Z_\ell, \tag{3.69}$$

which generate the gauge symmetries and commute with the Hamiltonian

$$\left[H^{\mathbb{Z}_2}, A_v \right] = 0 \quad \forall v \in \mathbb{L}.$$

In particular, each term of the Hamiltonian commutes with the Gauss operators, which means that the bond algebra they generate is gauge-invariant, This bond-algebra satisfy three simple relations:

(i) all the bonds square to the identity,

(ii) each spin Z anti-commutes with two adjacent plaquettes operators U

(iii) each plaquette operator U anti-commutes with four spins Z.

The model $H^{\mathbb{Z}_2}$ is dual to the $d = 2$ QIM. The Hamiltonian of the latter in two-dimensions is

$$H^{\text{Ising}} = -\sum_i \left(\sigma_i^z \sigma_{i+\hat{1}}^z + \sigma_i^z \sigma_{i+\hat{2}}^z + h\sigma_i^x \right), \qquad (3.70)$$

where the index i runs over the sites. One recognizes as separate bonds the terms $\sigma_i^z \sigma_{i+\hat{1}}^z$, $\sigma_i^z \sigma_{i+\hat{2}}^z$, and σ_i^x. It is immediate to see that these bonds satisfy the same relations of the bonds of $H^{\mathbb{Z}_2}$.

The dual model of $H^{\mathbb{Z}_2}$ lives on the dual lattice. Therefore we identify a plaquette p in the gauge model with a site i of the QIM, while x will refer to the lower left site of the plaquette p. With this notation, we can now build the duality mapping $\Phi^{2\text{d}}$ as follows:

$$\Phi^{2\text{d}}(Z_{(x,\hat{1})}) = \sigma_{(i-\hat{2})}^z \sigma_i^z, \quad \Phi^{2\text{d}}(Z_{(x,\hat{2})}) = \sigma_{(i-\hat{1})}^z \sigma_i^z, \quad \Phi^{2\text{d}}(U_p) = \sigma_i^x. \quad (3.71)$$

Applying to $\Phi^{2\text{d}}$ to $H^{\mathbb{Z}_2}$ we obtain

$$\Phi^{2\text{d}}(H^{\mathbb{Z}_2}) = -\sum_i \sigma_i^x - \lambda \sum_i \left(\sigma_{(i-\hat{2})}^z \sigma_i^z + \sigma_{(i-\hat{1})}^z \sigma_i^z \right) = \lambda H^{\text{Ising}}(\lambda^{-1})$$

Thus, $\Phi^{2\text{d}}$ maps $H^{\mathbb{Z}_2}$ to H^{Ising}, up to a multiplicative constant, if we identify the constants $\lambda \leftrightarrow h^{-1}$.

From (3.71), one readily obtains

$$\Phi^{2\text{d}}(G_x) = \mathbb{1},$$

which means that $\Phi^{2\text{d}}$ is in fact a *gauge-reducing duality*. Therefore, H^{Ising} represents all the physics contained in H_{gauge}, but without all the redundant d.o.f. Notice that we started with the "raw" Hamiltonian (3.68) and obtained $\Phi^{2\text{d}}$ without the need of gauge-fixing.

The reason why it is possible to encode the physical content of the gauge model in a simpler QIM is the following. The physical states of a pure gauge model is made of closed electric loops and each electric loop can be thought as containing magnetic flux. So, each physical state can be fully described by indicating which plaquettes contains magnetic flux and which do not. The electric lines naturally arises as domain walls between plaquettes with different flux.

Basically, the duality mapping $\Phi^{2\text{d}}$ assigns to each plaquette a spin-$\frac{1}{2}$ d.o.f, indicating the flux state. Everything else readily follows. The plaquette operator U_p flips the state of the plaquette, therefore it should be mapped to an operator that flips the spin in p, thus σ^x. The electric fields $V_{(x,\hat{1})}$ and $V_{(x,\hat{2})}$ are just domain walls between plaquettes, therefore they should be mapped to interaction terms like $\sigma_{i-\hat{1}}^z \sigma_i^z$ and $\sigma_{i-\hat{2}}^z \sigma_i^z$.

This duality can be extended to $\mathbb{Z}_N$ models in straightforward manner [128]. This requires substituting the Pauli matrices with an equivalent set of operators, that act on a N-dimensional local Hilbert space and satisfy an algebra similar to the Schwinger-Weyl algebra (3.31). These operators are the *clock operators* that define the Quantum Clock Models. We will discuss these models in a bit.

3.5 Dualities of the ladder models

In this section we discuss the main result in [5], which is a construction of a duality map between LGTs on a *ladder geometry* and *Quantum Clock Models*. Before proceeding with construction of the duality map, we briefly describe what are QCMs.

3.5.1 Quantum clock models

Quantum Clock Models (QCMs) are a class of models that generalizes the QIM [129, 130]. They show a resemblance to the $\mathbb{Z}_N$ LGT models we introduced previously, in Sec. 3.2. In fact, this similarity will later be exploited in order to obtain a gauge-reducing duality of the $\mathbb{Z}_N$ LGT ladder models.

The Hamiltonian (3.60) of QIM, with trasverse field, uses Pauli matrices σ^z and σ^x as basic operators and they have the fundamental property that they *anticommutes* on the same site, $\{\sigma_i^z, \sigma_i^x\} = 0$ This relation rewritten as

$$\sigma_i^z \sigma_i^x = -\sigma_i^x \sigma_i^z, \qquad (3.72)$$

which be read as follows: *if the two operators are exchanged, then a phase -1 is acquired.* Another important fact about Pauli matrices we want highlight is that they *square to the identity*:

$$(\sigma_i^x)^2 = (\sigma_i^z)^2 = \mathbb{1}. \qquad (3.73)$$

QCM are generalizations of the QIM, but not to higher spins. A p-state QCM (or simply a p-clock model) utilizes a set of unitary operators that generalizes (3.72) and (3.73) in the following sense: the operators σ^x and σ^z are promoted to the *clock operators* X and Z, respectively; they are $p \times p$ unitary matrices whose exchange produces a phase $\omega = e^{i2\pi/p}$ and their p-th power is equal to the identity. The algebraic properties of these clock operators X and Z can be summarized as follows:

$$\begin{aligned} XZ &= \omega ZX, & X^p &= Z^p = \mathbb{1}_p, \\ X^\dagger &= X^{-1} = X^{p-1}, & Z^\dagger &= Z^{-1} = Z^{p-1} \end{aligned} \qquad (3.74)$$

We see that the Schwinger-Weyl algebra in (3.31) and the clock operator algebra in (3.74) are basically the same, but there are some key differences to point out betweens a $\mathbb{Z}_N$ LGT and a p-clock model.

The d.o.f of a $\mathbb{Z}_N$ LGT live on the links of the lattice while in a p-clock model they live on the sites. But the most important aspect is that we don't have any gauge symmetry in a p-clock model, hence we do not have to impose any local constraints or physical conditions. These models can be derived as the quantum Hamiltonians of the classical 2D vector Potts model, which is a discretization of the 2D planar XY model [7].

A typical p-clock model Hamiltonian with transverse field has the form

$$H^{N\text{-clock}}(\lambda) = -\sum_i Z_i Z_{i+1} - \lambda \sum_i X_i + \text{h.c.} \tag{3.75}$$

which is, as expected, very similar to the quantum Ising Hamiltonian in (3.60). Furthermore, just like the latter, p-clock models with only transverse field are *self-dual*: the clocks can be mapped into the kinks (or domain walls) and one would obtain the same exact Hamiltonian description but with inverted transverse field [7]. For $p < 5$, the clock models present a self dual point for $\lambda = 1$, that separates an ordered phase from a disordered one. On the other hand, for $p \geq 5$ we have an intermediate continuous critical phase between the ordered and disordered phase with two BKT transition points, which are related to each other through the self-duality [131].

These models have been thoroughly studied, even with the addition of a longitudinal field proportional to Z_i [132] or chiral interactions. In particular, in the case of chiral interactions, it was shown [133] that the Hamiltonian (3.75) can be mapped to a parafermionic chain through a Fradkin-Kadanoff transformation, and in presence of a $\mathbb{Z}_3$ symmetry, it shows three different phases [134], if open boundaries are implemented: a trivial, a topological and an incommensurate (IC) phase. The case which presents a real longitudinal field term was considered in [135], where some of the critical exponents have been estimated. The general case, where chiral interactions are included in a $\mathbb{Z}_N$ model, has been studied in [133]. Here, the author considered the model as an extension of the Ising/Majorana chain and found the edge modes of the theory. He also calculated the points, in the parameter space, where the model is integrable or 'superintegrable'. All these studies are motivated by theoretical interest and recent experiments, which can be analysed by the above models [136].

3.5.2 Gauge-reducing duality onto clock models

In this section we will show one of the main result of [5]: how to construct a mapping of the $\mathbb{Z}_N$ ladder LGT onto a N-clock model on a chain with a transversal field and a longitudinal field, the latter depending on the super-selection sector of the ladder LGT.

The first step is the decomposition of the set of bonds in (3.40). Obviously, the magnetic terms $U_\square$ have to be separated from the electric terms V_ℓ, but the latter cannot be all treated the same. It is clear from the geometry of the ladder, that the links ℓ^0 have a different role when compared with the links $\ell^\uparrow$ and $\ell^\downarrow$, because the former are *domain walls* while the latter are not. Therefore, the duality transformation has to distinguish between the vertical links and horizontal links. Furthermore, also the top links $\ell^\uparrow$ and bottom links $\ell^\downarrow$ have to be treated separately because the electric operator on them have different commutation relations with the plaquette operators. In fact, using the notation introduced in Sec. 3.3, we have

$$U_i V_i^\downarrow = \omega V_i^\downarrow U_i, \qquad U_i V_i^\uparrow = \omega^{-1} V_i^\uparrow U_i. \tag{3.76}$$

and indeed they acquire different phases.

The plan is to associate to each plaquette a clock degree of freedom, hence we identify a plaquette $\square_i$ with a site i of a clock chain and the magnetic flux of a plaquette becomes the "fundamental gauge invariant degree of freedom" of the LGT ladder model. Given the fact that we are working in the electric basis, we chose for convenience to map the $\mathbb{Z}_N$ magnetic operator U_i to the "momentum" operator X_i of the N-clock chain. The electric field on a vertical link ℓ^0 is the result of the flux difference between the two plaquettes that it separates, which suggests that the operator V^0 have to be mapped to a kinetic-type term like $Z_i^\dagger Z_{i-1}$. This can be readily verified. From (3.51) we get

$$V_i^0 U_i = \omega^{-1} U_i V_i^0, \qquad V_i^0 U_{x-1} = \omega U_{x-1} V_i^0,$$

therefore the maps
$$U_i \mapsto X_i, \qquad V_i^0 \mapsto Z_i^\dagger Z_{i-1},$$

clearly conserves the commutation relations of U_i and V_i^0.

For now we are left with task of finding a suitable mapping of $V^\uparrow$ and $V^\downarrow$. With respect to the other bonds of the theory, both of them commute with V^0 while for (3.76) holds for U_i. Hence, a suitable and general mapping of $V^\uparrow$ and $V^\downarrow$ can be:
$$V_i^\downarrow \mapsto c_i^\downarrow Z_i, \qquad V_i^\uparrow \mapsto c_i^\uparrow Z_i^\dagger, \tag{3.77}$$

where $c_i^\downarrow$ and $c_i^\uparrow$ are complex numbers. Although, they cannot be any complex number. Both $V_i^\downarrow$ and $V_i^\uparrow$ have to be mapped onto unitary operators, which limits the numbers $c_i^\downarrow$ and $c_i^\uparrow$ to be *complex phases*.

To further constraint the value of these coefficients, we can use the Gauss law. In particular, given the fact that we are looking for a gauge-reducing duality, the aim is to make the Gauss law trivial. Using the mappings (3.5.2) and (3.77) in (3.52) yields

$$
\begin{aligned}
G_i^\uparrow &\mapsto (c_i^\uparrow Z_i^\dagger)(c_{i-1}^\uparrow Z_{i-1}^\dagger)(Z_i^\dagger Z_{i-1})^\dagger = c_i^\uparrow (c_{i-1}^\uparrow)^*, \\
G_i^\downarrow &\mapsto (c_i^\downarrow Z_i^\dagger)(Z_i^\dagger Z_{i-1})(c_{i-1}^\downarrow Z_{i-1}^\dagger) = c_i^\downarrow (c_{i-1}^\downarrow)^*
\end{aligned}
\tag{3.78}
$$

Gauss law have to be satisfied in a pure gauge theory, which mean that we have to impose $G_i^\uparrow = \mathbb{1}$ and $G_i^\downarrow = \mathbb{1}$ for all i. This is only possible if

$$
c_i^\downarrow = c^\downarrow, \qquad c_i^\uparrow = c^\uparrow, \qquad \forall i.
\tag{3.79}
$$

Furthermore, thanks to (3.78) we also know how to introduce static matter into this duality, because it can be thought as a violation of the Gauss law. We just have to change the phases $c_i^\uparrow$ and $c_i^\downarrow$.

The last factor to consider is how the $c^\uparrow$ and $c^\downarrow$ are related on the same site i. In this regard, the super-selection sectors of the theory come to the rescue. As established in Sec. 3.3, the super-selection sectors are identified by the eigenvalue of S_2 in (3.39), which in the ladder geometry becomes

$$
S_2 = V_i^\uparrow V_i^\downarrow
\tag{3.80}
$$

for any fixed x. Its eigenvalue are simply ω^k, for $k = 0, \ldots, N-1$.

Given a super-selection sector ω^k, using the mapping (3.77) on (3.80) yields

$$
S_2 \longmapsto (c^\uparrow Z_i^\dagger)(c^\downarrow Z_i) = c^\uparrow c^\downarrow = \omega^k.
\tag{3.81}
$$

Here, one is free to choose $c^\uparrow$ and $c^\downarrow$, given that their product has to be equal to ω^k. This freedom corresponds to a *global* symmetry of the system and it has nothing to due with the gauge symmetries, because the latter has already been solved. We choose to fix $c^\uparrow$ to 1 and $c^\downarrow$ to ω^k:

$$
c^\uparrow = 1, \qquad c^\downarrow = \omega^k.
\tag{3.82}
$$

In conclusion, we summarize the duality mapping for the super-selection sector ω^k of the $\mathbb{Z}_N$ LGT on a ladder:

$$
\begin{aligned}
U_i &\longmapsto X_i, & V_i^0 &\longmapsto Z_i^\dagger Z_{i-1}, \\
V_i^\uparrow &\longmapsto Z_i^\dagger, & V_i^\downarrow &\longmapsto \omega^k Z_i.
\end{aligned}
\tag{3.83}
$$

With the duality (3.83), from (3.53) in the sector $(\omega^k, 1)$ we obtain

$$H^{N\text{-lad}}(\lambda) \longmapsto \lambda H^{N\text{-dual}}(\lambda^{-1}) \tag{3.84}$$

where $H^{N\text{-dual}}$ is the dual N-clock Hamiltonian:

$$H^{N\text{-dual}}(\lambda^{-1}) = -\sum_i \left(Z_i^\dagger Z_{i-1} + \lambda^{-1} X_i + (1+\omega^k)Z_i + \text{h.c.} \right) \tag{3.85}$$

We see that (3.85) is a clock model with both *transversal* and *longitudinal* fields. In particular, the longitudinal field carries the information of the super-selection sector of the ladder model.

Interestingly, for N even the sector $k = N/2$ has a special role. Within this sector $\omega^k = -1$, for which the *longitudinal field disappears* and $H^{N\text{-clock}}$ reduces to self-dual quantum clock models with a known quantum phase transition. This phase transitions for $k = N/2$ can be put in correspondence with a *confined-deconfined* transition, which will be discussed in much more detail in the next section.

Let us remark that the complex coupling $(1 + \omega^n)$ does not make the Hamiltonian (3.85) necessarily chiral [133, 137]. In fact, one can get the real Hamiltonian

$$H^{N\text{-dual}}(\lambda^{-1}) = H^{N\text{-clock}}(\lambda^{-1}) - 2\cos\left(\frac{\pi n}{N}\right) \sum_i \left(Z_i + Z_i^\dagger \right). \tag{3.86}$$

by absorbing the complex phase in the Z_i-operators, with the transformation $Z_i \mapsto \omega^{-n/2} Z_i$. This transformation globally rotates the eigenvalues of the Z_i-operators, while preserving the algebra relations. For n even, this is just a permutation of the eigenvalues, meaning that it does not affect the Hamiltonian spectrum. Instead, for n odd, up to a reorder, the eigenvalues are shifted by an angle π/N, i.e. half the phase of ω. In the latter case we will denote the rotated Z_i operator with $\tilde{Z}_i$. The energy contribution of the extra term in (3.86) depends on the real part of these eigenvalues and for n odd we obtain that the lowest energy state is no longer unique, in fact it is doubly degenerate. This means that for $\lambda \to \infty$, where the extra term becomes dominant, we expect an ordered phase with a doubly degenerate ground state. Finally, one can easily prove that the sectors n and $N - n$ are equivalent [1].

3.6 A case study: $N = 2, 3$ and 4

In this section we present the results of the numerical investigations of [5]. But first, we present the reasoning for the choice of order parameters used for

---

[1]For the sector $N - n$ we have that the overall factor $\cos(\pi(N-n)/N)$ is just $-\cos(\pi n/N)$. The minus sign can then be again absorbed into the Z's operators. This overall operation is equivalent to the mapping $Z \mapsto \omega^{-n/2} Z$ for the sector $N - n$.
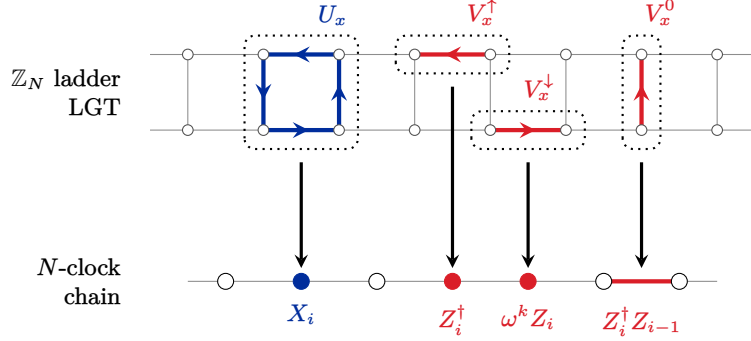
Figure 3.15. Visual representation of the duality transformation from the $\mathbb{Z}_N$ ladder LGT to the N-clock model. The plaquette operator U_i and the electric operators $V^\uparrow$ and $V^\downarrow$ map to one-site operators in the clock model, while the remaining electric operator V^0 maps to a hopping term between nearest neighbouring sites.

investigating the phase diagram, and second we show how the duality have been used for resolving the Gauss law in numerics.

3.6.1 Investigating the phase diagram

We wish to study the phase diagram of the $\mathbb{Z}_N$ LGT phase diagram, in particular we are interested in any deconfined-confined phase transition (DCPT). In a pure gauge theory, these phases are investigated with non-local order parameters like the *WL* (WL) (not be confused with the non-contractible WLs in (3.39)). This is because we expect the deconfined phase to be a topological phase, which can be investigated only with non-local order parameters.

Given a closed region $\mathcal{R}$, a WL operator $W_\mathcal{R}$ is defined as

$$W_\mathcal{R} = \prod_{\square \in \mathcal{R}} U_\square. \tag{3.87}$$

Alternatively, considering the oriented boundary $\partial\mathcal{R}$ one can write

$$W_\mathcal{R} = \prod_{\ell \in \partial\mathcal{R}} U_\ell, \tag{3.88}$$

where the Hermitian conjugate is implied every time we move in the negative directions. It is also implied that the curve $\partial\mathcal{R}$ is a contractible loop. As explained in Sec. 1.2.2, quark confinement is related to the expectation value $\langle W_\mathcal{R} \rangle$ of a WL, which can be thought as a gauge field average over the region $\mathcal{R}$. In particular, in the presence of quark confinement the gauge field average follows an *area law*, where it decays exponentially with the area enclosed by $\mathcal{R}$. On the other hand, in the deconfined phase we have a *perimeter law*, where the gauge field average decays exponentially with the perimeter of $\mathcal{R}$.
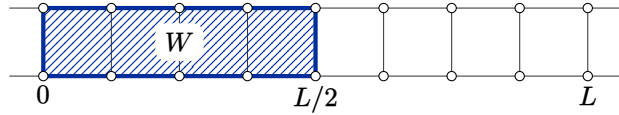
Figure 3.16. Half-ladder Wilson loop on the ladder. Notice that W can only grow in one direction, meaning there is no difference in scaling between the area and the perimeter. Nonetheless, it still can be used for distinguishing phases.

Unfortunately on a ladder geometry there is not much difference between the area and the perimeter of a WL. In fact, in units of the lattice spacing, the area of a WL over n plaquettes is n while its perimeter is just $2n + 2$. They both grow linearly. Nonetheless, we can still look at the behaviour of the WL, for a fixed length, at different couplings λ, for the following reason.

When the coupling λ in (3.40) is equal to zero, the TC is recovered and in any of its topological sector the ground state is the equal superposition of all the states with any number of closed electrical loops, in a similar fashion to coherent states. This makes the TC a *quantum loop gas*, which is a *deconfined phase*. Furthermore, the operator $W_\mathcal{R}$ in (3.87) creates an electrical loop around the region $\mathcal{R}$. From the ground state constraints of the TC (3.7), it can easily be proved that $W_\mathcal{R}$ leaves its ground states unchanged, showing in fact that they behaves as coherent states, which leads to $\langle W_\mathcal{R} \rangle = 1$.

Therefore, $\langle W_\mathcal{R} \rangle \approx 1$ signals a deconfined phase and, on the other hand, a vanishing $\langle W_\mathcal{R} \rangle \approx 0$ would correspond to confined phase. This is what is expected in the opposite limit, $\lambda \to \infty$, when only the electric term survives. For this reason, even tough we lack an area/perimeter law on the ladder geometry it is still sensible to look at the behaviour of the WL. Analogous models in two-dimensions show that there is indeed a transition for non-zero λ [116–118].

In the dual clock model picture, the WL translates to a disorder operator [126], which means that a deconfined phase can be thought of as a paramagnetic (or disordered) phase, while the confined phase is like a ferromagnetic (or ordered) phase. Moreover, the longitudinal field breaks the N-fold symmetry of the ferromagnetic phase into a one-fold or two-fold degeneracy, depending on the parity (n even/odd) of the super-selection sector.

For the reasons showed above, we have decided to study the $\mathbb{Z}_N$ LGT on a ladder by evaluating the half-ladder WL (see Fig. 3.16):

$$W = U_1 U_2 \cdots U_{L/2}. \tag{3.89}$$

Additionally, we have also decided to study each physical subspace $\mathcal{H}_{\text{phys}}^{(n)}$ (for $n = 0, \ldots, N-1$) separately, because we wanted to investigate if the choice of super-selection sector has any effect on the phase diagram. This motivated us
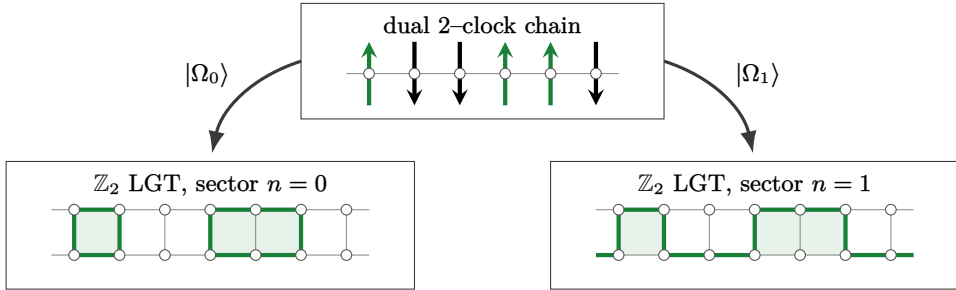
Figure 3.17. Duality between the states of a 2–chain and the states of a $\mathbb{Z}_2$ ladder LGT in the different sectors $n = 0$ (no non-contractible electric loop) and $n = 1$ (one non-contractible loop around the ladder). In the sector $n = 0$ it is evident that all the physical states contains closed electric loops. On the other hand, in the sector $n = 1$ the physical states are all the possible deformation of the electric string that goes around the ladder.

to use ED, where the state space can be implemented exactly. The physical subspace $\mathcal{H}_{\text{phys}}^{(n)}$ has dimension N^L, much smaller than N^{3L} (the dimension of the total Hilbert space), hence it allows for larger lattice sizes for ED.

3.6.2 Implementing the Gauss law in numerics

In order to proceed with ED one has to provide two things:

- the basic operators of the theory (U_ℓ and V_ℓ);

- the physical Hilbert space, given a lattice with specified size and boundary conditions.

The former is fairly standard, while the latter is the most challenging and interesting aspect to implement.

If one has to work with only physical states, then one has to check the Gauss law for every site. With the brute-force method one has to generate all the possible states and then filter out all the states that violate Gauss law. This method, like any brute-force method, is not very efficient. To better exemplify this, consider a $\mathbb{Z}_2$ theory on a $L \times L$ periodic lattice, which have L^2 sites and $2L^2$ links. There are therefore 2^{2L^2} possible configurations and for each one up to L^2 checks (one per site) has to be performed. Moreover, it can be showed that there are only 2^{L^2} *physical* states. As a result, the construction of the physical Hilbert space involves $O(L^2 2^{2L^2})$ operations in a search space of 2^{2L^2} objects for finding only 2^{L^2} elements. All of this makes the inefficiency of this brute-force method very clear, even for moderately small lattices.

The approach adopted in this work exploits the duality in Sec. 3.5 and represents an *exponential speedup* with respect to the brute-force method. It

is not a search or pattern-matching algorithm, each physical configuration is procedurally generated from the states of the dual clock model.

Given a $\mathbb{Z}_N$ LGT on a lattice of size $L \times L$, we consider the dual N-clock model on a similar lattice with $A = L^2$ sites. In its Hilbert space $\mathcal{H}_{N\text{-clock}}$ there is no gauge constraint or to apply, hence the basis is the set of states $|\{s_i\}\rangle \equiv |s_0 s_1 \cdots s_{A-1}\rangle$ with each $s_i = 0, \ldots, N - 1$. Each state s_i of the dual clock model corresponds to the flux state in the i-th plaquette of the gauge model. Additionally, the operators U_i and $U_i^\dagger$ act as "creation" or "annihilation" operators on the flux state (respectively), meaning that they increase or decrease the flux in the i-th plaquette. Hence, if we establish first what the $|0 \cdots 0\rangle$ clock state would correspond in the gauge model, then we can proceed to obtain the dual to a generic state $|\{s_i\}\rangle$ by applying the U_i operators. The clock state $|0 \cdots 0\rangle$ is the Fock vacuum from which every other clock state can be obtained, by applying the X_i clock operators. The corresponding state in the gauge model would be a state with no flux in the plaquettes. In this regard, the "Fock vacuum" is not unique. There is one vacuum for each super-selection sector.

Therefore, from a clock state $|\{s_i\}\rangle$ we can obtain the dual gauge state model in the (m, n) sector, by means of powers of U_i:

$$|\{s_i\}\rangle \longmapsto \prod_{i=0}^{A-1} U_i^{s_i} |\Omega_{(n,m)}\rangle, \qquad (3.90)$$

where U_i is the plaquette operator on the i-th plaquette and $|\Omega_{(m,n)}\rangle$ is the "Fock vacuum" of the (m, n) sector.

Moreover, the "Fock vacua" $|\Omega_{(n,m)}\rangle$ can be obtained easily, thanks to (3.49):

$$|\Omega_{(n,m)}\rangle = (\overline{W}_1)^n (\overline{W}_2)^m |\Omega_{(0,0)}\rangle, \qquad (3.91)$$

where $\left|\Omega_{(0,0)}\right\rangle$ is just the state $|000 \cdots 0\rangle$ in the electric basis of the gauge model, where all the links are in zero electric field state (see Fig. 3.18).

As one can deduce, the information about the super-selection sector of the LGT model is carried out in the Hamiltonian $H_{N\text{-clock}}$ of the dual clock model and not in the structure of $\mathcal{H}_{N\text{-clock}}$ itself. This means that is possible to build each sector $\mathcal{H}_{\text{phys}}^{(n,m)}$ in (3.45) from $\mathcal{H}_{N\text{-clock}}$, with the appropriate $\left|\Omega_{(n,m)}\right\rangle$. In order to simplify notation, we will denote the vacua of the ladder model simply as $|\Omega_n\rangle$ for the n-th sector.

If we want to quantify the obtained speedup with this method, in the case of a $\mathbb{Z}_2$ theory on a square lattice $L \times L$ there are 2^{L^2} possible clock configurations. For each configuration, there are at most L^2 magnetic fluxes to apply. This translates into $O(L^2 2^{L^2})$ operations, which is an exponential
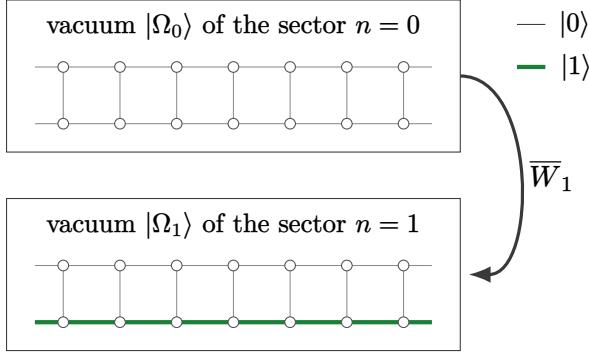
Figure 3.18. The different "Fock vacua" $|\Omega_0\rangle$ and $|\Omega_1\rangle$ of the $\mathbb{Z}_2$ ladder LGT. The latter can be obtained from the former by applying the WL operator W_1. The states $|0\rangle$ and $|1\rangle$ refers to the eigenstates of the electric field operator V, which is just σ_z in the $\mathbb{Z}_2$ model.

speedup with respect to the brute-force (notice the lack of a factor 2 in the exponent) and is easily generalizable for any $\mathbb{Z}_N$. Although, it remains an open question whether a similar method can be applied for gauge theories with non-Abelian finite groups.

3.6.3 Numerical results

In the following, we present the results with $N = 2, 3$ and 4, for different lengths.

Results for $N = 2$

As a warm up, we consider the $\mathbb{Z}_2$ ladder LGT, with lengths $L = 10, 12, \ldots, 18$. This model is equivalent to a $p = 2$ clock model, which is just the quantum Ising chain, with only two super-selection sectors for $n = 0$ and $n = 1$. The dual Hamiltonian (3.86) for $\mathbb{Z}_2$ and sector $n = 0$ is

$$H_{n=0}^{2\text{-dual}}(\lambda^{-1}) = H^{2\text{-clock}}(\lambda^{-1}) - 2\sum_i \left(Z_i + Z_i^\dagger \right), \qquad (3.92)$$

while for $n = 1$ we just have

$$H_{n=1}^{2\text{-dual}}(\lambda^{-1}) = H^{2\text{-clock}}(\lambda^{-1}). \qquad (3.93)$$

When $n = 1$ the Hamiltonian $H^{2\text{-dual}}$ contains only the transverse field, hence it is integrable [132]. Thus, we expect a critical point for $\lambda \simeq 1$, which will be a DCPT in the gauge model language. This is clearly seen in the behaviour of the half-ladder WL, as shown in the lower panel of Fig. 3.19. For $n = 0$, both the transverse and longitudinal fields are present, hence the model is no longer integrable [138–140] and we expect to always see a confined phase,
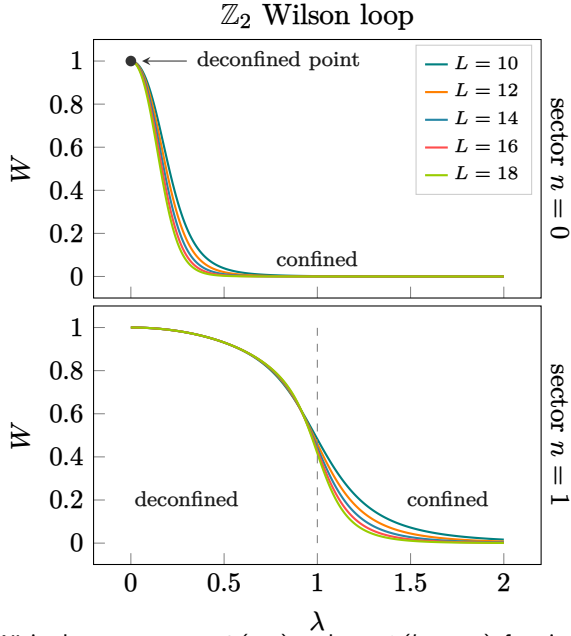
Figure 3.19. $\mathbb{Z}_2$ WL in the sectors $n = 0$ (*top*) and $n = 1$ (*bottom*), for sizes $L = 10, 12, \ldots, 18$. The sector $n = 0$ presents only a deconfined point at $\lambda = 0$ and then decays rapidly into a confined phase, while the sector $n = 1$ has a phase transition for $\lambda \simeq 1$.

except for $\lambda = 0$. This is indeed confirmed by the behaviour of the half-ladder WL shown in the upper panel of Fig. 3.19.

Notice that for $n = 0$ in Fig. 3.19, there is a lack of line crossings between values of WL for different L. This suggests that in the thermodynamic limit, we will have a single point $\langle W \rangle \neq 0$ for $\lambda = 0$, and a flat line $\langle W \rangle = 0$ for $\lambda \neq 0$, confirming the prediction of a always confining phase (excluded $\lambda = 0$).

We can further characterize the phases of the two sectors by looking at the structure of the ground state, for $\lambda < 1$ and $\lambda > 1$, which is possible thanks to the exact diagonalization. In particular, in the deconfined phase of the sector $n = 1$, the ground state is a superposition of the deformations of the non-contractible electric string that makes the $n = 1$ vacuum $|\Omega_1\rangle$. For this reason, this phase can be thought as a *kink condensate* [126] (which is equivalent to a paramagnetic phase), where each kink corresponds to a deformation of the string. Instead, for $\lambda > 1$, where we have confinement (as in the $n = 0$ sector), the ground state is essentially a product state, akin to a ferromagnetic state. This analysis has been performed at the end of Sec. 3.6.3.

Results for $N = 3$

The $\mathbb{Z}_3$ LGT is studied for lengths $L = 7, 9, 11$ and 13. This model can be mapped to a 3-clock model, which is equivalent to a 3-state quantum Potts

model with a longitudinal field, which is present in all sectors, as one can see from (3.86). The dual Hamiltonian $H^{3\text{-dual}}(\lambda^{-1})$ for the sector $n = 0$ is

$$H^{3\text{-dual}}_{n=0}(\lambda^{-1}) = H^{3\text{-clock}}(\lambda^{-1}) - 2\sum_i \left(Z_i + Z_i^\dagger\right), \qquad (3.94)$$

while for $n = 1$ and 2 (which are symmetric to each other) we have

$$H^{3\text{-dual}}_{n=1,2}(\lambda^{-1}) = H^{3\text{-clock}}(\lambda^{-1}) - 2\cos\left(\frac{\pi}{3}\right)\sum_i \left(\tilde{Z}_i + \tilde{Z}_i^\dagger\right). \qquad (3.95)$$

Remember that $\tilde{Z}_i$ stands for the Z_i operator with eigenvalues shifted by $\omega^{1/2} = e^{i\pi/N}$. In all three cases we have a longitudinal field, which is expected to disrupt any paramagnetic state. Thus, we do not expect to observe a phase transition, and this is confirmed by the behaviour observed in Fig. 3.20. Meanwhile, all the sectors present a deconfined point at $\lambda = 0$, as expected.

In the case $n = 0$, for $\lambda > 0$ we recognize a quick transition to a confined phase, similar to what happens in [141]. This behaviour is similar to what has been observed for the $\mathbb{Z}_2$ and $n = 0$ case in Fig. 3.19, hence the same reasoning apply. While for $n = 1$ and 2 (which are equivalent), the model exhibits a smoother *crossover* to an ordered phase characterized by a doubly-degenerate ground state, for $\lambda > 1$. Notice that, as discussed above, the presence of the "skew" longitudinal field breaks the three-fold degeneracy expected in the ordered phase of the 3-clock model into a two-fold degeneracy only. Additionally, for $L = 13$ we notice that a slight bump start to appear. If some speculation is allowed, this fact, united with the crossover region, may suggest that there is some intermediate phase between the deconfined point and the confined region. For this kind of analysis, higher lattice sizes are necessary which means that ED is no longer adequate. Thankfully, now that we are confident in the duality between ladder LGTs and QCMs, we can directly study this region in the QCMs setup, by simulating (3.95) with for example DMRG.

Results for $N = 4$

The $\mathbb{Z}_4$ ladder LGT have four super-selection sectors. The behaviour of half-ladder WLs as function of λ is shown in Fig. 3.21. The Hamiltonian in the first sector, $n = 0$, is

$$H^{4\text{-dual}}_{n=0}(\lambda^{-1}) = H^{4\text{-clock}}(\lambda^{-1}) - 2\sum_i \left(Z_i + Z_i^\dagger\right), \qquad (3.96)$$

As in the previous models, for $n = 0$ we see a deconfined point at $\lambda = 0$, followed by a sharp transition to a confined phase. Likewise, the lack of line
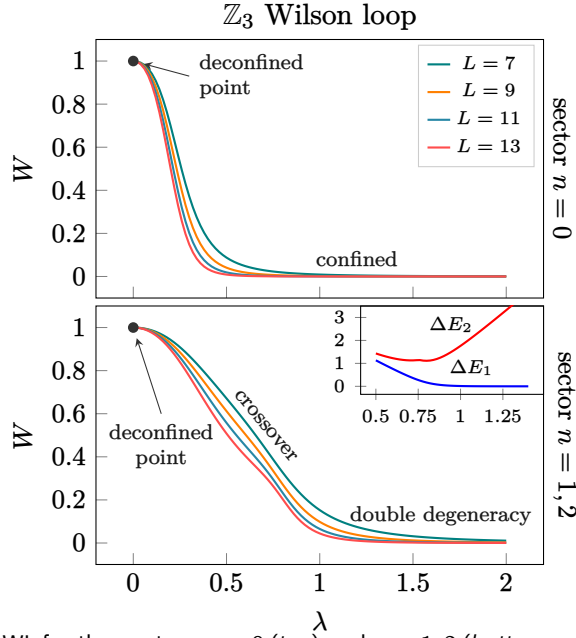
Figure 3.20. $\mathbb{Z}_3$ WL for the sectors $n = 0$ (*top*) and $n = 1, 2$ (*bottom*, which are equivalent), for sizes $L = 7, 9, 11$ and 13. Inset: energy differences $\Delta E_i = E_i - E_0$ for $i = 1, 2$, as a function of the coupling λ, in the sectors $n = 1, 2$, showing the emergence of a double-degenerate ground state for $\lambda > 1$.

crossings of the WL at different L suggests that in the limit $L \to \infty$ we will only have $\langle W \rangle \neq 0$ for $\lambda = 0$.

The dual Hamiltonian of the sector $n = 2$,

$$H_{n=2}^{4\text{-dual}}(\lambda^{-1}) = H^{4\text{-clock}}(\lambda^{-1}), \tag{3.97}$$

has no longitudinal field, it is the only one to present a clear DCPT for $\lambda \approx 1$, as it is expected from the fact that the 4-clock model is equivalent to two decoupled Ising chains [7].

In the two equivalent sectors $n = 1$ and 3, where the dual Hamiltonian is

$$H_{n=1,3}^{4\text{-dual}}(\lambda^{-1}) = H^{4\text{-clock}}(\lambda^{-1}) - 2\cos\left(\frac{\pi}{4}\right) \sum_i \left(\tilde{Z}_i + \tilde{Z}_i^\dagger\right), \tag{3.98}$$

the longitudinal field is non-zero and the WL shows a peculiar behaviour, at least for the largest size ($L = 10$) of the chain: it decreases fast as soon $\lambda > 0$, to stabilize to a finite value in the region $0.5 \lesssim \lambda \lesssim 1$, before tending to zero. It is comparable to $\mathbb{Z}_3$ and $n = 1, 2$ situation, where a slight bump appear when the size L is increased. The characteristics of this phase (with the crossover region for $\mathbb{Z}_3$ and $n = 1, 2$) would deserve a deeper analysis, that we plan to do in a future work. For $\lambda \gtrsim 1$, the system enters a deconfined phase with a double degenerate ground state, as for the $\mathbb{Z}_3$ model.
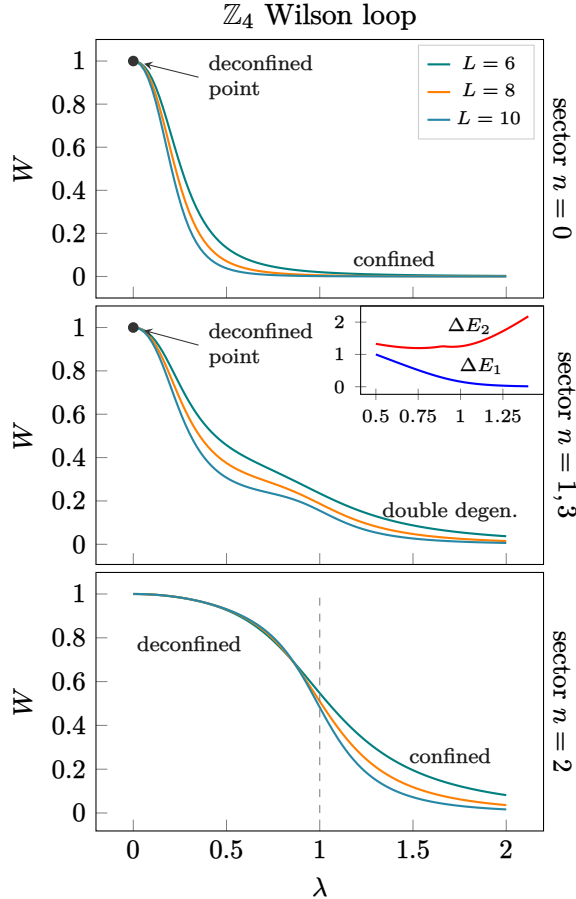
Figure 3.21. $\mathbb{Z}_4$ WL for sectors $n = 0, \ldots, 3$ and sizes $L = 6, \ldots, 10$. Only the sector $n = 2$ has a clear deconfined-confined phase transition, as expected from the duality with the 4-clock model.

Distribution of the amplitudes of the ground state

In the $N = 2$ case, we further differentiate the phase diagrams of the two sectors by looking at the ground state amplitudes distribution, for $\lambda < 1$ and $\lambda > 1$. Obviously, the ground state can be written as a superposition of the gauge invariant states of $\mathcal{H}_{\text{phys}}$ in the given sector

$$|\Psi_{\text{g.s.}}\rangle = \sum_n c_n |n\rangle, \tag{3.99}$$

The basis $|n\rangle$ and the amplitudes c_n are sorted in a decreasing order with respect to the modulus of the latter. The first state of the list, with amplitude c_1, is always the Fock vacuum $|\Omega\rangle$ of the sector, hence we consider the distribution of the ratios $|c_n/c_1|$, which are plotted in Fig. 3.22–3.23 for $\lambda = 0.1$ and $\lambda = 1.5$, respectively. The most interesting one is at $\lambda = 0.1$, where the difference between the deconfined phase in the sector $n = 1$ and the

confined one in the sector $n = 0$ can be seen. In particular, in the deconfined phase the ground state is a superposition of deformations of the Fock vacuum, i.e the non-contractible electric string, which can be thought as a *kink condensate* [126] (or as a paramagnetic phase), where each kink corresponds to a deformation of the string. Meanwhile, for $\lambda > 1$, where we have confinement in both sectors, the ground state is essentially a product state, akin to a ferromagnetic state. This is explained in Fig. 3.22 and Fig. 3.23.

3.7 Concluding remarks

In this work, we proposed an exact gauge preserving duality transformation that maps the $\mathbb{Z}_N$ lattice gauge theory on a ladder onto a 1D $N-$clock model in a transversal field, coupled to a possibly complex longitudinal field which depends on the super-selection sector.

This map allowed us to perform numerical simulations with an ED algorithm with sizes up to $L = 18, 13, 10$ for $N = 2, 3, 4$ respectively. To study the phases of the model and a possible DCPT transition, we calculated the Wilson loops in the different topological sectors, finding an unusual behaviour in the sectors with n odd (mod N), possibly suggesting the emergence of a new phase, such as for example the incommensurate phase appearing in chiral clock models [134, 137, 142], whose characterization requires however to consider longer sizes of the chain in order to evaluate the asymptotic behaviour of correlators.

This will be the subject of future work, in which we can also consider the possibility to include static and dynamical matter in the lattice gauge model. Another possible direction would be the extension of these duality transformations to non-Abelian gauge theories.
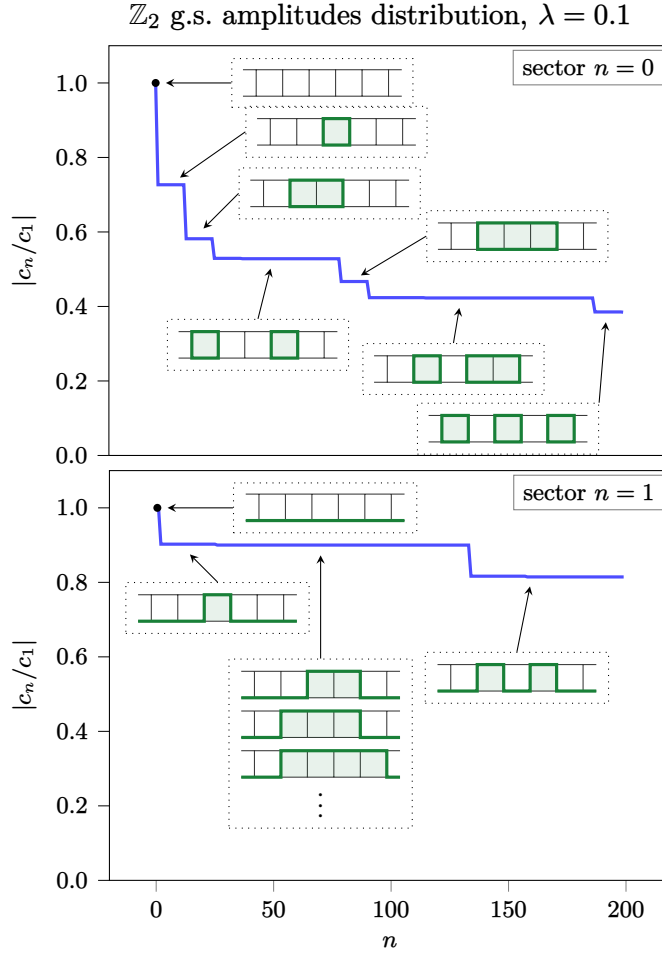
Figure 3.22. $\mathbb{Z}_2$ ground state amplitude distribution for $\lambda = 0.1$ of the first 200 states and with lattice size 12×2. *Top*: distribution of the ratios $|c_n/c_1|$ for the sector $n = 0$ (see (3.99)). We see that the heaviest states that enters the ground state, apart from the vacuum that sets the scale, are made of small electric loops, typical of a confined phase. *Bottom*: the same distribution of ratios for the sector $n = 1$. We see that the heaviest states are made of bigger and bigger deformations of the electric string that goes around the ladder. This happens because the energy contributions depends only on the domain walls between two plaquettes with different flux content. This behaviour is similar to the so-called *kink condensation* in spin chains [126], where the disordered state can be expressed as a superposition of all possible configuration of kinks (i.e. domain walls between two differently ordered regions). In the language of the duality, this deconfined phase then maps to the paramagnetic phase of the quantum Ising model with *only* transverse field.
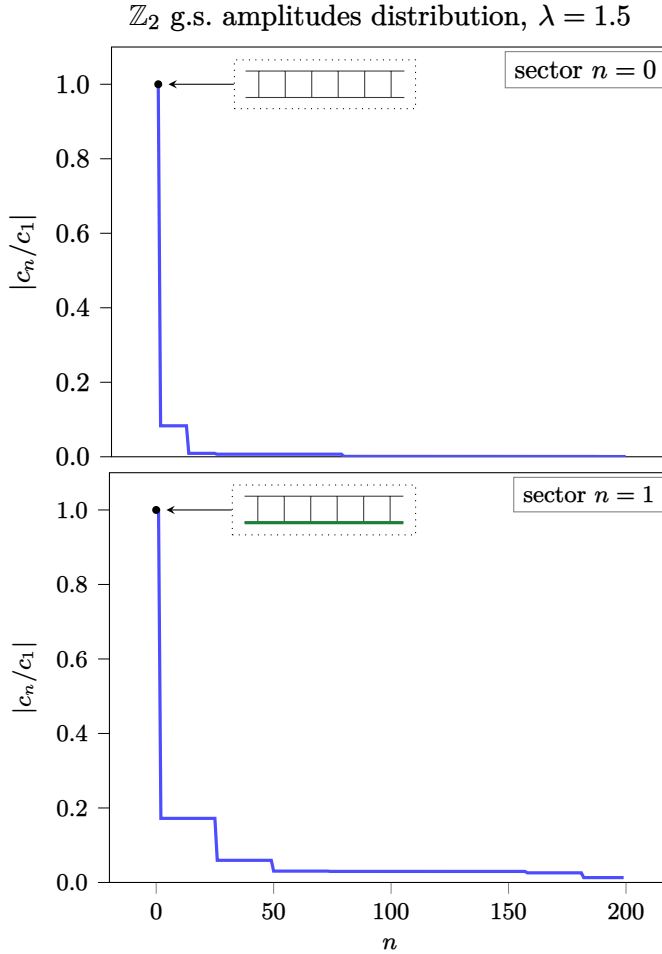
Figure 3.23. $\mathbb{Z}_2$ ground state amplitude distribution for $\lambda = 1.5$ of the first 200 states and with lattice size 12×2. *Top*: distribution of the ratios $|c_n/c_1|$ for the sector $n = 0$ (see (3.99)). *Bottom*: the same distribution of ratios for the sector $n = 1$. For both sectors $n = 0$ (*top*) and $n = 1$ (*bottom*) we are in a confined phase, which corresponds to a ferromagnetic phase in the dual model (the QIM). Here we see a polarized state where the domain walls are suppressed and the ground state is essentially a product state.

Finite Group Gauge Theories

In this chapter we present the work [6], where a class of finite group LGT in the Hamiltonian formulation are considered.

One of the main results of [6] is the construction of an electric term, that admits an interpretation of as a *Laplacian operator on the group*. This construction is valid in both Abelian or non-Abelian case. The characterization of the Hamiltonian using the finite-group Laplacian may be used to obtain non-trivial physical information about the theory.

Another important finding of [6], is the construction of the physical, gauge-invariant Hilbert space, independently of the choice of Hamiltonian. This relies on the use of *spin network states*, which are particularly suitable in the case of finite groups. Based on this fact, we derive a simple formula for computing the dimension of the physical Hilbert space.

Finally, we illustrate the use of the gauge-invariant basis by constructing the Hamiltonian for a gauge theory based on the dihedral group and compute some quantities of interest via ED.

4.1 Ingredients for finite groups

In this section we develop an Hamiltonian approach to finite group LGT, by showcasing the necessary ingredients. These main ingredients are basically the Hilbert space and the Hamiltonian operator. Regarding the Hilbert space, we will show that are two possible choices of basis, that are roughly analogous to a "position basis" and "momentum basis". The first would corresponds to the group element basis, while the second to the irreducible representation basis.

As for the Hamiltonian operator, we will focus more on the electric term because the magnetic term is pretty straightforward. As anticipated, the electric Hamiltonian admits an interpretation as a certain natural Laplacian operator on the group. This Laplacian is non-unique, which means that for a given gauge group G we can have an entire family of LGTs. This construction extends the electric term used in the Kogut-Susskind formulation [8] of LGTs,

based on Lie groups, to finite groups. At the end of the section we will also review the question of Lorentz invariance and classification of the possible models.

4.1.1   The Hilbert space and gauge invariance

In the Hamiltonian formulation of LGTs [8, 95, 98], time is continuous while the d spatial dimensions are discretized into a hypercubic lattice $\mathbb{L}$. The definition of the Hilbert space for both a compact Lie group or a finite group is substantially the same. As we have seen in Sec. 1.2, a group element $g \in G$ is assigned to each spatial lattice link $\ell \in \mathbb{L}$, where G is the gauge group. Links are oriented, and if a link is traversed in the opposite orientation, then g is replaced with g^{-1}.

In the Lie group case, one would typically write $U_\mu(x) = \exp\{(iA_\mu(x))\} \in G$ for the gauge field variable assigned to the lattice link $(x, \hat{\mu})$, where $A_\mu(x)$ is the vector potential. Note that finite groups have no Lie algebras, so we work with group-valued quantities as far as possible. In what follows, we write $g \in G$ for a group element indifferently for both finite and Lie groups G.

A classical configuration is given by a choice of group element g on each lattice link, which means that the configuration space is exactly G. In a quantum theory, the configuration space G has to be upgraded to a Hilbert space $\mathcal{H}^G$, spanned by the elements of G:

$$\mathcal{H}^G \equiv \mathrm{span}\{|g\rangle : g \in G\}, \tag{4.1}$$

Therefore, an element $|\psi\rangle$ of $\mathcal{H}^G$ can be written as

$$|\psi\rangle = \int \mathrm{d}g \, \psi(g) \, |g\rangle, \tag{4.2}$$

where $\int \mathrm{d}g$ is the Haar measure of G, if G is a compact Lie group. In the case of a finite group, (4.2) becomes simply

$$|\psi\rangle = \sum_{g \in G} \psi(g) \, |g\rangle, \tag{4.3}$$

where a Haar measure is not needed and a simple sum is sufficient. The basis $\{|g\rangle : g \in G\}$ can be considered as the analogous of a "position basis". In the case of a Lie group, the wavefunction $\psi(g)$ is square-integrable with respect to the Haar measure. Therefore, the Hilbert space $\mathcal{H}^G$ on each link can be identified with $L^2(G)$, i.e. the space of square-integrable functions on G [98]. Instead, for a finite group the Hilbert space $\mathcal{H}^G$ is simply the *group algebra* $\mathbb{C}[G]$, which is the complex vector space spanned by the group element basis.

The overall Hilbert space $\mathcal{H}_{\text{tot}}$ is then given by a tensor product over the links:

$$\mathcal{H}_{\text{tot}} = \bigotimes_{\ell \in \mathbb{L}} \mathcal{H}_\ell^G, \tag{4.4}$$

where $\mathcal{H}_\ell^G$ is the Hilbert space of the single link ℓ. Note that for a finite group, $\mathbb{C}[G]$ has finite dimension, because it is spanned by the finitely-many group element states $\{|g\rangle\}$. Therefore the Hilbert space on each link is finite-dimensional and $\mathcal{H}_{\text{tot}}$ is finite-dimensional on a finite lattice, with $\dim \mathcal{H}_{\text{tot}} = |G|^L$ where L is the number of links. For a Lie group, on the other hand, we have infinitely many basis states $\{|g\rangle\}$ and therefore the Hilbert space is infinite-dimensional *on each link*.

In the Hamiltonian formulation of gauge theories, the statement that the theory is invariant under gauge transformations translates at the level of the Hilbert space by restricting the allowed states only to those which are gauge-invariant. In particular, on the single-link Hilbert space one can define left and right "translation operators", in the analogy where $\{|g\rangle\}$ is a position basis in group space [95],

$$L_g |h\rangle = |gh\rangle, \qquad R_g |h\rangle = \left|hg^{-1}\right\rangle. \tag{4.5}$$

A local gauge transformation is given by a choice of group element $g_x \in G$ at every site x of the lattice [98]. This acts on the overall Hilbert space $\mathcal{H}_{\text{tot}}$ via the operator

$$\mathcal{G}(\{g_x\}) = \bigotimes_{l=\langle xy\rangle \in \text{links}} L_{g_x} R_{g_y}, \tag{4.6}$$

where $\{g_x\}$ is an arbitrary choice of group elements g_x at each lattice site x, and the link l connects the points x and y. In other words, each link state $|g_l\rangle$ transforms as $|g_l\rangle \mapsto |g_x g_l g_y^{-1}\rangle$.

The only physical states are those which satisfy the so-called "Gauss' law" constraint [8, 20, 98]

$$\mathcal{G}(\{g_x\}) |\psi\rangle = |\psi\rangle, \tag{4.7}$$

for any possible choice of local assignments $\{g_x\}$ of group variables to lattice sites. The Gauss law (4.7) is an exponentiated version of the usual Gauss law formulated in terms of Lie algebra generators. The states which satisfy (4.7) form the physical, gauge-invariant Hilbert space $\mathcal{H}_{\text{phys}}$. Note that the condition (4.7) only involves group-valued quantities and is thus valid for both Lie groups and finite groups. In the case of finite groups, the condition simplifies because it is sufficient to impose invariance against a set of generators of the finite group.

One can also straightforwardly include matter fields such as fermion fields which live on each lattice site. Under a gauge transformation, they transform as $\Psi(x) \to R(g_x)\Psi(x)$, where R is some representation of the gauge group.

4.1.2 The representation basis

It turns out to be fruitful to introduce a different basis of the overall Hilbert space $\mathcal{H}$, "dual" to the group element basis. The operators L_g and R_g introduced in (4.5) are unitary representations of G, known as the *left* and *right regular* representations [143, 144]. This is because $L_g L_h = L_{gh}$ and $(L_g)^{-1} = L_{g^{-1}} = (L_g)^\dagger$, as can be explicitly checked by acting on the group element basis, and the same holds for R. Their representation theory leads to the Peter-Weyl theorem [98, 144] (see also App. A.3). It works for both compact Lie groups and finite groups and it can be summarized as

$$\mathcal{H}^G = \bigoplus_{j \in \Sigma} V_j^* \otimes V_j, \tag{4.8}$$

where j is a label for the irreducible representationss (irreps) of G, and Σ is the set of all irreps of G. For more details see App. A, where we collected some general results on representation theory.

Here V_j is the representation vector space corresponding to the representation j, and V_j^* is its dual. For both compact Lie groups and finite groups the irreps are finite-dimensional and can be chosen to be unitary. For a finite group, Σ *is a finite set*, while it is *countably infinite* for a compact Lie group [143, 144]. In terms of the Peter-Weyl decomposition, the left and right regular representations take a particularly simple form [145],

$$L_g R_h = \bigoplus_j \rho_j(g)^* \otimes \rho_j(h), \tag{4.9}$$

where ρ_j is the matrix of the j-th irrep of G. The individual action of either L_g or R_h may be obtained by setting either g or h to the identity. The formula (4.9) is especially useful because, as we will see in Sec. 4.2, it simplifies the action of the Gauss' law constraint (4.7).

The Peter-Weyl theorem provides an alternative basis for the single-link Hilbert space. For each irrep j one chooses appropriate bases for V_j^* and V_j, which we denote $\{|jm\rangle\}$ and $\{|jn\rangle\}$ respectively, where $1 \leq m, n \leq \dim j$. Here $\dim j \equiv \dim V_j$ is the dimension of the representation. On each representation subspace, we use the shorthand notation $|jmn\rangle \equiv |jm\rangle \otimes |jn\rangle$. Then the "representation basis" for $\mathcal{H}^G$ is given by the set $\{|jmn\rangle\}$ for all $j \in \Sigma$

and $1 \leq m, n \leq \dim j$. In terms of the group element basis, one has [95]

$$\langle g | jmn \rangle = \sqrt{\frac{\dim(j)}{|G|}} \, [\rho_j(g)]_{mn} \, , \qquad (4.10)$$

where the bases $\{|jm\rangle\}$, $\{|jn\rangle\}$ are chosen so that ρ_j is unitary. It should be emphasized that (4.10) is valid for both finite and compact Lie groups; $|G|$ is either the order of the finite group or the volume $|G| \equiv \int dU \, 1$ given by the possibly unnormalized Haar measure [98, 145]. It is a basic result of the representation theory of finite groups that $\sum_j (\dim j)^2 = |G|$, which ensures that the group element basis and the representation basis have the same number of states [143].

Consider now the case $G = \mathbb{Z}_N$. It can be written down as

$$\mathbb{Z}_N = \{1, r, r^2, \ldots, r^{N-1}\},$$

where r is the generator, while the irreps are simply

$$\rho_j(r^k) = \langle r^k | j \rangle = \omega_N^{kj} \qquad \text{for } j = 0, 1, \ldots, N-1 \qquad (4.11)$$

with $\omega_N = e^{2\pi i/N}$. Using (4.10), the bases $\{|r^k\rangle\}$ and $\{|j\rangle\}$ are related by

$$|j\rangle = \sum_{k=0}^{N-1} |r^k\rangle \langle r^k | j \rangle = \frac{1}{\sqrt{N}} \sum_{k=0}^{N-1} |r^k\rangle \, \omega_N^{kj} . \qquad (4.12)$$

We have rediscovered the discrete Fourier transform. This allows us to think of (4.10) as a "non-Abelian Fourier transform", when the group G is non-Abelian. In the case of the dihedral group D_4 (which will be considered later in this chapter), we have four one-dimensional representations, each of which spans a one-dimensional subspace of $\mathbb{C}[G]$. Then, have a two-dimensional representation which spans a $2^2 = 4$ dimensional subspace of $\mathbb{C}[G]$ through the four basis elements $|jmn\rangle$ for $1 \leq m, n \leq 2$. We have summarized the representation theory of some groups of interest in App. B.

Since every group admits a trivial, one-dimensional irrep with $\rho(g) \equiv 1$, we always have a singlet representation state $|0\rangle$, which may be extended to the whole lattice to form the "electric vacuum" $|0_E\rangle$,

$$|0_E\rangle = \bigotimes_{\ell \in \mathbb{L}} |0\rangle_\ell \, , \qquad |0\rangle_\ell = \frac{1}{\sqrt{|G|}} \sum_g |g\rangle_\ell \, , \qquad (4.13)$$

where we used (4.10) to express $|0\rangle_\ell$ in the group element basis.

4.1.3 The Hamiltonian

A generic LGT Hamiltonian H is made of two parts, the electric part H_E and the magnetic part H_B, i.e. $H = H_E + H_B$. These have to be considered separately and a for a simple reason. The magnetic term involves only the spatial component of the field strength tensor, i.e., $\mathbf{B}^2 \sim F^{ij} F_{ij}$, while the electric term involves also the temporal components, i.e., $\mathbf{E}^2 \sim F^{0i} F_{0i}$. Given that in the Hamiltonian formalism time is continuous while space is discrete, the two terms cannot be treated on the same footing. This differs from the Wilson action approach, where the magnetic and electric are treated equally because it has to be Lorentz-invariant.

The Hamiltonian for a LGT takes the general form [8, 95]

$$H = \lambda_E \sum_{\ell \in \mathbb{L}} h_E + \lambda_B \sum_{\square} h_B(g_{\square}), \qquad (4.14)$$

where h_E is an operator that depends only on each lattice link, while h_B depends on the lattice plaquettes $\square$. The symbol $g_{\square}$ stands for the product of the link variables around a plaquette $\square$, i.e. $g_{\square} = g_1 g_2 g_3^{-1} g_4^{-1}$. It is also possible to add matter fields, but we focus here on the pure gauge theory.

If the gauge group is a Lie group, each group element $g = e^{iX}$ can be written as the exponential of a Lie algebra element X. Then one also has infinitesimal generators of left-translations $\hat{\ell}_L^a$ such that

$$L_{e^{iT^a}} = \exp\left\{\left(i\hat{\ell}_L^a\right)\right\},$$

where T^a is a Lie algebra basis and a a color index [98]. In other words, $\hat{\ell}_L$ is the Lie algebra representation corresponding to the group representation L, and plays the role of the chromo-electric field.

The Lie group Hamiltonian, also known as the Kogut-Susskind Hamiltonian, is then given by [8, 98]

$$h_E = \sum_a \left(\hat{\ell}_L^a\right)^2 \quad \text{and} \quad h_B = 2(\dim \rho - \operatorname{Re} \operatorname{tr}\{\rho(g_{\square})\}), \qquad (4.15)$$

where ρ is the fundamental representation of $\mathrm{SU}(N)$, with couplings $\lambda_E = g^2/2$ and $\lambda_B = 1/g^2$ in terms of a coupling constant g (the lattice spacing is set to 1). As the group element basis may be thought of as a "position basis" in group space, the infinitesimal generators of translations $\hat{\ell}_L^a$ may be thought of as "momentum" operators in group space. Then the electric Hamiltonian h_E, which is the sum of the squares of the "momenta" in all directions, is a *Laplacian in group space*. Applying the Peter-Weyl decomposition (4.9) to $\hat{\ell}_L^a$,

one finds that [98, 145]

$$h_E = \sum_a \left(\hat{\ell}_L^a\right)^2 = \sum_{jmn} C(j) \left|jmn\right\rangle \left\langle jmn\right|, \tag{4.16}$$

where $C(j)$ is the quadratic Casimir operator, which depends only on the representation $C(j)$. For U(1), for example $C(j) = j^2$, while for SU(2) one finds $C(j) = j(j+1)$.

We note that the magnetic Hamiltonian depends only on group-valued quantities and is therefore well-defined for both Lie groups and finite groups. On the other hand, the electric Hamiltonian depends on the infinitesimal Lie algebra through $\hat{\ell}_L^a$ and therefore *the definition does not extend to finite groups*. Nonetheless, the decomposition (4.16) is well-defined also for finite groups, but one must leave the coefficients $C(j)$ unsatisfactorily unspecified because finite groups do not have a Casimir operator [95].

If one thinks of a finite group as a natural discretization of some parent Lie group, the natural choice of electric Hamiltonian is a discrete Laplacian on the finite group. The geometric structure of a finite group is that of a graph, with group elements as vertices and the group operation defining the edges. This is called a *Cayley graph*. The discrete Laplacian on the finite group is then naturally given by the graph Laplacian of the Cayley graph. This choice also preserves the interpretation of the electric Hamiltonian as a quantum-mechanical rotor in group space [8].

We explain the construction of the finite group Laplacian in detail in Sec. 4.1.4, and the resulting Hamiltonian takes the form of (4.14) with

$$h_E = \sum_{g \in \Gamma} (1 - L_g) \quad \text{and} \quad h_B = h_B(g_\square), \tag{4.17}$$

where $\Gamma \subset G$ is a subset of the group (*not* a subgroup) such that

1. $1 \notin \Gamma$, i.e. Γ doesn't contain the identity element.

2. $\Gamma^{-1} = \Gamma$, i.e. it is invariant under inversion of group elements. In other words, if $g \in \Gamma$, then $g^{-1} \in \Gamma$ also.

3. $g\Gamma g^{-1} = \Gamma$, i.e. it is invariant under conjugation. In other words, Γ is a union of conjugacy classes of G.

These conditions on Γ ensure that the electric Hamiltonian is gauge-invariant. On the other hand, as usual, the magnetic term is gauge-invariant as long as h_B is any real function such that $h_B(g_1 g_\square g_1^{-1}) = h_B(g_\square)$ for any $g_1 \in G$. As explained in Sec. 4.1.5, the Hamiltonian (4.17) includes as a special case

the transfer-matrix Hamiltonian obtained in [146] which consists in a certain specific choice of subset Γ. The choice of Γ is in fact not unique, a fact which we will also discuss in later sections.

While the magnetic Hamiltonian h_B is diagonal in the group element basis, the electric Hamiltonian h_E is diagonal in the representation basis. In fact, h_E in (4.17) in the irrep basis becomes

$$h_E = \sum_{jmn} h_E(j) \, |jmn\rangle \, \langle jmn| \quad \text{with} \quad h_E(j) = |\Gamma| - \frac{1}{\dim j} \sum_{g \in \Gamma} \chi_j(g), \quad (4.18)$$

where $|\Gamma|$ is the number of elements in Γ and χ_j is the character of the irrep labelled j. The electric Hamiltonian may be interpreted as an "on-link" hopping term within group space; in fact, up to a constant, it may be written as

$$h_E = -\sum_{g \in \Gamma} \sum_{h \in G} |gh\rangle \, \langle h|, \quad (4.19)$$

and it favours each link to sit in the electric ground state (4.13), which is fully delocalized in group space. On the other hand, the magnetic term is a plaquette-based potential which pushes plaquettes close to the identity. The competition between the two non-commuting terms gives rise to non-trivial dynamics.

We would like to emphasize that the description of the electric Hamiltonian h_E in (4.17) as the graph Laplacian of the Cayley graph associated with the group is not simply an interesting analogy, but also a tool which may be used to extract information on the Hamiltonian itself.

As an example, we note the well-known fact that the smallest eigenvalue of a graph Laplacian is always zero (given by the trivial representation state (4.13)) and its degeneracy equals the number of connected components of the graph [147]. Moreover, it is not hard to show that if Γ does not generate the group G, but rather only a subgroup $\langle\Gamma\rangle < G$, then the Cayley graph splits into connected components which are identified with the cosets of $\langle\Gamma\rangle$ in G. The number of such components, and therefore the degeneracy of the ground state of h_E on each link, is given by

$$\text{electric ground state degeneracy} = \frac{|G|}{|\langle\Gamma\rangle|}. \quad (4.20)$$

This is the degeneracy of h_E on each link; the degeneracy of the electric Hamiltonian $H_E = \sum_{\text{links}} h_E$ on the Hilbert space of the whole lattice is larger. If, instead, Γ generates the whole group, then the electric Hamiltonian is not degenerate. A detailed proof can be found in Appendix C.1. The degeneracy
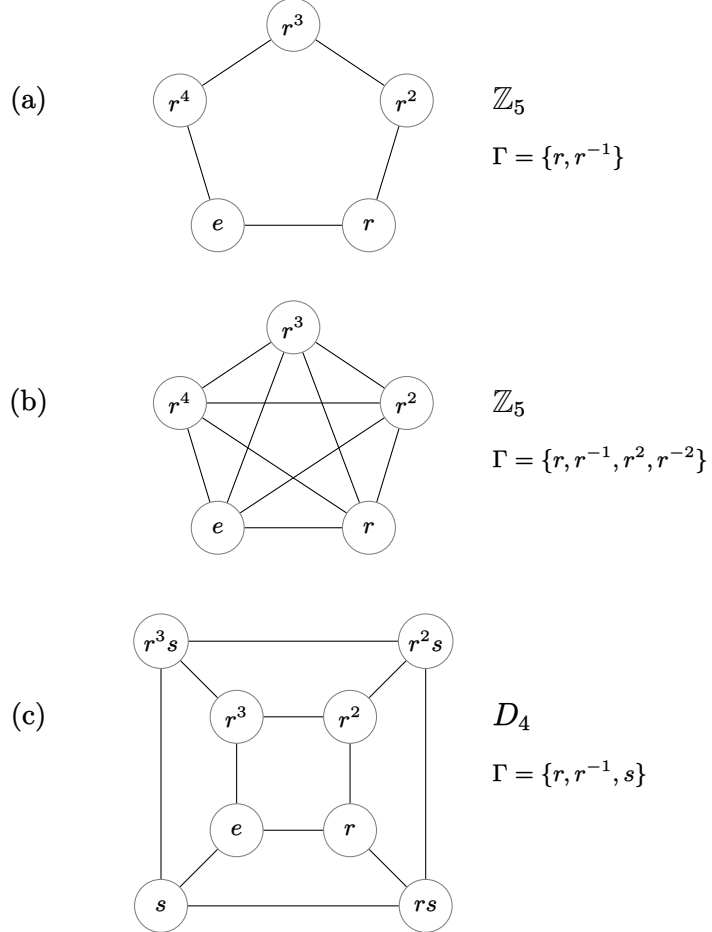
Figure 4.1. 5 Examples of Cayley graphs. (a) and (b) show $\mathbb{Z}_5$ with $\Gamma = \{g, g^{-1}\}$ and $\Gamma = \{g, g^2, g^{-1}, g^{-2}\}$ respectively. (c) shows D_4 with $\Gamma = \{r, r^{-1}, s\}$

of the electric ground state is not only an important feature of the theory, but also technically important for methods such as adiabatic quantum simulation.

As we will see at the end of Sec. 4.1.4, an electric Hamiltonian with degenerate ground state can be constructed in the simple case of the dihedral group D_4.

4.1.4 The finite group Laplacian

In this section we explain in detail the construction of the finite group Laplacian, which we take as the electric Hamiltonian, as the graph Laplacian of the Cayley graph of the finite group. Given a finite group G, we choose a set of generators $\Gamma \subset G$, which we require to be invariant under inversion and conjugation. In other words, $\Gamma^{-1} = \Gamma$ and $g\Gamma g^{-1} = \Gamma$ for any $g \in G$ [147].

We choose Γ not to include the identity element and we note that the choice of Γ is not unique.

The Cayley graph has the group elements as vertices, and we place an edge between $g \in G$ and $h \in G$ if $hg^{-1} \in \Gamma$. The result is a simple undirected graph. Examples of Cayley graphs for the groups $\mathbb{Z}_5$ and D_4 are shown in Fig. 4.1. Given any graph, its Laplacian is defined as [147]

$$\Delta = D - A, \tag{4.21}$$

where A is the adjacency matrix and D is the degree matrix. Each of these matrices acts on the vector space of graph vertices, which in the case of a Cayley graph can be identified with the group algebra $\mathbb{C}[G]$. The degree matrix is always diagonal, and in this case $D = |\Gamma|\mathbb{1}$. The adjacency matrix A is given by

$$A_{gh} = \begin{cases} 1 & gh^{-1} \in \Gamma \\ 0 & \text{otherwise} \end{cases} \tag{4.22}$$

for group elements g, h. On a basis element, one has

$$A|g\rangle \equiv \sum_h A_{hg}|h\rangle = \sum_{k\in\Gamma}|gk\rangle = \sum_{k\in\Gamma}\left|gk^{-1}\right\rangle = \sum_{k\in\Gamma}R_k|g\rangle, \tag{4.23}$$

where R_k is the right regular representation, and we used the closure of Γ under inversion. Therefore as an operator on $\mathbb{C}[G]$,

$$A = \sum_{k\in\Gamma}R_k = \bigoplus_j \mathbb{1}_j \otimes \left(\sum_{k\in\Gamma}\rho_j(k)\right), \tag{4.24}$$

where we used the Peter-Weyl decomposition of R_k (4.9). Then we see that

$$\left(\sum_{k\in\Gamma}\rho_j(k)\right)\rho_j(g) = \sum_{k\in\Gamma}\rho_j(kg) = \sum_{k\in\Gamma}\rho_j(gkg^{-1}g) = \rho_j(g)\left(\sum_{k\in\Gamma}\rho_j(k)\right), \tag{4.25}$$

where we used the closure of Γ under conjugation.

Hence the operator $\left(\sum_{k\in\Gamma}\rho_j(k)\right)$ commutes with the irreducible representation ρ_j and as such is proportional to the identity by Schur's lemma [143]. The constant of proportionality can be readily computed by taking a trace. This therefore implies

$$A = \sum_j \lambda_j P_j, \qquad \lambda_j = \frac{1}{\dim j}\sum_{k\in\Gamma}\chi_j(k). \tag{4.26}$$

where $P_j = \sum_{mn} |jmn\rangle \langle jmn|$ is the projector onto the j-th representation subspace, and χ_j is the character of the irrep labelled j. Therefore the Laplacian of the Cayley graph is given by

$$\Delta = \sum_j f(j) P_j, \qquad f(j) = |\Gamma| - \frac{1}{\dim(j)} \sum_{k \in \Gamma} \chi_j(k). \qquad (4.27)$$

which is the same form as the electric Hamiltonian in the representation basis, (4.18). For any finite group, this formula defines the electric energy $f(j)$ to be assigned to each irrep.

We give some examples of this construction. For the group $\mathbb{Z}_N$ it is natural to construct the electric eigenvalues $f(j)$ with the generating set $\Gamma = \{r, r^{-1}\}$ where r is a generator of $\mathbb{Z}_N$, which results in

$$f(j) = f(N-j) = 4\sin^2\left(\frac{\pi j}{N}\right), \qquad (4.28)$$

which is the same as in [111]. Moreover for large N,

$$f(j) \to \frac{4\pi^2}{N^2} j^2 \qquad N \text{ large}, \qquad (4.29)$$

which is proportional to the Casimir eigenvalues of U(1) gauge theory [111]. Thus both a truncation of U(1) theory and proper $\mathbb{Z}_N$ theory naively approach U(1) theory for large N, albeit in different ways. One can however choose a different generating set, such as $\Gamma = \{r, r^{-1}, r^2, r^{-2}\}$ and the corresponding eigenvalues would be

$$f(j) = f(N-j) = 4\sin^2\left(\frac{\pi j}{N}\right) + 4\sin^2\left(\frac{2\pi j}{N}\right). \qquad (4.30)$$

For the dihedral group D_4 we can choose for example

$$\Gamma_1 = \{r, r^3, s, r^2 s\},$$

which gives rise to the eigenvalues $f(j)$ shown in Table 4.1, where the representations are ordered like in the character table in Table B.1 in Appendix B.2. Note that Γ_1 generates the whole group.

By looking at its character table, we may in fact classify all possible choices of Γ for D_4. In fact, D_4 has five conjugacy classes:

$$C_0 = \{e\}, \quad C_1 = \{r, r^3\}, \quad C_2 = \{r^2\}, \quad C_3 = \{s, r^2 s\}, \quad C_4 = \{rs, r^3 s\}.$$

One can check that, as is generally true, $\sum_i |C_i| = 8 = |G|$. In this case, all conjugacy classes are invariant under inversion, i.e. $C_i^{-1} = C_i$. Hence any

		$f(j)$				
Γ	j	0	1	2	3	4
$\Gamma_1 = \{r, r^3, s, r^2 s\}$		0	4	4	8	4
$\Gamma_2 = \{r, r^3, s, rs, r^2 s, r^3 s\}$		0	8	8	8	6
$\Gamma_3 = \{r, r^2, r^3\}$		0	4	0	4	5

Table 4.1. Eigenvalues of the single-link electric Hamiltonian $f(j)$ for the finite group D_4, with three choices of generating sets: Γ_1, Γ_2, and Γ_3 respectively.

union of the C_i's ($i \neq 0$) is a valid choice for Γ. There are 2^4 such possibilities. Note that this is not true in general, in which case one must choose conjugacy classes to ensure that $\Gamma^{-1} = \Gamma$. In the next sections we will consider in more detail two specific cases:

$$\Gamma_2 = C_1 \cup C_3 \cup C_4 = \{r, r^3, s, rs, r^2 s, r^3 s\} \quad \text{and} \quad \Gamma_3 = C_1 \cup C_2 = \{r, r^2, r^3\}.$$

The choice of Γ_2 is especially interesting, because it corresponds to the Hamiltonian arising from the transfer-matrix procedure when h_B is the real part of the trace of the faithful irrep of D_4; therefore, this choice gives rise to a manifestly Lorentz-invariant theory. Note that also Γ_2 generates the whole group. On the other hand, the set $\Gamma_3 = \{r, r^2, r^3\}$ does not generate the whole group, but only the subgroup of rotations; this is reflected in the electric eigenvalues in Table 4.1, with the electric ground state being two-fold degenerate on each link.

4.1.5 Action formulation and Lorentz invariance

The Kogut-Susskind Hamiltonian (4.15) may be obtained via the transfer-matrix formulation from the Euclidean Wilson action [148, 149]

$$S = -\frac{2}{g^2} \sum_{\square} \mathrm{Re}\,\mathrm{tr}\{\rho(g_{\square})\}, \tag{4.31}$$

where g is the coupling. In the path-integral formulation, the lattice is fully discretized and thus plaquettes extend also in the time direction. The action (4.31) is also perfectly valid for finite groups, as one simply replaces the integration measure over the Lie group with a sum over the elements of a finite group. The representation ρ can be chosen to be any faithful representation of the finite group (not necessarily irreducible). One may then repeat the transfer-matrix formulation for an arbitrary finite group [146]. Starting from the action (4.31), the transfer-matrix procedure gives rise to a Hamiltonian of

the form (4.17) that we've described, with

$$\Gamma = \{g \in G,\ g \neq 1,\ \max[\mathrm{Re}\,\mathrm{tr}\{\rho(g)\}]\} \quad \text{and} \quad h_B = -2\,\mathrm{Re}\,\mathrm{tr}\,\rho. \qquad (4.32)$$

In other words, the magnetic Hamiltonian is directly inherited from the action, while the electric Hamiltonian takes the form of the finite-group Laplacian with a specific choice of Γ. In the example of the gauge group D_4, if we choose the faithful, two-dimensional irrep for h_B, then $\mathrm{Re}\,\mathrm{tr}\,\rho(g)$ can equal $2, 0, -2$ on the different conjugacy classes (see the character table of D_4 in Table B.1). Since $\mathrm{Re}\,\mathrm{tr}\,\rho(1) = 2$, then Γ consists of all group elements g such that $\mathrm{Re}\,\mathrm{tr}\,\rho(g) = 0$. This gives rise to the generating set Γ_2 anticipated in Sec. 4.1.4.

These considerations are especially important for the Lorentz invariance of the theory. While the lattice discretization breaks the Lorentz symmetry to the subgroup of Euclidean cubic rotations, as long as this subgroup is preserved one expects to recover Lorentz invariance in the continuum limit. In particular, the action (4.31) is manifestly invariant under Euclidean cubic rotations and, therefore, one expects that it gives rise to a Hamiltonian which describes a Lorentz-invariant theory in the continuum. Intuitively, a Lorentz transformation can swap the electric and magnetic fields, and it is therefore not surprising that in a Lorentz-invariant theory the electric and magnetic Hamiltonians must satisfy specific relations with each other.

In particular, finite-group Hamiltonians of the form (4.17) which however do not respect the relations (4.32) cannot arise from an action of the form (4.31). For example, they could come from an action in which plaquettes extending in one direction (the "time" direction) are weighted differently. For such Hamiltonians, it is unclear whether they describe a Lorentz-invariant theory. This includes in particular setting $h_E(j) = j^2$ for subgroups of U(1) and $h_E(j) = j(j+1)$ for subgroups of SU(2) in (4.18), while keeping h_B unchanged. In all such cases, the remnant Lorentz symmetry is explicitly broken. While Lorentz symmetry is required in particle physics applications, it might not be necessarily required in other cases, such as some condensed matter applications, and one may thus independently choose Γ and h_B.

4.1.6 Classification of the possible theories

The construction of finite group LGTs with Hamiltonian (4.17) involves a few arbitrary choices which can be classified. Since the Hilbert space is fixed to the physical, gauge-invariant Hilbert space $\mathcal{H}_{\mathrm{phys}}$, the only possible choices involve the various terms in the Hamiltonian. Given a gauge group G in d spatial dimensions, one may arbitrarily choose:

1. A set Γ of group elements which does not contain the identity, and is invariant under both inversion and conjugation $\Gamma^{-1} = \Gamma$ and $g\Gamma g^{-1}$.

2. A choice for the magnetic Hamiltonian $h_B = h_B(g_\square)$. Since it must be real and satisfy $h_B(g_1 g_\square g_1^{-1}) = h_B(g_\square)$, i.e. it is a *class function*, by a well-known result [143] it may be expanded in a sum of characters of irreducible representations, $h_B(g) = \sum_j c_j \chi_j(g)$ for coefficients c_j which may be chosen arbitrarily, while ensuring that $h_B(g)$ is real. Most typically $h_B = -2\,\mathrm{Re}\,\mathrm{tr}\,\rho$, where ρ is some representation (not necessarily an irrep).

3. If present, possible choices of representations and Hamiltonians in the matter sector.

4. One can also add a Chern-Simons term as in [150]. This is especially interesting for quantum simulation, because such theories have a sign problem.

Further considerations involve the Lorentz symmetry, as explained in Sec. 4.1.5. Moreover, one may want to choose representations which are non-trivial when restricted to the center of the gauge group [151, 152].

We note that the above construction allows further generalizations. In particular, the discretized d-dimensional space does not have to take the form of a hypercubic lattice, but more generally can be a Bravais or non-Bravais lattice, or even a cell complex. No difference arises for the electric term, which is link-based, and the plaquette variable in the magnetic term is replaced by an an elementary closed loop in the lattice.

4.2 The physical Hilbert space

As we remarked in Sec. 4.1.1, while the overall Hilbert space of the pure gauge theory is $\mathcal{H}_{\mathrm{tot}} = \bigotimes_\ell \mathcal{H}_\ell^G$, only those states that satisfy the so-called "Gauss' law" constraint (4.7) are to be considered physical [8, 20, 98].

For gauge theories based on most compact Lie groups, the Wilson loops (despite being overcomplete) span the space of gauge-invariant states [153, 154]. This, however, is not necessarily true for finite groups [153, 155]; this means that in some cases, it is possible to construct different gauge-invariant states, which nevertheless have identical Wilson loops. We mention that this difficulty does not arise for Abelian finite groups such as $\mathbb{Z}_N$, in which case the Wilson loops *do* span the physical Hilbert space $\mathcal{H}_{\mathrm{phys}}$.

As will be discussed in Sec. 4.2.1, the gauge-invariant Hilbert space for pure gauge theories may be described in terms of *spin network states*. This basis
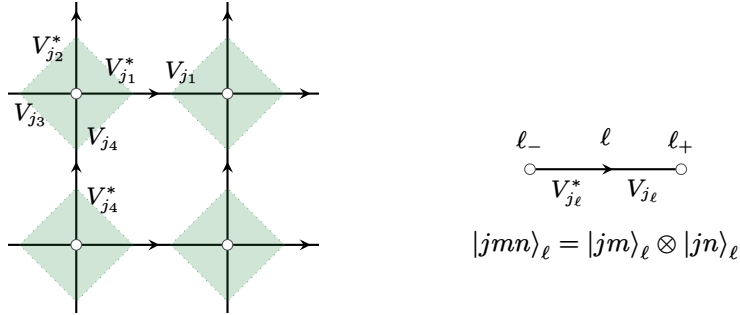
Figure 4.2. Decomposition of the total Hilbert space $\mathcal{H}_{\text{tot}}$. Each link space can be decomposed into two factors $V_{j_\ell}^*$ and V_{j_ℓ}. The factors around the same site $x \in \mathbb{L}$ can be then grouped together. These terms, represented as green regions in the picture, corresponds to the terms in square brackets in (4.34). Therefore, for each irrep configuration $\{j\}$ the space $\mathcal{H}_{\text{tot}}$ is site-wise decomposed, making it possible to solve Gauss's law at each site.

turns out to be particularly suitable for finite gauge groups and in Sec. 4.2.2 we give a simple formula to compute the dimension of the physical Hilbert space for any finite gauge group.

4.2.1 Spin network states

The physical Hilbert space of pure gauge theories with either Lie or finite gauge group can be explicitly described in terms of *spin network states* [156, 157]. Spin network states can be defined indifferently when the d-dimensional space is discretized as an arbitrary graph, and are thus valid in arbitrary dimension with arbitrary lattices and boundary conditions.

The first key observation is that the action of the Gauss' law operator (4.7) is block-diagonal in the representation basis, as can be seen from (4.9). Then starting from the Hilbert space in the representation basis (4.8), we can, as usual, permute the summation and product, obtaining

$$\mathcal{H}_{\text{tot}} = \bigotimes_{\mathbb{L}} \bigoplus_{j \in \Sigma} V_j^* \otimes V_j = \bigoplus_{\{j\} \in \{\Sigma\}} \bigotimes_{\ell \in \mathbb{L}} V_{j_\ell}^* \otimes V_{j_\ell}. \tag{4.33}$$

where now $\{j\}$ is an assignment of an irrep j_ℓ to each lattice link ℓ, and $\{\Sigma\}$ is the set of the possible assignments. The second key observation is that the gauge transformations (4.7) are given by an independent group-valued variable g_x at each site x of the lattice.

Moreover, due to (4.9) the gauge transformation associated to one site x acts at most on one of the spaces V_j or V_j^* associated to a link, but it cannot act on both. One can then split the two vector spaces V_j and V_j^* associated with each link and reorder the V's in the tensor product over links so that

$$G(\{j\}_x) = \cdots$$
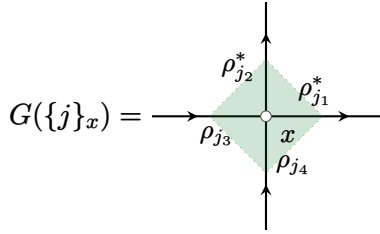
Figure 4.3. Gauss operator in the representation basis. Notice that it acts on a single block (green region) of the total Hilbert space decomposition (4.34).

V_j's are now grouped together according to the *sites* $x \in \mathbb{L}$ and not the links,

$$\mathcal{H}_{\text{tot}} = \bigoplus_{\{j\} \in \{\Sigma\}} \bigotimes_{x \in \mathbb{L}} \left[\left(\bigotimes_{\ell_- = x} V_{j_\ell}^* \right) \otimes \left(\bigotimes_{\ell_+ = x} V_{j_\ell} \right) \right], \qquad (4.34)$$

where by ℓ_+ and ℓ_- we denote respectively the target and source vertex of link ℓ (see Fig. 4.4).

We can repeat the same set of operations for the gauge transformation operator (4.6), which is therefore given by

$$\mathcal{G}(\{g_x\}) = \bigoplus_{\{j\} \in \{\Sigma\}} \bigotimes_{x \in \mathbb{L}} \left[\left(\bigotimes_{\ell_- = x} \rho_{j_\ell}^*(g_x) \right) \otimes \left(\bigotimes_{\ell_+ = x} \rho_{j_\ell}(g_x) \right) . \right] \qquad (4.35)$$

In the above decomposition, the gauge transformations now act independently for each x and the Gauss' law constraint (4.7) gives the physical Hilbert space

$$\mathcal{H}_{\text{phys}} = \bigoplus_{\{j\} \in \{\Sigma\}} \bigotimes_{x \in \mathbb{L}} \text{Inv} \left[\left(\bigotimes_{\ell_- = x} V_{j_\ell}^* \right) \otimes \left(\bigotimes_{\ell_+ = x} V_{j_\ell} \right) \right]. \qquad (4.36)$$

Given a representation ρ (not necessarily irreducible) with representation space V_ρ, the *set of invariant vectors* $\text{Inv}(V_\rho)$ is the set of vectors $v \in V_\rho$ such that $\rho(g)v = v$ for all $g \in G$. Note that this is a *separate notion* from that of an "invariant subspace".

In order to make the reasoning so far more clear, we stress that we were able di re-arrange the terms that enter $\mathcal{H}_{\text{tot}}$ in the representation basis in (4.33). The obtained result (4.34) shows a sum over the irrep configurations $\{j\}$ and for each configuration we have a product of representation spaces *over the sites*. Then, in each of these new representation spaces we can solve Gauss' law. In fact, the set of invariant vectors is just the set of solutions to the Gauss' law on a given site and irrep configuration around it.

The characterization of the Hilbert space (4.36) implies that any physical, gauge-invariant state $|\Psi\rangle$ (i.e. a state which satisfies the Gauss' law (4.7)) may be expanded in a basis of *spin network states*,

$$|\Psi\rangle = \sum_{\{j\}} \sum_A \Psi(\{j\}; A) |\{j\}, A\rangle, \qquad |\{j\}, A\rangle = \bigotimes_{x \in \mathbb{L}} |\{j\}_x, a_x\rangle, \qquad (4.37)$$

where $\{j\}$ is an assignment of irreps to lattice links and $A = (a_1, \ldots a_V)$ is a multi-index which labels the choice of a basis element of invariant states at each site. With $\{j\}_x$ we denote the irreps assigned to the links connected to site x.

For a hypercubic lattice in d dimensions with periodic boundary conditions, each site is connected to $2d$ links and therefore $2d$ terms appear in the tensor product within each Inv in (4.36). If instead we choose open boundary conditions, the sites in the bulk will again be connected to $2d$ links, but the sites on the boundary will be connected to fewer links and thus fewer terms will appear in the tensor product for those sites. In the general case, the number of terms in the tensor product within each Inv will thus depend on the site.

We choose to work directly with the spaces of invariant vectors rather than with spaces of intertwiners more commonly employed in the literature on spin-network states [156, 157]. We also would like to note that the physical Hilbert space (4.36) contains *all* gauge-invariant states, possibly also including states in sectors with a non-contractible Wilson line.

The calculation of a basis of invariant states (or, equivalently, of the intertwiners) can be difficult in the Lie group case, especially since they admit infinitely many irreps. On the other hand, since the number of links connected to each site is finite and independent of the lattice volume, one needs only compute the invariant states of a finite number of tensor product representations which does not scale with the lattice volume.

This can be achieved in practice by explicitly writing out the matrices of the tensor product representation

$$\rho(g) \equiv \left(\bigotimes_{\ell_- = x} \rho_{j_\ell}^* \right) \otimes \left(\bigotimes_{\ell_+ = x} \rho_{j_\ell} \right)$$

and solving the simultaneous equations $\rho(g)v = v$ for a set of generators of G. In a d-dimensional periodic hypercubic lattice, the number of terms in the tensor product equals $2d$ and the maximum dimension of the tensor product representation is bounded by $(\dim j)^{2d} \leq |G|^d$, owing to $\sum_j (\dim j)^2 = |G|$, independently from the lattice volume.

As an example, we work out explicitly the case of a 2×2 square lattice with periodic boundary conditions. As shown in Fig. 4.4, this system has four
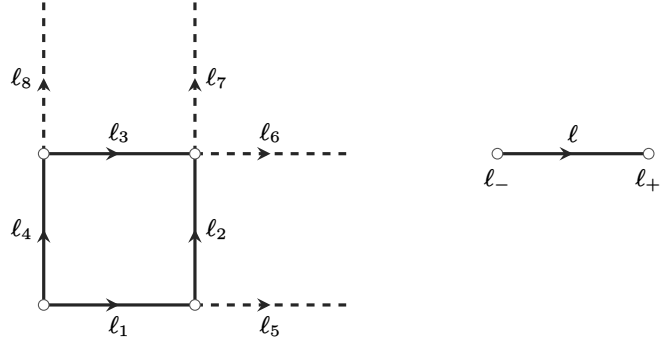
Figure 4.4. *Left*: a 2×2 square lattice with periodic boundary conditions, showing the labels of the links. *Right*: labelling of sites attached to a link.

vertices and eight links. Expanding explicitly (4.36) we see that in this case

$$
\mathcal{H}_{\text{phys}} = \bigoplus_{j_1, \ldots j_8} \left(\text{Inv} \left[V_{j_1}^* V_{j_4}^* V_{j_5} V_{j_8} \right] \otimes \text{Inv} \left[V_{j_5}^* V_{j_2}^* V_{j_1} V_{j_7} \right] \otimes \right.
$$

$$
\left. \otimes \text{Inv} \left[V_{j_6}^* V_{j_7}^* V_{j_3} V_{j_2} \right] \otimes \text{Inv} \left[V_{j_3}^* V_{j_8}^* V_{j_6} V_{j_4} \right] \right), \quad (4.38)
$$

where tensor product symbol inside the invariant space brackets has been omitted in order to lighten the notation. Now consider a single invariant space $\text{Inv} \left[V_{j_1}^* V_{j_2}^* V_{j_3} V_{j_4} \right]$ with arbitrary assignment of irreps. This vector space admits an orthonormal basis $\{ |j_1 j_2 j_3 j_4; a_5 \rangle \}$ where $1 \leq a \leq \dim \text{Inv} \left[V_{j_1}^* V_{j_2}^* V_{j_3} V_{j_4} \right]$ indexes the basis vector. We can expand the basis vectors explicitly in terms of the bases of the V_j as (see also the discussion around (4.10))

$$
|j_1 j_2 j_3 j_4; a_5 \rangle = \sum_{m_1, m_2, n_3, n_4} \psi^{j_1 j_2 j_3 j_4}(m_1 m_2 n_3 n_4 | a) \times
$$

$$
\times |j_1 m_1 \rangle |j_2 m_2 \rangle |j_3 n_3 \rangle |j_4 n_4 \rangle . \quad (4.39)
$$

The basis vectors can be chosen to be orthonormal. By virtue of spanning the space $\text{Inv} \left[V_{j_1}^* \otimes V_{j_2}^* \otimes V_{j_3} \otimes V_{j_4} \right]$, they are invariant vectors of the tensor product representation $\rho \equiv \rho_{j_1}^* \otimes \rho_{j_2}^* \otimes \rho_{j_3} \otimes \rho_{j_4}$; as such, they satisfy $\rho(g) |j_1 j_2 j_3 j_4; a \rangle = |j_1 j_2 j_3 j_4; a \rangle$ for all $g \in G$. The coefficients of the expansion $\psi^{j_1 j_2 j_3 j_4}(m_1 m_2 n_3 n_4 | a)$ may be easily computed, for example by writing the tensor product representation matrices $\rho(g)$ explicitly and then solving the simultaneous equations $\rho(g) v = v$. The dimension of the space of invariant vectors depends on the four representations assigned to the relevant site.

Now let $A = (a_1, a_2, a_3, a_4)$, which implicitly depends on $\{j\}$ (because the range of each a_x depends on the irreps assigned around the site x). Given any

assignment of irreps $\{j\}$, A is a choice of a basis vector of invariant states at the four sites. Therefore an orthonormal basis for the gauge invariant Hilbert space is given by

$$|\{j\}; A\rangle = |j_1 j_4 j_5 j_8; a_1\rangle \otimes |j_5 j_2 j_1 j_7; a_2\rangle \otimes |j_6 j_7 j_3 j_2; a_3\rangle \otimes |j_3 j_8 j_6 j_4; a_4\rangle . \quad (4.40)$$

for any possible assignment $\{j\}$ of irreps to links, and then all possible choices A of an invariant vector at each of the four sites. The spin-network states $|\{j\}; A\rangle$ then form a basis of the gauge-invariant Hilbert space $\mathcal{H}_{\text{phys}}$. Expanding the tensor product, we find an explicit expression for these states in terms of the representation basis,

$$\begin{aligned}|\{j\}; A\rangle = \sum_{\{m,n\}} & \psi^{j_1 j_4 j_5 j_8}(m_1 m_4 n_5 n_8 | a_1) \psi^{j_5 j_2 j_1 j_7}(m_5 m_2 n_1 n_7 | a_2) \times \\ & \times \psi^{j_6 j_7 j_3 j_2}(m_6 m_7 n_3 n_2 | a_3) \psi^{j_3 j_8 j_6 j_4}(m_3 m_8 n_6 n_4 | a_4) \times \\ & \times |j_1 m_1 n_1\rangle |j_2 m_2 n_2\rangle \cdots |j_8 m_8 n_8\rangle .\end{aligned} \quad (4.41)$$

where the sum is over all the indices m_ℓ and n_ℓ ($\ell = 1, \ldots, 8$), the ordering of the vector spaces V_j's was restored, and shorthand $|jmn\rangle = |jm\rangle \otimes |jn\rangle$ was used. We note in particular that despite having introduced a splitting of the variables at each link, in the final answer this splitting disappears and the spin-network states can be entirely expressed in terms of the representation basis $|jmn\rangle$.

4.2.2 The dimension of the physical Hilbert space

As we have seen in the previous section, spin network states give an explicit description of the physical Hilbert space $\mathcal{H}_{\text{phys}}$ as

$$\mathcal{H}_{\text{phys}} = \bigoplus_{\{\rho\} \in \{\Sigma\}} \bigotimes_{v \in \mathbb{L}} \text{Inv} \left[\left(\bigotimes_{\ell_- = v} V_{\rho_l}^* \right) \otimes \left(\bigotimes_{\ell_+ = v} V_{\rho_l} \right) \right]. \quad (4.42)$$

where $\text{Inv}(\rho)$ is the space of invariant vectors of the representation ρ, $\{\rho\}$ is an assignment of irreps to links and $\{\Sigma\}$ is the set of such possible assignments. For a finite group,

$$\dim \text{Inv}(\rho) = \frac{1}{|G|} \sum_{g \in G} \chi_\rho(g). \quad (4.43)$$

where χ_ρ is the character of ρ. A proof of this result can be found in Appendix C.2. This fact can be used to obtain a general formula for the dimension of the $\mathcal{H}_{\text{phys}}$, which is valid for any lattice in any dimension with any boundary conditions. On a connected lattice with L links and V sites, we will show that

$$\dim \mathcal{H}_{\text{phys}} = \sum_C \left(\frac{|G|}{|C|} \right)^{L-V} . \quad (4.44)$$

where the sum runs over all conjugacy classes C of the group, and $|C|$ is the size of C. The ratio $|G|/|C|$ is always an integer by the orbit-stabilizer theorem [143]. Since for a connected graph $L - V \geq -1$, the $\dim \mathcal{H}_{\text{phys}}$ in (4.44) is always an integer. This is clear for $L - V \geq 0$; when $L - V = -1$ the graph is a tree and since $\sum_C |C| = |G|$, we find $\dim \mathcal{H}_{\text{phys}} = 1$; this is to be expected because on a tree the gauge degrees of freedom can be used to rotate away the physical ones.

Using (4.43), together with the fact that the character of a tensor product is given by the product of the characters, we may readily prove (4.44). From the general formula for the gauge-invariant Hilbert space, we have

$$\dim \mathcal{H}_{\text{phys}} = \sum_{j_1 \cdots j_L} \prod_{x \in \mathbb{L}} \dim \text{Inv} \left[\left(\bigotimes_{\ell_- = x} V_{\rho_l}^* \right) \otimes \left(\bigotimes_{\ell_+ = x} V_{\rho_l} \right) \right]$$

$$= \frac{1}{|G|^V} \sum_{j_1 \cdots j_L} \sum_{g_1 \cdots g_V} \prod_{x \in \mathbb{L}} \left(\prod_{\ell_- = x} \chi_{j_\ell}^*(g_x) \right) \left(\prod_{\ell_+ = x} \chi_{j_\ell}(g_x) \right).$$

Within the product over all sites, there are exactly $2L$ factors of characters χ, as each link contributes two representation spaces V and each representation space gives rise to a character. Thus grouping characters by link, we obtain

$$\dim \mathcal{H}_{\text{phys}} = \frac{1}{|G|^V} \sum_{g_1 g_2 \cdots g_V} \prod_{\ell = \langle xx' \rangle \in \mathbb{L}} \langle g_x, g_{x'} \rangle. \tag{4.45}$$

where we denoted $\langle g, h \rangle = \sum_j \chi_j(g)^* \chi_j(h)$. It is a well-known result that $\langle g, h \rangle$ is zero unless g and h belong to the same conjugacy class, in which case $\langle g, h \rangle = |G|/|C|$ where C is the conjugacy class of both g and h [143]. If any two adjacent sites x and x' have g_x and $g_{x'}$ in different conjugacy classes, then $\langle g_x, g_{x'} \rangle = 0$ and the corresponding term in the sum is zero. Assuming that the lattice is connected, this implies that the product over all links is zero unless all the g_x at each site x belong to the same conjugacy class. Then, since $\langle g_x, g_{x'} \rangle$ is constant on conjugacy classes, we can write

$$\dim \mathcal{H}_{\text{phys}} = \frac{1}{|G|^V} \sum_C \sum_{g_1 g_2 \cdots g_V \in C} \frac{|G|^L}{|C|^L} = \sum_C \left(\frac{|G|}{|C|} \right)^{L-V}. \tag{4.46}$$

which concludes the proof. In the Abelian case the above formula simplifies as all conjugacy classes are singlets and therefore $\dim \mathcal{H}_{\text{phys}} = |G|^{L-V+1}$. Thus finite Abelian groups have the largest physical Hilbert space among all groups of the same order. For periodic boundary conditions in a hypercubic lattice, $L = Vd$ and as such $\dim \mathcal{H} = |G|^{Vd}$, while $\dim \mathcal{H}_{\text{phys}} \approx |G|^{V(d-1)}$, so that the physical Hilbert space has roughly the same size as the overall Hilbert space

Size	BCs	L	V	$L-V$	$\dim \mathcal{H}_{\text{phys}}$	$\dim \mathcal{H}$
2×2	open	4	4	0	5	4096
	periodic	8	4	4	8960	1.6×10^7
2×3	open	7	6	1	28	2.1×10^6
	periodic	12	6	6	536576	6.9×10^{10}
3×3	open	12	9	3	1216	6.9×10^{10}
	periodic	18	9	9	2.7×10^8	1.8×10^{16}

Table 4.2. Dimension of the physical subspace of D_4 gauge theory on some small lattices in $2+1$ dimensions, compared to the dimension of the total Hilbert space. L is the number of links and V is the number of vertices. Numbers above 10^7 are approximated values.

in one lower dimension. Nonetheless, both spaces grow exponentially with the lattice size.

As a further example, we consider the dimension of the Hilbert space for pure D_4 gauge theory. Using (4.44), we find for $G = D_4$ on a lattice with L links and V sites (see also [158]),

$$\dim \mathcal{H}_{\text{phys}} = 8^{L-V} \left(2 + \frac{3}{2^{L-V}} \right). \tag{4.47}$$

The dimension of the physical Hilbert space for some two-dimensional finite square lattices in $2+1$ dimensions is shown in Table 4.2. We see that its size grows quickly with the lattice size. We point out that even for a 2×2 periodic lattice with a small group such as D_4 it is not practical to write down all possible gauge-invariant states. Unless the structure happens to be very sparse, writing down the 8960 physical basis elements in terms of the $|G|^L = 8^8$ basis elements in the representation basis using 4B floating point numbers would require roughly $600\,\text{GB}$ of memory. For a 3×3 periodic lattice this number rises to $20\,\text{YB}$ or $2 \cdot 10^{16}\,\text{GB}$.

Finally, we remark that since matter fields are site-based, the spin-network states may be extended to this case as well; the physical Hilbert space would then be given again by (4.36) with an extra factor of the matter Hilbert space at each site within each Inv. The detailed description of the gauge-invariant Hilbert space with matter fields will be given in a future publication.

4.3   A case study: D_4

In this section we consider pure gauge theory with gauge group $G = D_4$, the dihedral group with eight elements, on a small 2×2 periodic lattice (see

Fig. 4.4). We compute the Hamiltonian in the gauge-invariant spin-network basis and diagonalize it exactly.

4.3.1 Implementation of the physical Hilbert space

As remarked in Sec. 4.2.2, the physical Hilbert space of this theory has dimension equal to 8960 and it's not practical to store the gauge-invariant states directly. Instead, we compute numerically the basis of invariant states at a site for all possible combinations of irreps assigned to the four links attached to the site. In other words, we compute the coefficients ψ of (4.39).

Then, the gauge-invariant states can be stored just as labels of the choice of irreps on the links, and invariant vectors at each site. When the coefficients of a physical state are needed, it is sufficient to call the appropriate ψ's based on the label of the state. Therefore one has to store just the invariant vectors of a single vertex and the labels of the physical states, without needing to expand (4.41) and save the full result. This greatly cuts down on the amount of memory necessary for storing the gauge-invariant basis.

Let's try to quantify this gain. In the D_4 gauge theory in two dimensions, we found that the total number of invariant vectors for a vertex is 164. The size of the invariant vectors depends on the irreps configuration around the vertex, but they are at most 16-dimensional. Using single-precision float (which requires 4B), in the worst case scenario (all vectors are 16-dimensional) the storage for the invariant vectors would require only around 10KB. This is a fixed storage cost independent of the lattice size. On a 2×2 periodic lattice, in order to label the states we would need 8 integers (irrep index) plus 4 integers (invariant vector choice at each vertex). With 8960 states and 2B per integer, the total storage cost would amount to ~ 230KB, a huge decrease from the 600GB estimated before. In the case of a 3×3 lattice, the storage cost would increase to ~ 15GB, orders of magnitude less than 2×10^{16}GB. Using these coefficients ψ, we then compute the matrix elements of the electric and magnetic Hamiltonians separately in the spin-network basis (4.41).

4.3.2 Explicit computation of the Hamiltonian

The electric Hamiltonian is diagonal, and the magnetic Hamiltonian is off-diagonal. In units of $\lambda_E + \lambda_B$ the Hamiltonian can be written as

$$H = \lambda H_E + (1 - \lambda) H_B \quad \text{where} \quad \lambda = \frac{\lambda_E}{\lambda_E + \lambda_B} \in [0, 1]. \tag{4.48}$$

In practice, for each λ, H is a 8960×8960 matrix. As expected for spin-network states [157], we find H to be very sparse: around 1% of the elements

$$\Gamma_1 = \{r, r^3, s, r^2 s\} \qquad \Gamma_2 = \{r, r^3, s, rs, r^2 s, r^3 s\} \qquad \Gamma_3 = \{r, r^2, r^3\}$$
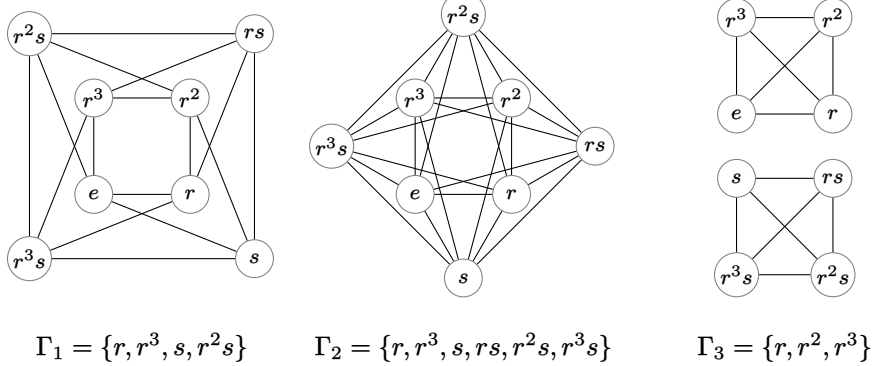
Figure 4.5. The different Cayley graphs of the group D_4. Notice that only the third choice is disconnected, leading to a two-fold degeneracy in the electric Hamiltonian on each link.

are non-zero. A plot of the non-zero elements elements of H_B is shown in Fig. 4.6.

The electric and magnetic Hamiltonians were chosen as in (4.17). In particular, we chose $h_B = -2 \operatorname{tr} \rho_4$ where ρ_4 is the two-dimensional irrep of D_4 and considered the three different choices of the set Γ for h_E described in Sec. 4.1.4. These are:

$$\begin{aligned}
\Gamma_1 &= \{r, r^3, s, r^2 s\}, \\
\Gamma_2 &= \{r, r^3, s, rs, r^2 s, r^3 s\}, \\
\Gamma_3 &= \{r, r^2, r^3\}.
\end{aligned}$$

Their Cayley graphs is shown in Fig. 4.5. We recall that the electric Hamiltonian is two-fold degenerate on each link with Γ_3 but is not degenerate for Γ_1, Γ_2. The choice of Γ_2, unlike the other two, gives rise to a Lorentz-invariant theory.

Working in the spin state basis, computing the matrix elements of $H_E = \sum_\ell h_E$ is rather easy, because is diagonal in the irrep basis:

$$\langle \{j\}', A' | H_E | \{j\}, A \rangle = \delta(\{j\}, \{j\}') \delta(A, A') \sum_{\ell \in \mathbb{L}} f(j_\ell) \qquad (4.49)$$

The difficult part comes from the magnetic Hamiltonian $H_B = \sum_\square h_B(g_\square)$.

In order to compute the matrix elements of H_B, one can use the group elements base, where it is diagonal. In this basis we have

$$\operatorname{tr} \rho_4 = 2 \sum_{g_1 \cdots g_4} \operatorname{Re} \chi_4(g_\square) |g_1 g_2 g_3 g_4\rangle\langle g_1 g_2 g_3 g_4| . \qquad (4.50)$$

The above $|g_1 g_2 g_3 g_4\rangle$ can shorten as $|g_\square\rangle$. We denote with $|\{jmn\}_\square\rangle$ the state $|j_1 m_1 n_1 \cdots j_4 m_4 n_4\rangle$ for the links around the plaquette $\square$. Then, a matrix

element of (4.50) in the $|jmn_\square\rangle$ basis can be computed as

$$\langle \{jmn\}'_\square | \operatorname{tr} \rho_4 | \{jmn\}_\square \rangle = 2 \sum_{g_\square} \operatorname{Re} \chi_4(g_\square) \, \langle \{jmn\}'_\square | g_\square \rangle \, \langle g_\square | \{jmn\}_\square \rangle$$

(4.51)

The terms $\langle \{jmn\}_\square | g_\square \rangle$ can be obtained from (4.10). The coefficients (4.51) depends on the representations and can be precomputed. We will refer to then as $C(\{jmn\}'_\square, \{jmn\}_\square)$.

These coefficients can be used to compute the matrix elements of H_B in the full (non gauge-invariant) irrep basis $|\{jmn\}\rangle$:

$$\langle \{jmn\}' | H_B | \{jmn\} \rangle = -\sum_\square \left(\prod_{\ell \in \square} \delta(j'_\ell m'_\ell n'_\ell, j_\ell m_\ell n_\ell) \right) \times$$
$$\times C(\{jmn\}'_\square, \{jmn\}_\square). \quad (4.52)$$

Thus, using (4.41), we finally obtain the expression for the magnetic in the gauge-invariant basis:

$$\langle \{j\}', A' | H_B | \{j\}, A \rangle = -\sum_\square \sum_{\{mn\}} \sum_{\{mn\}'} \left(\prod_{\ell \in \square} \delta(j'_\ell m'_\ell n'_\ell, j_\ell m_\ell n_\ell) \right)$$
$$\times C(\{jmn\}'_\square, \{jmn\}_\square)$$
$$\times \psi^{j'_1 j'_4 j'_5 j'_8}(m'_1 m'_4 n'_5 n'_8 | a'_1) \psi^{j_1 j_4 j_5 j_8}(m_1 m_4 n_5 n_8 | a_1)$$
$$\times \psi^{j'_5 j'_2 j'_1 j'_7}(m'_5 m'_2 n'_1 n'_7 | a'_2) \psi^{j_5 j_2 j_1 j_7}(m_5 m_2 n_1 n_7 | a_2)$$
$$\times \psi^{j'_6 j'_7 j'_3 j'_2}(m'_6 m'_7 n'_3 n'_2 | a'_3) \psi^{j_6 j_7 j_3 j_2}(m_6 m_7 n_3 n_2 | a_3)$$
$$\times \psi^{j'_3 j'_8 j'_6 j'_4}(m'_3 m'_8 n'_6 n'_4 | a'_4) \psi^{j_3 j_8 j_6 j_4}(m_3 m_8 n_6 n_4 | a_4).$$

(4.53)

Notice that when $|\{j\}', A'\rangle$ and $|\{j\}, A\rangle$ are fixed, only the indices $\{mn\}$ and $\{mn\}'$ are free. Additionally, each index m or n of the invariant vectors ψ is contracted with an index of the plaquette coefficients C. The same goes for the primed indices. This means that the terms of the sum over the plaquette can be computed as *tensor contractions*. Using numerical libraries that efficiently implements tensors, one can greatly improve the computation time.

Another note that is important to point out is the role of the delta functions in (4.53). These are what make the magnetic Hamiltonian sparse, combined with the structure of C. The only non-zero matrix elements are only those between two states whose irrep configuration coincide outside a plaquette $\square$. Then, inside the plaquette $\square$ also the coefficients C's has to be non-zero. It is easy to see that these two facts greatly restrict what matrix elements of H_B can be non-zero.
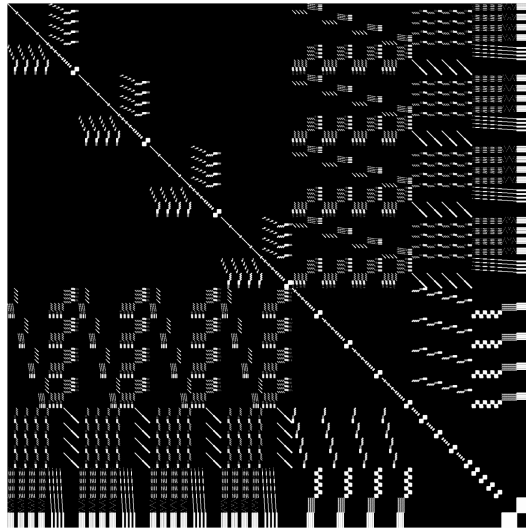
Figure 4.6. Plot of the 8960-dimensional Hamiltonian matrix H_B. The non-zero elements are presented as white dots, which have been enlarged in order to make them visible against the black background. It can be noticed that there is a lot of regular structure, which suggests that may be methods for further compressing the Hamiltonian. Note that the diagonal lines are just slightly offset from the true diagonal at the matrix, which contains only zeros.

4.3.3 Numerical results

Ground state energy and gap

Looking at the ground state energy in Fig. 4.7, one sees that the system evolves from a electric ground state to a magnetic one, with a transition around $0.6 \lesssim \lambda \lesssim 0.8$, for all three case. This is because the Hamiltonian at $\lambda = 0$ coincide with H_E and h_E has always a zero eigenvalue, while at $\lambda = 1$ the Hamiltonian reduces to H_B, which is the same in all three cases. Therefore, a transition is expected for an intermediate value of λ.

The energy gap corresponds to the difference $E_1 - E_0$, where E_1 is the energy of the first excited state. When the energy gaps are considered, we notice a clear difference between Γ_3 and the rest. For Γ_1 and Γ_2 the gap closes, signalling the aforementioned transition. While for Γ_3 the picture is quite different. The electric Hamiltonian is degenerate, as it is expected from the fact that Γ_3 does not generate the whole D_4. This degeneracy is slightly lifted for $\lambda > 0$ but the scale of the gap remains much smaller than in the other two cases. At this lattice size we are not able to exclude finite size effects for this lifted degeneracy.

107

Electric and magnetic expectation values

The ground state expectation values of the electric and magnetic Hamiltonians are shown in Fig. 4.9. The plaquette Wilson loop is equal to H_B apart from an overall prefactor of 8, and therefore its behaviour is also shown in Fig. 4.9 (right). We note that our data for the ground state energies agrees with that obtained in [158] with a different method.

One possible way to locate the transition point is to identify it as the point of sharpest variation of $\langle H_E \rangle$ and/or $\langle H_B \rangle$ (i.e. the maximum of the absolute value of their derivative with respect to λ). With this identification, the transition points given by either $\langle H_E \rangle$ or $\langle H_B \rangle$ coincide at $\lambda_1^* = 0.67(1)$ and $\lambda_2^* = 0.76(1)$ for Γ_1 and Γ_2, but show a small difference for Γ_3, at $\lambda_{3,E}^* = 0.63(1)$ and $\lambda_{3,B}^* = 0.61(1)$.

Fidelity susceptibility

Another way to locate the transition points is through the peaks of *fidelity susceptibility* [159, 160]. Calling $|\psi_0(\lambda)\rangle$ the ground state of $H(\lambda)$, one can look at the fidelity susceptibility [159]

$$\chi(\lambda) = -\frac{\partial^2}{\partial \epsilon^2} \log |\langle \psi_0(\lambda)|\psi_0(\lambda + \epsilon)\rangle|^2 \Big|_{\epsilon=0}, \qquad (4.54)$$

which is expected to peak at the transition [160]. Fig. 4.11 shows $\chi(\lambda)$ for the three cases and its peak identifies the transition point as $\lambda_{1,\chi}^* = 0.67(1)$, $\lambda_{2,\chi}^* = 0.76(1)$ and $\lambda_{3,\chi}^* = 0.62(1)$, in agreement with the previous method.

Overall, these results point towards the expected picture of a two-phase structure for all three cases. The data for Γ_1 and Γ_2 is consistent with the usual picture of a confining phase at small λ and a deconfined phase at large λ. For Γ_3, the gap is much smaller, especially at small λ, which complicates the interpretation of this phase as confining. Of course, due to the small volume these results are only qualitative and preliminary; a study with larger volumes would be required in order to properly establish the phase structure. However, they point to the possibility that theories with electric degeneracy may display different behaviour and phase structure compared to those with no electric degeneracy.
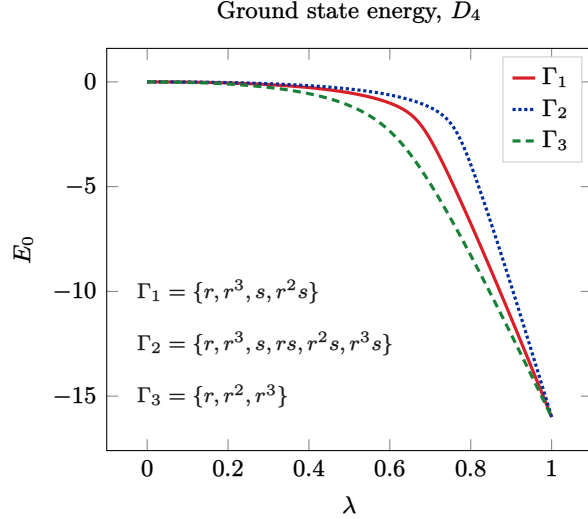
Figure 4.7. Ground state energy of the D_4 gauge theory, for the three different generating Γ_1, Γ_2 and Γ_3. For $\lambda = 1$, the Hamiltonian is equivalent for all the three cases, because is just H_B. While, for $\lambda = 0$ the ground state energy is zero because in all thee cases H_E has always zero eigenvalues. It can be seen that the transition points is always in the region $0.6 \lesssim \lambda \lesssim 0.8$.
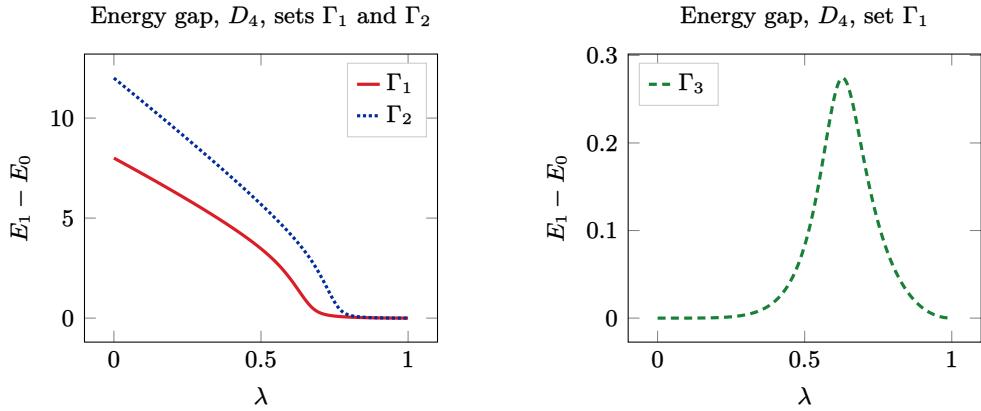
Figure 4.8. *Left:* Energy gap $E_1 - E_0$ for Γ_1 and Γ_2. *Right:* Energy gap $E_1 - E_0$ for only Γ_3. While the behaviour of the ground state energy may seem the same for all the three generating sets (see Fig. 4.7), the same cannot be said for the energy gaps. This is motivated from the fact that Γ_3 does not generate the whole group, so there is a two-fold degeneracy in the electric eigenvalues for each link.
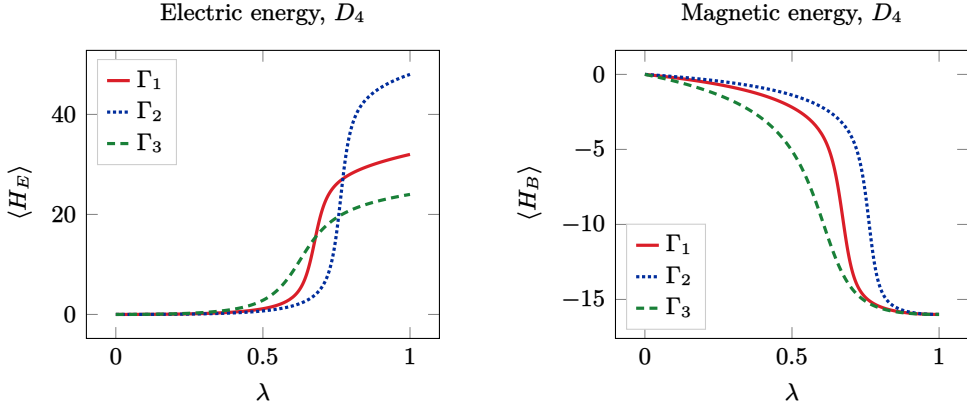
Figure 4.9. Expectation values $\langle H_E \rangle$ (*left*) and $\langle H_B \rangle$ (*right*). They confirm the picture suggested from Fig. 4.7, where there is a transition region for $0.6 \lesssim \lambda \lesssim 0.8$.
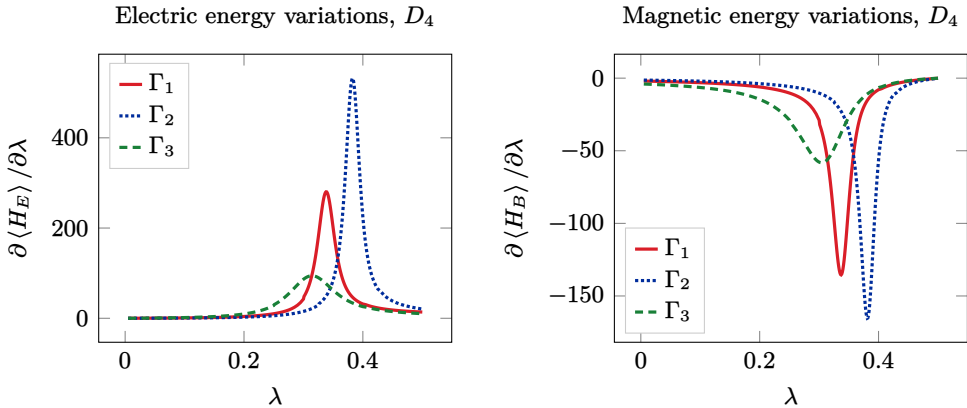
Figure 4.10. Variations of the expectation values $\langle H_E \rangle$ (*left*) and $\langle H_B \rangle$ (*right*). The location of the peaks can be used identifying the transition points. They coincide for Γ_1 ($\lambda^* = 0.67(1)$ and Γ_2 ($\lambda^* = 0.76(1)$)) and slightly differs for Γ_3 ($\lambda_E^* = 0.63(1)$ and $\lambda_B^* = 0.61(1)$). It should be noted that for Γ_3 the peak is much smoother, so the identification of the transition point is much more difficult.
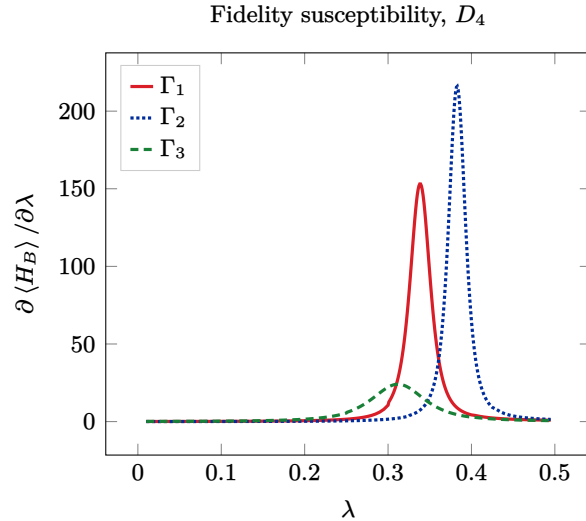
Figure 4.11. Fidelity susceptibility $\chi(\lambda)$ for D_4 for all the three sets Γ_1, Γ_2 and Γ_3. The peaks of $\chi(\lambda)$ identifies the transition points for each case. The position of such peaks are compatible with those in Fig. 4.10. We find $\lambda_{1,\chi}^* = 0.67(1)$, $\lambda_{2,\chi}^* = 0.76(1)$ and $\lambda_{3,\chi}^* = 0.62(1)$ for Γ_1, Γ_2 and Γ_3, respectively.

4.4 Concluding remarks

In this work we considered Hamiltonians for gauge theories with a finite gauge group and we have shown that the electric term may be interpreted as a natural Laplacian operator on the finite group, constructed as the graph Laplacian of its Cayley graph. The choice of generating set of the Cayley graph has a simple relation with the ground state degeneracy of the electric Hamiltonian. We have also given careful consideration to the various choices involved in constructing a finite group gauge theory and their consequences.

Independently from the choice of Hamiltonian, we have shown that the physical, gauge-invariant Hilbert space of pure gauge theories may be explicitly described in terms of spin-network states, which are particularly suitable for finite groups. This also allows us to derive a simple formula to compute the dimension of the physical Hilbert space on an arbitrary lattice. Using the spin-network basis, we diagonalized D_4 gauge theory on a small periodic lattice with different Hamiltonians. Due to the small system size, these results are only suggestive, but they point to the possibility that theories with a degenerate electric Hamiltonian may have a different phase structure than commonly expected.

The methods employed in this work may be extended in several directions. The graph Laplacian construction may be adapted to those approaches where a Lie group is discretized to a finite subset, not necessarily a subgroup [103].

In that case the finite subset may be seen as a weighted graph, with the edge weights representing the distance between group elements in the parent Lie group.

As we have seen, working directly in the gauge-invariant basis reduces the size of the Hilbert space and and implements the Gauss' law exactly, at the expense of higher complexity of the Hamiltonian. It would be worthwhile to explore whether the gauge-invariant basis can be efficiently implemented, for example in a quantum circuit. It is also possible to extend the spin-network basis to gauge theories coupled to matter fields, and we will treat this case in a future publication.

Finally, it would be very interesting to explore the possibility of a non-standard mechanism to obtain a continuum limit for finite group gauge theories; for example, this is possible in quantum link models via the D-theory formulation [161, 162].

chapter five

Conclusions

In this thesis two works by the author have been presented [5, 6], both about LGTs with finite groups. Before moving to their discussion, a proper context has been given by first introducing the general topic of LGTs (Chap. 1) and Quantum Simulation (Chap. 2).

The first work [5], discussed in Chap. 3, focuses on the use of dualities in Abelian LGTs. Using a systematic formal approach, that makes use of bond-algebras, it was possible to obtain a duality transformation from Abelian models on a quasi one-dimensional lattice (the ladder) to a class of one-dimensional non-gauge models, called Quantum Clock Models. This map highlights how the physics of a gauge model can depends on super-selection rules, which is often an overlooked aspect. Depending on the selected rules we can have a deconfined-confined phase transition, or none. Or even a new intermediate phase for which not much is known, as it happened for the $\mathbb{Z}_3$ case within the sector $n \neq 0$ or the $\mathbb{Z}_4$ case for $n \neq 0, 2$.

The second work [6], discussed in Chap. 4, treats a general framework for formulating non-Abelian LGTs, in the Hamiltonian formulation, focusing on two key aspects: the electric term and the physical Hilbert space. Regarding the former, it introduces a novel perspective where the electric term can be interpreted as a Laplacian on the Cayley graph of the group. This new interpretation can be considered quite natural, because it generalize the Lie group case where the electric term is a Laplacian on the group manifold. Furthermore, it has been shown that a complete description of the physical Hilbert space, for any group, is possible through the use of spin-network states. Such a achievement can have major consequences, as it can lead to more efficients implementations of LGTs where no resources has to be wasted on redundant degrees of freedom.

In conclusion, both works show some novel point of view on the subject of LGTs for Quantum Simulation, that the author hopes to be beneficial for the whole community working on these topics.

Some results in representation theory

In this appendix we sum up some of the basic results of representation theory of finite and compact Lie groups. All the representation theory here presented is taken over the complex field $\mathbb{C}$.

A.1 Basic results

A finite group only has finitely many representations up to equivalence, and they are all unitary:

Theorem 1. *Let G be a finite group and Σ the set of equivalence classes of irreducible representations (irreps) of G. Then, Σ is finite, and the representative of each class can be chosen to be unitary.*

We can then state the following:

Theorem 2 (Burnside)**.** *Let G be a finite group. Then:*

1. *If $\dim(j)$ is the dimension of the j-th inequivalent irreps of G, and there are M such irreps, then*

$$\sum_{j=1}^{M} \dim(j)^2 = |G|,\qquad (A.1)$$

where $|G|$ is the order of the group.

2. *The number of inequivalent irreducible representations of G is equal to the number of conjugacy classes of G.*

An immediate consequence follows:

Corollary 1. *If G is a finite Abelian group, then it has precisely $|G|$ inequivalent irreps.*

Similar results apply to compact groups. First of all,

Theorem 3. *The irreps of a compact Lie group are finite-dimensional.*

Moreover,

Theorem 4. *Let G be a compact Lie group and Σ the set of equivalence classes of irreducible representations of G. Then, Σ is countable, and the representative of each class can be chosen to be unitary.*

Given the irreps $\{\pi_j\}$ of a group (compact Lie or finite), these satisfy the so-called *orthogonality theorem*. The statement for compact Lie groups is the following:

Theorem 5 (Orthogonality theorem for compact Lie groups). *Let $\{\pi_j\}$ be unitary irreps of G. Then*

$$\int \mathrm{d}g [\pi_j(g)]^*_{nm} [\pi_{j'}(g)]_{n'm'} = \frac{Vol(G)}{\dim(j)} \delta_{jj'} \delta_{nn'} \delta_{mm'}, \tag{A.2}$$

where the volume of the group is the volume corresponding to the chosen Haar measure.

While the statement for finite groups needs some little adjustments:

Theorem 6 (Orthogonality theorem for finite groups). *Let $\{\pi_j\}$ be unitary irreps of G. Then*

$$\sum_{g \in G} [\pi_j(g)]^*_{nm} [\pi_{j'}(g)]_{n'm'} = \frac{|G|}{\dim(j)} d_{jj'} \delta_{nn'} \delta_{mm'} \tag{A.3}$$

A useful corollary is that the sum of all matrices of a non-trivial irrep j is zero:

$$\int \mathrm{d}g \pi_j(g) = 0 \quad \text{or} \quad \sum_{g \in G} \pi_j(g) = 0, \tag{A.4}$$

where the former equation correspond to compact groups while the latter to finite groups. This follows by taking j' equal to the trivial representation, whose matrice elements are all equal to the identity. Then if j is non-trivial, the right-hand side of the orthogonality theorem is always zero. Taking $m' = n'$ on the left-hand side gives the claim

A.2 Character theory

In this section, we will only be concerned with finite groups. The irreps of a finite group G are the function $\chi : G \to \mathbb{C}$ defined as the traces of irreps of G:

$$\chi_j(g) = \operatorname{tr} \pi_j(g). \tag{A.5}$$

There are as many irreducible charactes as there airreducible representations. We will use the the following result:

Theorem 7. *The characters* $\{\chi_j\}$ *of a group* G *form a basis for the space of class functions on* G.

A class function f satisfies

$$f(axa^{-1}) = f(x) \qquad \text{for all } x, a \in G, \tag{A.6}$$

which means that it is constant on conjugacy classes. We will also needthe following

Theorem 8 (Orthogonality theorem for characters). *The irreducible characters of a finite group are orthonormal, in the sense that*

$$\frac{1}{|G|} \sum_{g \ inG} \chi_i^*(g)\chi_j(g) = \delta_{ij}. \tag{A.7}$$

The characters also satisfy a different kind of orthogonality relation, where one sums over characters rather than over group elements:

Theorem 9. *The irreducible characters* $\{\chi_i\}$ *of a finite group satisfy*

$$\sum_i \chi^*(g)\chi_i(h) = \begin{cases} |G|/|C(g)| & g \text{ and } h \text{ are conjugate} \\ 0 & \text{otherwise} \end{cases} \tag{A.8}$$

where i indices the irreducible characters and $|C(g)|$ *is the sice of the conjugacy class of g.*

Finally, we can define the *convolution* of two class functions ϕ and ψ:

$$(\phi * \psi)(g) = \sum_{h \in G} \phi(gh^{-1})\psi(h). \tag{A.9}$$

The convolution is symmetric, $\phi * \psi = \psi * \phi$. We will use the fact that the convolution of two characters is again a character,

$$\chi_i * \chi_j = \frac{|G|}{\dim(j)} \delta_{ij}\chi_j. \tag{A.10}$$

This can be showed with a direct computation.

A.3 Peter-Weyl theorem

The Peter-Weyl theorem is instrumental in the formulation of the Hamiltonian in Sec. 4.1.2. See [144, 163] for the Lie group case and [143] for the finite group case. The statement for compact Lie groups is:

Theorem 10 (Peter-Weyl for compact Lie groups). *Let G be a compact Lie group. Then*

  (i) *The space of square-integrable functions on G can be decomposed as a sum of representation spaces. More precisely, V_j is the vector space for the irreps π_j, then*

$$L^2(G) = \bigoplus_{j \in \Sigma} V_j^* \otimes V_j. \tag{A.11}$$

 (ii) *The matrix elements of all the inequivalent irreps of G form an orthogonal basis for $L^2(G)$.*

(iii) *If $\{|g\rangle\}$ is the orthonormal group element basis for $L^2(G)$, then the orthonormal matrix element basis $|jmn\rangle$ satisfies*

$$\langle g|jmn\rangle = \sqrt{\frac{\dim(j)}{\text{Vol}(G)}} [\pi_j(g)]_{mn}. \tag{A.12}$$

Note that there are multiple ways of writing the Peter-Weyl decomposition, as

$$V^* \otimes V \simeq \text{End}V \simeq V^{\oplus \dim V} \tag{A.13}$$

As we will see later, these correspond to different ways of seeing $L^2(G)$ as a representation space.

Note that part *(i)* can be understood as a generalisation of the Fourier decomposition. In fact, since U(1) is Abelian, all of its irreps are one-dimensional and are given by matrix elements of the form $\{e^{inx}\}$ for $x \in S^1 = [0, 2\pi)$. Then the Peter-Weyl theorem states that any square-integrable function on $U(1) \simeq S^1$ can be written as a Fourier series.

Recall that matrix elements are defined as follows. Consider the examples of SU(2) [98], but the generalisation is easy. As we know, the irreps of SU(2) are labeled by a half integer $j \in \frac{1}{2}\mathbb{Z}^+$. Then in this case

$$L^2(G) = \bigoplus_{j \ in \frac{1}{2}\mathbb{Z}^+} V_j^* \otimes V_j, \tag{A.14}$$

where $V_j = \mathbb{C}^{2j+1}$ We have irreps π_j for each j and the matrix elements are literally the elements of the matrices representing a certain $U \in$ SU(2) as a

function of U. More precisely, they are functions

$$[\pi_j(\cdot)]_{mn} = \mathrm{SU}(2) \to \mathbb{C}, \qquad g \mapsto [\pi_j(g)]_{mn}, \qquad (A.15)$$

where $-j \leq m, n \leq j$ in integer steps. In the general case, it is more natural to take $1 \leq m, n \leq \dim(j)$.

In part *(iii)* $\mathrm{Vol}(G)$ is the volume of the group given by the chosen Haar measure. The resul of part *(iii)* can be readily derived as a consequence of *(ii)* and the orthogonality theorems for representations. The non-trivial statement is that the matrix elements of representations space $L^2(G)$, while the orthogonality is an algebraic statement. In fact, by *(ii)* the matrix elements $[\pi_j]_{mn}$ for a basis for the space of wave-functions $L^2(G)$. The corresponding states are then given by

$$|jmn\rangle = C_{jmn} \int \mathrm{d}U \, [\pi_j(U)]_{mn} \, |U\rangle, \qquad (A.16)$$

where the constant C_{jmn} can be chosen to ensure that the $|jmn\rangle$ are normalized. Then we can compute their inner product,

$$\langle j'm'n' | jmn \rangle = C^*_{j'm'n'} C_{jmn} \frac{\mathrm{Vol}(G)}{\dim(j)} \delta_{jj'} \delta_{mm'} \delta_{nn'}.$$

It follows that the representation basis $\{|jmn\rangle\}$ is orthonormal with an appropriate choice of constants,

$$C_{jmn} = \sqrt{\frac{\dim(j)}{\mathrm{Vol}(G)}}$$

for compact Lie groups. Everything we have said here also holds for finite groups, with the replacement $\mathrm{Vol}(G) \to |G|$.

Crucially, the Peter-Weyl theorem also holds for finite groups [143, Sec. 6.2]:

Theorem 11 (Peter-Weyl for finite groups). *Let G be a finite groups. Then*

(i) *The group algebra on G can be decomposed as a sum of representation spaces. More precisely, if V_j is the vector space for the j-th irrep π_j, then*

$$\mathbb{C}[G] = \bigoplus_{j \in \Sigma} V_j^* \otimes V_j. \qquad (A.17)$$

(ii) *The matrix elements of all the inequivalent irreps of G form an orthogonal basis for $\mathbb{C}[G]$.*

(iii) If $\{|g\rangle\}$ is the orthonormal group element basis for $\mathbb{C}[G]$, then the orthonormal matrix element basis $\{|jmn\rangle\}$ can be chosen to satisfy

$$\langle g|jmn\rangle = \sqrt{\frac{\dim(j)}{|G|}}[\pi_j(g)]_{mn}. \qquad (A.18)$$

The result is essentially the same as in the compact case. Note that in the finite group case there is no issue of convergence, and as such we do not need to specify further information on the group algebra. The duality relation can be shown to hold in the same manner as for compact Lie groups.

Some groups of interest

B.1   The cyclic groups $\mathbb{Z}_N$

The cyclic group of order N, which we denote as $\mathbb{Z}_N$, consists of the powers $1, r, \ldots, r^{N-1}$ of an element r such that $r^N = 1$. This can be written formally as

$$\mathbb{Z}_N = \langle r | r^N = 1 \rangle. \tag{B.1}$$

The group $\mathbb{Z}_N$ can be realized as the group fo rotations through angles $2\pi k/N$ around an axis.

It is an Abelian group, therefore all its irreps are of degree 1. Such a representation associates with r a complex number $\chi(r) = \omega$, and with r^k the number $\chi(r^k) = \omega^k$. Since $r^N = 1$, we have $\omega^N = 1$, that is, ω is a root of unity of degree N, which means

$$\omega = e^{i 2\pi j/N}, \qquad \text{for } j = 0, 1, \ldots, N - 1. \tag{B.2}$$

Thus, all the irreps are labeled by an integer $j = 0, \ldots, N - 1$ and are all of degree 1. So we do not need to specify the matrix elements obviously. The characters $\chi_0, \chi_1, \ldots, \chi_{N-1}$ are given by

$$\chi_j(r^k) = e^{i 2\pi k j/N}. \tag{B.3}$$

It is immediate to see that $\chi_n \chi_{n'} = \chi_{n+n'}$, where $n + n'$ is taken modulo N. Because $\mathbb{Z}_N$ is Abelian, all its conjugacy classes are singlets, i.e. contains only one element, hence we have N conjugacy classes.

Regarding the basis of the group algebra $\mathbb{C}[\mathbb{Z}_N]$, the group basis $\{|r^k\rangle\}$ and the irreps basis $|j\rangle$ are related by the trasformation

$$|j\rangle = \sum_{k=0}^{N-1} |r^k\rangle \langle r^k | j\rangle = \frac{1}{\sqrt{N}} \sum_{k=0}^{N-1} \omega^{kj} |r^k\rangle, \tag{B.4}$$

which is just the *quantum Fourier transform.*

Moreover, ρ_h and ρ^{N-h} are isomorphic. Hence we may assume $0 \leq h \leq N/2$. The extreme cases $h = 0$ and $h = N/2$ are uninteresting: The former corresponds to the one-dimensional irrep with character $\psi_0 + \psi_1$, while the latter to $\psi_2 + \psi_3$. On the other hand, for $0 < h < N/2$, the representation ρ_h are *irreducible*. The corresponding characters χ_h are given by:

$$\chi_h(r^k) = \omega^{hk} + \omega^{-hk} = 2\cos\frac{2\pi hk}{N} \quad \text{and} \quad \chi_h(r^k s) = 0 \qquad \text{(B.9)}$$

The irreducible representations of degree 1 and 2 constructed above are the *only irreducible representations* of D_N, up to isomorphism. In fact, thesum of the squares of their degrees

$$4 \times 1 + \left(\frac{N}{2} - 1\right) \times 4 = 2N$$

equals to the order of D_N (see (A.1)).

Irreps for N odd In the case of odd N we only have *two one-dimensional irreps*, with character table

	r	s
ψ_0	$+1$	$+1$
ψ_1	$+1$	-1

We are missing the irreps ψ_2 and ψ_3 of the previous case because $(-1)^N = +1$ is true only for N even.

The representations ρ_h of degree 2 are defined by the same formulas (B.7) as in the case where N is even. Those corresponding to $0 < h < N/2$ are irreducible and pairwise non-isomorphic. Observe that, since N is odd, the condition $h < n/2$ can also be written as $h \leq (n-1)/2$. The formulas of their characters is the same as (B.9).

These representations are the *only* ones. Indeed, it can be readily verified with formula (A.1) of Th. 2. The sum of the squares of their degrees is equal to

$$2 \times 1 + \frac{N-1}{2} \times 4 = 2N,$$

which is in fact the order of D_N.

The case $N = 4$ We describe in more detail the dihedral group D_4 of order 8. Its elements are

$$D_4 = \{1,\, r,\, r^2,\, r^3,\, s,\, rs,\, r^2s,\, r^3s\}$$

	$\{e\}$	$\{r, r^3\}$	$\{r^2\}$	$\{s, r^2s\}$	$\{rs, r^3s\}$
χ_0	$+1$	$+1$	$+1$	$+1$	$+1$
χ_1	$+1$	-1	$+1$	$+1$	-1
χ_2	$+1$	$+1$	$+1$	-1	-1
χ_3	$+1$	-1	$+1$	-1	$+1$
χ_4	$+2$	0	-2	0	0

Table B.1.   Character table of D_4

and it has 5 conjugacy classes:

$$\{e\}, \quad \{r, r^3\}, \quad \{r^2\}, \quad \{s, r^2\}, \quad \{rs, r^3s\}.$$

We also have 5 irreps $\{\rho_j\}$, which we number them with $j = 0, \ldots, 4$. For $j = 0, \ldots, 3$ we have the one-dimensional irreps, while for $j = 4$ we have the only two-dimensional irrep:

$$\rho_4(r) = \begin{pmatrix} i & 0 \\ 0 & -i \end{pmatrix} \quad \text{and} \quad \rho_4(s) = \begin{pmatrix} 0 & 1 \\ 1 & 0 \end{pmatrix}. \tag{B.10}$$

Alternatively, we can choose another two-dimensional representation $\bar{\pi}_4$ which uses only real matrices

$$\bar{\rho}_4(r) = \begin{pmatrix} 0 & -1 \\ 1 & 0 \end{pmatrix} \quad \text{and} \quad \bar{\rho}_4(s) = \begin{pmatrix} 1 & 0 \\ 0 & -1 \end{pmatrix} \tag{B.11}$$

and isomorphic to π_4. The character table is shown in Table B.1.

As the $j = 4$ is the only faithful representation, it is a natural choice for the magnetic Hamiltonian.

appendix C

Some proofs

C.1 Degeneracy of electric Hamiltonian

As discussed in Sec. 4, the degeneracy of the electric Hamiltonian given by
the finite group Laplacian Δ is directly related to the structure of the Cayley
graph. In particular, it is a standard result that the graph Laplacian always
has a zero mode and its degeneracy equals the number of connected compo-
nents of the graph [147]. Here we show that the Cayley graph is connected if
its generating set Γ generates the whole group. If instead $\langle \Gamma \rangle \neq G$, then the
Cayley graph splits into connected components identified with the cosets of
$\langle \Gamma \rangle$ in G; thus the degeneracy of the finite-group Laplacian Δ equals $|G|/|\langle \Gamma \rangle|$.

Any subset $\Gamma \in G$ generates a subgroup $\langle \Gamma \rangle < G$. The right cosets of
$\langle \Gamma \rangle$ are of the form $\langle \Gamma \rangle h$ for h in G. Since cosets partition the group, any
two group elements g_1 and g_2 will belong to some coset, say $g_1 \in \langle \Gamma \rangle h_1$ and
$g_2 \in \langle \Gamma \rangle h_2$. We want to show that there is an edge in the Cayley graph
between group elements g_1 and g_2 if and only if $\langle \Gamma \rangle h_1 = \langle \Gamma \rangle h_2$. The fact that
$g_i \in \langle \Gamma \rangle h_i$ means that $g_i = k_i h_i$ for some $k_i \in \langle \Gamma \rangle$. There is an edge between
g_1 and g_2 if and only if $g_1 g_2^{-1} = k_1 h_1 h_2^{-1} k_2 \in \Gamma$. But since $k_i \in \langle \Gamma \rangle$ this is
equivalent to saying that $h_1 h_2^{-1} \in \langle \Gamma \rangle$, which is equivalent to $\langle \Gamma \rangle h_1 = \langle \Gamma \rangle h_2$.
This concludes the proof.

C.2 Counting of invariant states

In Sec. 4.2.2 we used the fact that for a generic representation ρ, the dimension
of the space of invariant vectors is given by

$$\dim \mathrm{Inv}(\rho) = \frac{1}{|G|} \sum_{g \in G} \chi_\rho(g) \,, \qquad\qquad \text{(C.1)}$$

As is well known, if ρ is irreducible then the corresponding character sums to
zero and there are no invariant states. This is to be expected since irreducible
representations by definition have no non-trivial invariant subspaces, but any
invariant vector would span an invariant subspace.

Here we provide a proof of the above formula. If v is an invariant vector for the representation ρ, by definition it satisfies $\rho(g)v = v$ for all $g \in G$. Now we construct a projector onto the subspace of invariant vectors. We define the averaging map $\mathrm{Av} : V_\rho \to V_\rho$,

$$\mathrm{Av}(v) = \frac{1}{|G|} \sum_{g \in G} \rho(g)v \ . \tag{C.2}$$

The averaging map is the projector onto the subspace of invariant vector. In fact, given an arbitrary vector v, we see that $\mathrm{Av}(v)$ is invariant because

$$\rho(g)\mathrm{Av}(v) = \frac{1}{|G|} \sum_{h \in G} \rho(gh)v = \frac{1}{|G|} \sum_{h \in G} \rho(h)v = \mathrm{Av}(v) \ . \tag{C.3}$$

Therefore, Av maps the representation space to the subspace of invariant vectors $\mathrm{Av} : V_\rho \to \mathrm{Inv}(V_\rho)$. Moreover, if v is invariant, then $\mathrm{Av}(v) = v$, and more generally, $\mathrm{Av}^2 = \mathrm{Av}$ by a similar calculation. This means that Av is a projector onto the subspace of invariant vectors. Then the size of projected subspace is as usual given by the trace of the projector, $\dim \mathrm{Inv}(\rho) = \mathrm{tr}\{\mathrm{Av}\}$, which reproduces the above formula.

Acknowledgements

Living off borrowed time, the clock tick faster
That'd be the hour they knock the slick blaster
— MF DOOM

This thesis represent the end of almost ten years living in Bologna and studying Physics, which I can say without a doubt that have been the best years of my life so far.

First and foremost, I would like to thank my supervisor Elisa Ercolessi, for following and supporting me since my Master. If it was not for her courses on Statistical Mechanics and Quantum Many Body Theory, I would not have been inspired in doing Theoretical Physics.

Then, I would like to thank my parents and my family for their unconditional support of my studies, even though they still, to this day, have not a clear idea of what I do. Nonetheless, I am certain that this career choice of mine makes them proud.

Next, I would like to thank all the friends I have made over the years. From the classmates and office colleagues to the roommates, without forgetting all the people I have met outside the department. It is still astonishing to me how many relationships and close friends I have been able to build over the years, which feels like a blessing. They are the main reason I can rest assured these have been the best years of my life so far.

Last but not least, a special thanks to the jungle music scene of the 90s, and record labels like Moving Shadow, Good Looking Records, Suburban Base Records, etc. Without their sound, the writing of this thesis would have not been possible.

Acronyms

CM Condensed Matter

d.o.f degrees of freedom

DCPT deconfined-confined phase transition

DMRG Density Matrix Renormalization Group

ED Exact Diagonalization

irrep irreducible representations

LGT Lattice Gauge Theory

MC Monte Carlo

MPS Matrix Product State

PEPS Projected Entangled Pair State

QCD Quantum Chromodynamics

QCM Quantum Clock Model

QED Quantum Electrodynamics

QFT Quantum Field Theory

QIM Quantum Ising Model

QS Quantum Simulation

SM Statistical Mechanics

TC Toric Code

tHS 't Hooft string

TN Tensor Network

WL Wilson loop

YM Yang-Mills

List of Figures

Bibliography

1. M. C. Bañuls *et al.* "Simulating lattice gauge theories within quantum technologies". *The European Physical Journal D* **74,** 1–42 (2020).

2. K. G. Wilson. "Confinement of quarks". *Phys. Rev. D* **10,** 2445 (1974).

3. J. I. Cirac, P. Zoller. "Goals and opportunities in quantum simulation". *Nature Physics* **8,** 264–266 (Apr. 2012).

4. R. P. Feynman. "Simulating physics with computers". *Int. J. Theor. Phys.* **21** (ed L. Brown) 467–488 (1982).

5. S. Pradhan, A. Maroncelli, E. Ercolessi. *Discrete Abelian lattice gauge theories on a ladder and their dualities with quantum clock models.* 2022. arXiv: 2208.04182.

6. A. Mariani, S. Pradhan, E. Ercolessi. *Hamiltonians and gauge-invariant Hilbert space for Yang-Mills theories with finite gauge group.* arXiv: 2301.12224.

7. G. Ortiz, E. Cobanera, Z. Nussinov. "Dualities and the phase diagram of the *p*-clock model". *Nuclear Physics B* **854,** 780–814 (2012).

8. J. Kogut, L. Susskind. "Hamiltonian formulation of Wilson's lattice gauge theories". *Phys. Rev. D* **11,** 395–408 (2 Jan. 1975).

9. M. Creutz. *Quarks, gluons and lattices* (Cambridge Univ. Press, 1985).

10. M. E. Peskin, D. V. Schroeder. *An Introduction to quantum field theory* (Addison-Wesley, Reading, USA, 1995).

11. G. Aarts. "Introductory lectures on lattice QCD at nonzero baryon number". *Journal of Physics: Conference Series* **706,** 022004 (Apr. 2016).

12. C. E. DeTar, U. M. Heller. "QCD thermodynamics from the lattice". *The European Physical Journal A* **41,** 405–437 (July 2009).

13. M. Alford. "Color superconducting quark matter". *Annual Review of Nuclear and Particle Science* **51,** 131–160 (Dec. 2001).

14. G. Bhanot. "SU(3) lattice gauge theory in 4 dimensions with a modified Wilson action". *Physics Letters B* **108,** 337–340 (1982).

15. R. C. Edgar. "Generalised actions for lattice gauge models". *Nuclear Physics B* **200,** 345–354 (1982).

16. M. Creutz, M. Okawa. "Generalized actions in Zp lattice gauge theory". *Nuclear Physics B* **220,** 149–166 (1983).

17. S. Elitzur. "Impossibility of spontaneously breaking local symmetries". *Phys. Rev. D* **12,** 3978–3982 (12 Dec. 1975).

18. H. Nielsen, M. Ninomiya. "A no-go theorem for regularizing chiral fermions". *Physics Letters B* **105,** 219–223 (Oct. 1981).

19. L. Susskind. "Lattice fermions". *Phys. Rev. D* **16,** 3031–3039 (10 Nov. 1977).

20. D. Tong. *Gauge Theory.* 2018.

21. Y. Manin. "Computable and uncomputable". *Sovetskoye Radio, Moscow* **128** (1980).

22. I. M. Georgescu, S. Ashhab, F. Nori. "Quantum simulation". *Rev. Mod. Phys.* **86,** 153–185 (1 Mar. 2014).

23. P. Hauke, F. M. Cucchietti, L. Tagliacozzo, I. Deutsch, M. Lewenstein. "Can one trust quantum simulators?" *Reports on Progress in Physics* **75,** 082401 (July 2012).

24. V. M. Kendon, K. Nemoto, W. J. Munro. "Quantum analogue computing". *Philosophical Transactions of the Royal Society A: Mathematical, Physical and Engineering Sciences* **368,** 3609–3620 (2010).

25. I. Buluta, F. Nori. "Quantum Simulators". *Science* **326,** 108–111 (2009).

26. R. P. Feynman. "Quantum Mechanical Computers". *Optics News* **11,** 11–20 (Feb. 1985).

27. M. A. Nielsen, I. L. Chuang. *Quantum Computation and Quantum Information: 10th Anniversary Edition* (Cambridge University Press, 2010).

28. W. P. Schleich, H. Walther. *Elements of quantum information* (John Wiley & Sons, 2007).

29. J. Stolze, D. Suter. *Quantum computing: a short course from theory to experiment* (John Wiley & Sons, 2008).

30. S. Lloyd. "Universal Quantum Simulators". *Science* **273,** 1073–1078 (1996).

31. R. C. Wagner, M. S. Everitt, V. M. Kendon, M. L. Jones. *Universal Continuous Variable Quantum Computation in the Micromaser.* in *Unconventional Computation* (eds C. S. Calude, M. Hagiya, K. Morita, G. Rozenberg, J. Timmis) (Springer Berlin Heidelberg, Berlin, Heidelberg, 2010), 152–163.

32. D. E. Deutsch. "Quantum computational networks". *Proceedings of the Royal Society of London. A. Mathematical and Physical Sciences* **425,** 73–90 (1989).

33. E. Fredkin, T. Toffoli. "Conservative logic". *International Journal of Theoretical Physics* **21,** 219–253 (Apr. 1982).

34. A. Barenco *et al.* "Elementary gates for quantum computation". *Phys. Rev. A* **52,** 3457–3467 (5 Nov. 1995).

35. R. Somma, G. Ortiz, J. E. Gubernatis, E. Knill, R. Laflamme. "Simulating physical phenomena by quantum networks". *Phys. Rev. A* **65,** 042323 (4 Apr. 2002).

36. N. Wiebe, D. W. Berry, P. Høyer, B. C. Sanders. "Simulating quantum dynamics on a quantum computer". *Journal of Physics A: Mathematical and Theoretical* **44,** 445308 (Oct. 2011).

37. W. H. Zurek. "From quantum to classical". *Phys Today* **37.** arXiv: `quant-ph/0306072 [quant-ph]` (1991).

38. M. Schlosshauer. "The quantum-to-classical transition and decoherence". arXiv: `1404.2635` (2014).

39. M. Schlosshauer. "Quantum decoherence". *Physics Reports* **831,** 1–57 (Oct. 2019).

40. J. Preskill. "Fault-tolerant quantum computation". arXiv: `quant-ph/9712048` (1997).

41. P. Shor. *Fault-tolerant quantum computation.* in *Proceedings of 37th Conference on Foundations of Computer Science* (1996), 56–65.

42. J. Preskill. "Quantum Computing in the NISQ era and beyond". *Quantum* **2,** 79 (Aug. 2018).

43. H. Wei, X. Xue. "Quantum Isomorphic Simulation". arXiv: `quant-ph/9702050` (1997).

44. J. Argüello-Luengo, A. González-Tudela, T. Shi, P. Zoller, J. I. Cirac. "Analogue quantum chemistry simulation". *Nature* **574,** 215–218 (Oct. 2019).

45. A. Aspuru-Guzik, P. Walther. "Photonic quantum simulators". *Nature Physics* **8,** 285–291 (Apr. 2012).

46. R. Blatt, C. F. Roos. "Quantum simulations with trapped ions". *Nature Physics* **8,** 277–284 (Apr. 2012).

47. I. Bloch, J. Dalibard, S. Nascimbène. "Quantum simulations with ultracold quantum gases". *Nature Physics* **8,** 267–276 (Apr. 2012).

48. A. A. Houck, H. E. Türeci, J. Koch. "On-chip quantum simulation with superconducting circuits". *Nature Physics* **8,** 292–299 (Apr. 2012).

49. M. Lewenstein, A. Sanpera, V. Ahufinger. *Ultracold Atoms in Optical Lattices: Simulating quantum many-body systems* (Oxford University Press, June 2012).

50. W. Thomson. "VI. Mechanical integration of the general linear differential equation of any order with variable coefficients". *Proceedings of the Royal Society of London* **24,** 271–275 (1876).

51. I. Bloch, J. Dalibard, W. Zwerger. "Many-body physics with ultracold gases". *Rev. Mod. Phys.* **80,** 885–964 (3 July 2008).

52. D. G. Angelakis. "Quantum simulations with photons and polaritons". *Quantum Science and Technology (Springer, 2017),* 134 (2017).

53. S. Somaroo, C. H. Tseng, T. F. Havel, R. Laflamme, D. G. Cory. "Quantum Simulations on a Quantum Computer". *Phys. Rev. Lett.* **82,** 5381–5384 (26 June 1999).

54. A. Singha *et al.* "Two-Dimensional Mott-Hubbard Electrons in an Artificial Honeycomb Lattice". *Science* **332,** 1176–1179. eprint: `https://www.science.org/doi/pdf/10.1126/science.1204333` (2011).

55. A. W. Sandvik. "Computational Studies of Quantum Spin Systems". *AIP Conference Proceedings* **1297,** 135–338. eprint: `https://aip.scitation.org/doi/pdf/10.1063/1.3518900` (2010).

56. M. Troyer. *Computational quantum physics.* 2010.

57. U. Schollwöck. "The density-matrix renormalization group in the age of matrix product states". *Annals of Physics* **326.** January 2011 Special Issue, 96–192 (2011).

58. I. P. McCulloch. "From density-matrix renormalization group to matrix product states". *Journal of Statistical Mechanics: Theory and Experiment* **2007,** P10014 (Oct. 2007).

59. G. D. Chiara, M. Rizzi, D. Rossini, S. Montangero. "Density Matrix Renormalization Group for Dummies". *Journal of Computational and Theoretical Nanoscience* **5,** 1277–1288 (July 2008).

60. E. Stoudenmire, S. R. White. "Studying Two-Dimensional Systems with the Density Matrix Renormalization Group". *Annual Review of Condensed Matter Physics* **3,** 111–128 (2012).

61. R. Orús. "A practical introduction to tensor networks: Matrix product states and projected entangled pair states". *Annals of Physics* **349,** 117–158 (Oct. 2014).

62. F. Verstraete, J. I. Cirac. *Renormalization algorithms for Quantum-Many Body Systems in two and higher dimensions.* 2004. arXiv: 0407066.

63. F. Verstraete, V. Murg, J. Cirac. "Matrix product states, projected entangled pair states, and variational renormalization group methods for quantum spin systems". *Advances in Physics* **57,** 143–224 (2008).

64. F. Verstraete, D. Porras, J. I. Cirac. "Density Matrix Renormalization Group and Periodic Boundary Conditions: A Quantum Information Perspective". *Phys. Rev. Lett.* **93,** 227205 (22 Nov. 2004).

65. G. Vidal. "Class of Quantum Many-Body States That Can Be Efficiently Simulated". *Phys. Rev. Lett.* **101,** 110501 (11 Sept. 2008).

66. J. I. Cirac, F. Verstraete. "Renormalization and tensor product states in spin chains and lattices". *Journal of Physics A: Mathematical and Theoretical* **42,** 504004 (Dec. 2009).

67. G. Vidal, J. I. Latorre, E. Rico, A. Kitaev. "Entanglement in Quantum Critical Phenomena". *Physical Review Letters* **90** (June 2003).

68. P. Calabrese, J. Cardy. "Entanglement entropy and quantum field theory". *Journal of Statistical Mechanics: Theory and Experiment* **2004,** P06002 (June 2004).

69. P. Calabrese, J. Cardy. "Entanglement entropy and conformal field theory". *Journal of Physics A: Mathematical and Theoretical* **42,** 504005 (Dec. 2009).

70. M. Srednicki. "Entropy and area". *Physical Review Letters* **71,** 666–669 (Aug. 1993).

71. M. B. Plenio, J. Eisert, J. DreiSSig, M. Cramer. "Entropy, Entanglement, and Area: Analytical Results for Harmonic Lattice Systems". *Physical Review Letters* **94** (Feb. 2005).

72. I. Affleck, T. Kennedy, E. H. Lieb, H. Tasaki. "Rigorous results on valence-bond ground states in antiferromagnets". *Phys. Rev. Lett.* **59,** 799–802 (7 Aug. 1987).

73. J. Jordan, R. Orús, G. Vidal, F. Verstraete, J. I. Cirac. "Classical Simulation of Infinite-Size Quantum Lattice Systems in Two Spatial Dimensions". *Phys. Rev. Lett.* **101,** 250602 (25 Dec. 2008).

74. L. Tagliacozzo, G. Evenbly, G. Vidal. "Simulation of two-dimensional quantum systems using a tree tensor network that exploits the entropic area law". *Phys. Rev. B* **80,** 235127 (23 Dec. 2009).

75. M. Fannes, B. Nachtergaele, R. F. Werner. "Ground states of VBS models on cayley trees". *Journal of Statistical Physics* **66,** 939–973 (Feb. 1992).

76. G. Evenbly, G. Vidal. in *Strongly Correlated Systems: Numerical Methods* (eds A. Avella, F. Mancini) 99–130 (Springer Berlin Heidelberg, Berlin, Heidelberg, 2013).

77. G. Vidal. "Entanglement Renormalization". *Physical Review Letters* **99** (Nov. 2007).

78. G. Evenbly, G. Vidal. "Entanglement Renormalization in Two Spatial Dimensions". *Phys. Rev. Lett.* **102,** 180406 (18 May 2009).

79. H.-W. Lin *et al.* "Parton distributions and lattice QCD calculations: a community white paper". *Progress in Particle and Nuclear Physics* **100,** 107–160 (2018).

80. M. C. Bañuls, K. Cichy. "Review on novel methods for lattice gauge theories". *Reports on Progress in Physics* **83,** 024401 (Jan. 2020).

81. K. Cichy, M. Constantinou. "A Guide to Light-Cone PDFs from Lattice QCD: An Overview of Approaches, Techniques, and Results". *Advances in High Energy Physics* **2019,** 1–68 (June 2019).

82. S. Arora, B. Barak. *Computational complexity: a modern approach* (Cambridge University Press, 2009).

83. M. Troyer, U.-J. Wiese. "Computational Complexity and Fundamental Limitations to Fermionic Quantum Monte Carlo Simulations". *Phys. Rev. Lett.* **94,** 170201 (17 May 2005).

84. M. Dalmonte, S. Montangero. "Lattice gauge theory simulations in the quantum information era". *Contemporary Physics* **57,** 388–412. eprint: https://doi.org/10.1080/00107514.2016.1151199 (2016).

85. U.-J. Wiese. "Ultracold quantum gases and lattice systems: quantum simulation of lattice gauge theories". *Annalen der Physik* **525,** 777–796 (July 2013).

86. E. Zohar, J. I. Cirac, B. Reznik. "Quantum simulations of gauge theories with ultracold atoms: Local gauge invariance from angular-momentum conservation". *Phys. Rev. A* **88,** 023617 (2 Aug. 2013).

87. E. Zohar, J. I. Cirac, B. Reznik. "Quantum simulations of lattice gauge theories using ultracold atoms in optical lattices". *Reports on Progress in Physics* **79,** 014401 (2015).

88. E. Zohar, B. Reznik. "Confinement and Lattice Quantum-Electrodynamic Electric Flux Tubes Simulated with Ultracold Atoms". *Phys. Rev. Lett.* **107,** 275301 (27 Dec. 2011).

89. D. Banerjee *et al.* "Atomic Quantum Simulation of Dynamical Gauge Fields Coupled to Fermionic Matter: From String Breaking to Evolution after a Quench". *Phys. Rev. Lett.* **109,** 175302 (17 Oct. 2012).

90. P. Hauke, D. Marcos, M. Dalmonte, P. Zoller. "Quantum Simulation of a Lattice Schwinger Model in a Chain of Trapped Ions". *Phys. Rev. X* **3,** 041018 (4 Nov. 2013).

91. D. Yang *et al.* "Analog quantum simulation of (1+1)-dimensional lattice QED with trapped ions". *Phys. Rev. A* **94,** 052321 (5 Nov. 2016).

92. D. Marcos, P. Rabl, E. Rico, P. Zoller. "Superconducting Circuits for Quantum Simulation of Dynamical Gauge Fields". *Phys. Rev. Lett.* **111,** 110504 (11 Sept. 2013).

93. D. Marcos *et al.* "Two-dimensional lattice gauge theories with superconducting quantum circuits". *Annals of Physics* **351,** 634–654 (2014).

94. G. K. Brennen, G. Pupillo, E. Rico, T. M. Stace, D. Vodola. "Loops and Strings in a Superconducting Lattice Gauge Simulator". *Phys. Rev. Lett.* **117,** 240504 (24 Dec. 2016).

95. E. Zohar, M. Burrello. "Formulation of lattice gauge theories for quantum simulations". *Phys. Rev. D* **91,** 054506 (5 Mar. 2015).

96. E. Zohar, A. Farace, B. Reznik, J. I. Cirac. "Digital lattice gauge theories". *Phys. Rev. A* **95,** 023604 (2 Feb. 2017).

97. E. Zohar, A. Farace, B. Reznik, J. I. Cirac. "Digital Quantum Simulation of $\mathbb{Z}_2$ Lattice Gauge Theories with Dynamical Fermionic Matter". *Phys. Rev. Lett.* **118,** 070501 (7 Feb. 2017).

98. A. Milsted, T. J. Osborne. "Quantum Yang-Mills theory: An overview of a program". *Physical Review D* **98** (July 2018).

99. J. Bender, E. Zohar, A. Farace, J. I. Cirac. "Digital quantum simulation of lattice gauge theories in three spatial dimensions". *New Journal of Physics* **20,** 093001 (Sept. 2018).

100. X. Cui, Y. Shi, J.-C. Yang. "Circuit-based digital adiabatic quantum simulation and pseudoquantum simulation as new approaches to lattice gauge theory". *Journal of High Energy Physics* **2020,** 1–35 (2020).

101. T. Byrnes, Y. Yamamoto. "Simulating lattice gauge theories on a quantum computer". *Phys. Rev. A* **73,** 022328 (2 Feb. 2006).

102. S. Chandrasekharan, U. Wiese. "Quantum link models: A discrete approach to gauge theories". *Nuclear Physics B* **492,** 455–471 (1997).

103. D. C. Hackett *et al.* "Digitizing gauge fields: Lattice Monte Carlo results for future quantum computers". *Physical Review A* **99** (June 2019).

104. H. Lamm, S. Lawrence, Y. Yamauchi. "General methods for digital quantum simulation of gauge theories". *Phys. Rev. D* **100,** 034518 (3 Aug. 2019).

105. R. Brower, S. Chandrasekharan, U.-J. Wiese. "QCD as a quantum link model". *Phys. Rev. D* **60,** 094502 (9 Sept. 1999).

106. R. Savit. "Duality in field theory and statistical systems". *Rev. Mod. Phys.* **52,** 453–487 (2 Apr. 1980).

107. D. B. Kaplan, J. R. Stryker. "Gauss's law, duality, and the Hamiltonian formulation of U(1) lattice gauge theory". *Phys. Rev. D* **102,** 094515 (9 Nov. 2020).

108. E. Fradkin, S. H. Shenker. "Phase diagrams of lattice gauge theories with Higgs fields". *Phys. Rev. D* **19,** 3682–3697 (12 June 1979).

109. Y. Ji, H. Lamm, S. Z. and. "Gluon field digitization via group space decimation for quantum computers". *Physical Review D* **102** (Dec. 2020).

110. A. Alexandru *et al.* "Gluon Field Digitization for Quantum Computers". *Phys. Rev. D* **100,** 114501. arXiv: 1906.11213 [hep-lat] (2019).

111. S. Notarnicola *et al.* "Discrete Abelian gauge theories for quantum simulations of QED". *Journal of Physics A: Mathematical and Theoretical* **48,** 30FT01 (2015).

112. E. Ercolessi, P. Facchi, G. Magnifico, S. Pascazio, F. V. Pepe. "Phase transitions in Z_n gauge models: Towards quantum simulations of the Schwinger-Weyl QED". *Phys. Rev. D* **98,** 074503 (7 Oct. 2018).

113. J. Schwinger. "Unitary operator bases". *Proceedings of the National Academy of Sciences* **46,** 570–579 (1960).

114. J. Schwinger, B. Englert. *Symbolism of Atomic Measurements.* 2001.

115. H. Weyl. *The theory of groups and quantum mechanics* (Courier Corporation, 1950).

116. L. Tagliacozzo, G. Vidal. "Entanglement renormalization and gauge symmetry". *Phys. Rev. B* **83,** 115127 (2011).

117. A. Hamma, D. A. Lidar. "Adiabatic Preparation of Topological Order". *Phys. Rev. Lett.* **100,** 030502 (3 Jan. 2008).

118. S. Trebst, P. Werner, M. Troyer, K. Shtengel, C. Nayak. "Breakdown of a Topological Phase: Quantum Phase Transition in a Loop Gas Model with Tension". *Phys. Rev. Lett.* **98,** 070602 (7 Feb. 2007).

119. E. Cobanera, G. Ortiz, Z. Nussinov. "The bond-algebraic approach to dualities". *Advances in physics* **60,** 679–798 (2011).

120. H. A. Kramers, G. H. Wannier. "Statistics of the two-dimensional ferromagnet. Part I". *Phys. Rev.* **60,** 252 (1941).

121. L. Onsager. "Crystal Statistics. I. A Two-Dimensional Model with an Order-Disorder Transition". *Phys. Rev.* **65,** 117–149 (3-4 Feb. 1944).

122. T. D. Schultz, D. C. Mattis, E. H. Lieb. "Two-Dimensional Ising Model as a Soluble Problem of Many Fermions". *Rev. Mod. Phys.* **36,** 856–871 (3 July 1964).

123. P. Jordan, E. P. Wigner. "About the Pauli exclusion principle". *Z. Phys* **47,** 14–75 (1928).

124. E. Cobanera, G. Ortiz, Z. Nussinov. "Unified Approach to Quantum and Classical Dualities". *Phys. Rev. Lett.* **104,** 020402 (2 Jan. 2010).

125. Z. Nussinov, G. Ortiz. "Bond algebras and exact solvability of hamiltonians: Spin $S = 1/2$ multilayer systems". *Phys. Rev. B* **79,** 214440 (2009).

126. E. Fradkin, L. Susskind. "Order and disorder in gauge systems and magnets". *Phys. Rev. D* **17,** 2637 (1978).

127. E. Wigner. *Group theory and its application to the quantum mechanics of atomic spectra.* Trans. by J. J. Griffin (New York: Academic Press, 1959).

128. D. Radicevic. *Spin Structures and Exact Dualities in Low Dimensions.* 2019. arXiv: 1809.07757 [hep-th].

129. P. Fendley. "Free parafermions". *Journal of Physics A: Mathematical and Theoretical* **47,** 075001 (2014).

130. R. J. Baxter. "A simple solvable Z_N Hamiltonian". *Physics Letters A* **140,** 155–157 (1989).

131. G. Sun, T. Vekua, E. Cobanera, G. Ortiz. "Phase transitions in the Z_p and $U(1)$ clock models". *Phys. Rev. B* **100,** 094428 (2019).

132. R. J. Baxter. *Exactly solved models in statistical mechanics* (Elsevier, 2016).

133. P. Fendley. "Parafermionic edge zero modes in Z_n-invariant spin chains". *Journal of Statistical Mechanics: Theory and Experiment* **2012,** P11020 (Nov. 2012).

134. Y. Zhuang, H. J. Changlani, N. M. Tubman, T. L. Hughes. "Phase diagram of the Z_3 parafermionic chain with chiral interactions". *Phys. Rev. B* **92,** 035154 (3 July 2015).

135. R.-Z. Huang, S. Yin. "Nonequilibrium critical dynamics in the quantum chiral clock model". *Phys. Rev. B* **99,** 184104 (18 May 2019).

136. H. Bernien *et al.* "Probing many-body dynamics on a 51-atom quantum simulator". *Nature* **551,** 579–584 (2017).

137. S. Whitsitt, R. Samajdar, S. Sachdev. "Quantum field theory for the chiral clock transition in one spatial dimension". *Phys. Rev. B* **98,** 205118 (20 Nov. 2018).

138. M. C. Bañuls, J. I. Cirac, M. B. Hastings. "Strong and Weak Thermalization of Infinite Nonintegrable Quantum Systems". *Phys. Rev. Lett.* **106,** 050405 (5 Feb. 2011).

139. M. Kormos, M. Collura, G. Takács, P. Calabrese. "Real-time confinement following a quantum quench to a non-integrable model". *Nature Physics* **13,** 246–249 (2017).

140. O. Pomponio, M. A. Werner, G. Zarand, G. Takacs. "Bloch oscillations and the lack of the decay of the false vacuum in a one-dimensional quantum spin chain". *SciPost Phys.* **12,** 61 (2 2022).

141. J. Nyhegn, C.-M. Chung, M. Burrello. "$\mathbb{Z}_N$ lattice gauge theory in a ladder geometry". *Phys. Rev. Research* **3,** 013133 (1 Feb. 2021).

142. D. A. Huse, A. M. Szpilka, M. E. Fisher. "Melting and wetting transitions in the three-state chiral clock model". *Physica A: Statistical Mechanics and its Applications* **121,** 363–398 (1983).

143. J.-P. Serre. *Linear Representations of Finite Groups* (Springer, New York, NY, 1967).

144. A. W. Knapp. *Lie Groups: Beyond an Introduction* (Birkhäuser, Boston, 1996).

145. A. Mariani. *Finite-group Yang-Mills lattice gauge theories in the Hamiltonian formalism.*

146. D. Harlow, H. Ooguri. *Symmetries in quantum field theory and quantum gravity*. 2018. arXiv: 1810.05338.

147. F. R. K. Chung. *Spectral Graph Theory* (American Mathematical Society, 1997).

148. M. Creutz. "Gauge fixing, the transfer matrix, and confinement on a lattice". *Phys. Rev. D* **15,** 1128–1136 (4 Feb. 1977).

149. J. B. Kogut. "An introduction to lattice gauge theory and spin systems". *Rev. Mod. Phys.* **51,** 659–713 (4 Oct. 1979).

150. S. Caspar, D. Mesterházy, T. Olesen, N. Vlasii, U.-J. Wiese. "Doubled lattice Chern–Simons–Yang–Mills theories with discrete gauge group". *Annals of Physics* **374,** 255–290 (Nov. 2016).

151. K. Holland, U.-J. Wiese. in *At The Frontier of Particle Physics* 1909–1944 (World Scientific, Apr. 2001).

152. T. D. Cohen. "Center symmetry and area laws". *Physical Review D* **90** (Aug. 2014).

153. A. Sengupta. "Gauge Invariant Functions of Connections". *Proceedings of the American Mathematical Society* **121,** 897–905 (1994).

154. B. Durhuus. "On the structure of gauge invariant classical observables in lattice gauge theories". *Letters in Mathematical Physics* **4,** 515–522 (Nov. 1980).

155. S. X. Cui *et al.* "Kitaev's quantum double model as an error correcting code". *Quantum* **4,** 331 (Sept. 2020).

156. J. C. Baez. "Spin Networks in Gauge Theory". *Advances in Mathematics* **117,** 253–272 (Feb. 1996).

157. G. Burgio, R. D. Pietri, H. Morales-Técotl, L. Urrutia, J. Vergara. "The basis of the physical Hilbert space of lattice gauge theories". *Nuclear Physics B* **566,** 547–561 (Feb. 2000).

158. L. Marchese. *Quantum simulation of abelian and non-abelian gauge theories.*

159. W.-L. You, Y.-W. Li, S.-J. Gu. "Fidelity, dynamic structure factor, and susceptibility in critical phenomena". *Phys. Rev. E* **76,** 022101 (2 Aug. 2007).

160. L. Wang, Y.-H. Liu, J. Imri ka, P. N. Ma, M. Troyer. "Fidelity Susceptibility Made Simple: A Unified Quantum Monte Carlo Approach". *Phys. Rev. X* **5,** 031007 (3 July 2015).

161. R. Brower, S. Chandrasekharan, S. Riederer, U.-J. Wiese. "D-theory: field quantization by dimensional reduction of discrete variables". *Nuclear Physics B* **693,** 149–175 (Aug. 2004).

162. U.-J. Wiese. "D-Theory: A Quest for Nature's Regularization". *Nuclear Physics B - Proceedings Supplements* **153.** Proceedings of the Workshop on Computational Hadron Physics, 336–347 (2006).

163. T. Tao. *The Peter-Weyl theorem, and non-abelian Fourier analysis on compact groups.* 2011.